Filem AD-753257

Nonlinear Wave Interaction in a Plasma Column

by

Jean-Marc Larsen

SU-IPR Report No. 493

October 1972

This work was supported by the Joint Services Electronics Program (U.S. Army, U.S. Navy, and U.S. Air Force) under Contract N00014-67-A-0112-0044 and by the National Aeronautics and Space Administration under Contract NGL-05-020-176

INSTITUTE FOR PLASMA RESEARCH
STANFORD UNIVERSITY, STANFORD, CALIFORNIA

NONLINEAR WAVE INTERACTION IN A PLASMA COLUMN

by

Jean-Marc Larsen

SU-IPR Report No. 493

October 1972

This work was supported by the
Joint Services Electronics Program
(U.S. Army, U.S. Navy, and U.S. Air Force)
under Contract N00014-67-A-0112-0044
and by the
National Aeronautics and Space Administration
under Contract NGL-05-020-176

Institute for Plasma Research
Stanford University
Stanford, California

NONLINEAR WAVE INTERACTION IN A PLASMA COLUMN

by

Jean-Marc Larsen
Institute for Plasma Research
Stanford University
Stanford, California

This work is a theoretical and experimental study of two particular cases of nonlinear wave interaction in a plasma column. The frequencies of the waves are of the order of magnitude of the electron plasma frequency. Ion motions are neglected.

In the first part of the thesis, the nonlinear coupling of slow waves on a plasma column is studied by means of cold plasma theory. The quasistatic approximation is used to simplify the analysis. Waves in a metal tube filled with plasma, and on a uniform plasma column surrounded by an infinite dielectric, are considered in the limit of an infinite magnetic field parallel to the axis of the column. The case of a plasma column surrounded by an infinite dielectric in the absence of a magnetic field is also examined. The linear properties of slow waves are reviewed, and solutions are obtained for use in the nonlinear theory.

The simplest case of nonlinear wave interaction is the coupling of three waves whose frequencies and propagation constants satisfy synchronism conditions on frequency and wavenumber. The coupled mode equations describing the interaction are obtained by means of a Lagrangian description of a bounded cold plasma. When one of the waves is much stronger than the other two, the coupled mode equations can be solved easily. Two possible cases are considered: when the large amplitude wave has the highest frequency, parametric amplification occurs, and the other two waves grow exponentially; otherwise, the two small amplitude waves exchange their energies. The effect of wave damping is considered, and is introduced into the theory as a phenomenological loss factor. Some experimental results on mode conversion in the presence of loss are presented, and are discussed in relation to the theory.

The second part of the thesis is devoted to nonlinear scattering from a plasma column in an electromagnetic field having its magnetic

field parallel to the axis of the column. In the linear regime, the plasma column exhibits series of multipole resonances. A warm plasma analysis using a scalar electron pressure and a nonuniform electron density profile is presented. The quasistatic approximation is used in the column and, for simplicity, a parabolic static electron density profile is chosen. The theory is then extended to the nonlinear regime and the nonlinear scattered power is obtained. The excitation of two linear dipole resonances produces a nonlinear quadrupolar radiation pattern with minima in the direction of the incident wave and at right angle to it. In general, there is no nonlinear power radiated in the forward and backward directions. Numerical results for the nonlinear scattering coefficient are obtained in the special case of second harmonic generation at a linear dipole resonance.

Some observations of nonlinear scattering are presented, and the effect of the Earth's magnetic field and of discharge symmetry on the radiation pattern are discussed. The influence of collisional loss on the nonlinear scattering amplitude is also considered.

CONTENTS

CONTENTS (Cont.)

CONTENTS (Cont.)

TABLES

ILLUSTRATIONS

ILLUSTRATIONS (Cont.)

ILLUSTRATIONS (Cont.)

ILLUSTRATIONS (Cont.)

LIST OF SYMBOLS

Symbol		Page where defined on first use
	(1) Latin Alphabet	
$\underset{\sim}{A}$	an arbitrary vector	126
A_λ	an expression defined in Eq. (2.41)	23
$A_{3\ell}$	constant used in Eq. (5.65)	90
a	radius of plasma column	15
a_λ	constant used in Eq. (2.58)	27
$\underset{\sim}{B}$	magnetic flux density	14
B_0	static magnetic flux density in the z direction	2
$B_\perp$	transverse component of the Earth's magnetic flux density	112
B_ℓ	amplitude of the ℓ-th order term for the incoming wave in the glass	73
$B_{3\ell}$	constant used in Eq. (5.65)	90
b	outside diameter of glass tube	73
b_λ	constant used in Eq. (2.58)	27
$\underset{\sim}{C}$	an arbitrary vector	126
C_ℓ	amplitude of the ℓ-th order term for the outgoing wave in the glass	73
$C_{\ell p}$	constant used in Eq. (5.79)	93
$C_{\alpha\beta\gamma}$	coefficient depending on ω_λ and k_λ for $\lambda = \alpha,\beta,\gamma$, defined in Eq. (2.37)	23
c	speed of light	3
$c_{\ell i}$	coefficient of the i^{th} term in series given by Eq. (C.8)	130

Symbol		Page where defined on first use
$\underset{\sim}{D}$	electric displacement	79
D_ℓ	differential operator defined in Eq. (5.17)	75
d_ℓ	expression defined in Eq. (5.80)	94
$\underset{\sim}{E}$	electric field	2
$E_{\theta s}(\underset{\sim}{r})$	θ-component of the linear scattered electric field	80
$\mathcal{E}_{\lambda 2}$	three-dimensional energy density for Wave λ	21
$\mathcal{E}_{c3}$	three-dimensional coupling energy density .	21
e	electronic charge	8
e_λ	one-dimensional energy density for Wave λ .	21
e_c	one-dimensional coupling energy density . .	21
$F(s,\ell,m)$	expression defined in Eq. (C.23)	132
F_λ	expression defined in Eq. (2.53)	26
$F_{\ell 1}, F_{\ell 2}$	constants defined in Eq. (5.42)	80
$F_{3\ell 1}, F_{3\ell 2}$	constants defined in Eq. (5.79)	93
$F_{c\ell 1}, F_{c\ell 2}$	constants defined in Eq. (D.16)	136
$\mathcal{F}_j$	j-th component of the generalized energy-flux vector	19
$f(r)$	radial electron density profile	73
f_ℓ	expression defined in Eq. (D.13)	136
G_λ	expression defined in Eq. (4.28)	68
$G_\ell(\xi)$	series defined in Eq. (E.2)	137

Symbol		Page where defined on first use
$G_{mn}(r)$	function defined in Eq. (5.71)	92
$G_{\ell j}$	expression defined in Eq. (5.79)	93
$g_{\ell j}$	expression defined in Eq. (5.24)	76
$\underset{\sim}{H}$	magnetic field	15
$H_{z\ell}(\underset{\sim}{r})$	ℓ-th order term in the expansion of the magnetic field of a plane wave into cylindrical waves	73
H_0	magnetic field amplitude of the incident wave	73
$H_{0\lambda}$	magnetic field amplitude of incident Wave λ	87
$H_\ell^{(1)}(r)$	Hankel function of the first kind and order ℓ	73
$H_\ell^{(2)}(r)$	Hankel function of the second kind and order ℓ	73
$H_{zs}(\underset{\sim}{r})$	linear scattered magnetic field	80
$H_{z3}(\underset{\sim}{r})$	nonlinear magnetic field	87
$\mathcal{H}_{z\ell}(r)$	r-varying part of $H_{z\ell}(\underset{\sim}{r})$	73
$\mathcal{H}_{z3\ell}(r)$	r-varying part of the ℓ-th order term of $H_{z3}(\underset{\sim}{r})$	87
$h_{\ell j}(r)$	function defined in Eq. (5.22)	76
$h_{3\ell j}(r)$	function defined in Eq. (5.74)	92
$I_n(r)$	modified Bessel function of the first kind	2
$I_{\alpha\beta\gamma}$	expression defined in Eq. (2.43)	24

Symbol		Page where defined on first use
$I_{\ell j}$	expression defined in Eq. (5.80)	94
$\underset{\sim}{J}$	current density	15
$J_n(r)$	Bessel function of order n	3
J_{s3}	surface current density	135
$J_{s3\ell}$	ℓ-th component of J_{s3}	135
j	$(-1)^{1/2}$	2
$K_n(r)$	modified Bessel function of the second kind and order n	16
k	propagation constant	2
k_g	propagation constant in glass	73
k_p	plasma wavenumber defined in Eq. (5.29) . .	77
k_p	propagation constant in cold plasma	132
L	characteristic dimension of the discharge .	10
$\mathfrak{L}$	Lagrangian density	18
$\mathfrak{L}_j$	j-th order component of $\mathfrak{L}$	19
$L_{n\ell}$	constant defined in Eq. (5.42)	80
ℓ	radial wavenumber	3
ℓ	azimuthal wavenumber	73
M_ℓ	amplitude factor of $H_{z\ell}(\underset{\sim}{r})$.	73
m_e	electronic mass	8
N	electron density	8
N_0	DC electron density	15
$N_{\lambda\ell}(r)$	r-varying part of the ℓ-th component of the electron density associated with Wave λ.	89

Symbol		Page where defined on first use
$T_{3\ell}(r)$	function defined in Eq. (5.68)	91
$U_{mn}(r)$	function defined in Eq. (5.68)	91
V	output of receiver	49
V_ℓ	constant defined in Eq. (5.42)	80
V'_ℓ	constant defined in Eq. (5.42)	80
$V_{r\lambda\ell}(r)$	r-varying part of the ℓ-th component of the radial velocity associated with Wave λ	89
$V_{\theta\lambda\ell}(r)$	r-varying part of the ℓ-th component of the azimuthal velocity associated with Wave λ	89
$\underset{\sim}{v}$	electron velocity	8
v_g	group velocity	2
v_p	phase velocity	2
v_z	z component of $\underset{\sim}{v}$	15
$\underset{\sim}{v}_\lambda(\underset{\sim}{r})$	velocity associated with Wave λ	88
$W_{3\ell}$	amplitude of the ℓ-th order term for the reflected wave at ω_3, in the glass	88
$X_{3\ell}$	amplitude of the ℓ-th order term for the outgoing wave at ω_3, in the glass	88
x_j	j-th component of position vector $\underset{\sim}{r}$	19
$Y_{3\ell}$	nonlinear scattering amplitude	88
$Z_{3\ell}(r)$	function used in Eq. (5.67)	91
z	axial coordinate	2

Symbol		Page where defined on first use
	(2) Greek Alphabet	
α	an arbitrary variable	19
α	geometric parameter in parabolic profile . .	75
$\alpha(z)$	phase of wave	49
$\alpha_{n\ell}$	ℓ-th zero of $J_n(\beta r)$	16
α_r	phase of reference signal	49
α_λ	attenuation constant of Wave λ	36
β	effective wavenumber	4
β_λ	effective wavenumber for Wave λ	23
Γ	gain in dB/unit length	29
Γ	collision factor	74
Γ_N	normalized gain factor	29
Γ_λ	collision factor for Wave λ	88
γ	compression constant for electrons	74
Δk	departure from synchronism	36
ϵ	permittivity	18
ϵ_{eff}	effective permittivity	81
ϵ_g	relative permittivity	2
$\underleftrightarrow{\epsilon}_p$	equivalent permittivity tensor of a cold plasma in an infinite magnetic field	123
ϵ_p	equivalent permittivity of a cold plasma without magnetic field	134
ϵ_0	permittivity of free space	15
$\epsilon_\parallel$	component of $\underleftrightarrow{\epsilon}_p$ parallel to B_0	123

Symbol		Page where defined on first use
$\epsilon_\perp$	component of $\overleftrightarrow{\epsilon}_p$ perpendicular to B_0	123
ζ_D	ratio a/λ_D	129
θ	angular coordinate	2
κ	Boltzmann constant	73
λ_D	electronic Debye length	10
μ_0	permeability of free space	80
ν	effective momentum transfer collision frequency	71
ξ	normalized radius	129
$\underset{\sim}{\xi}$	generalized displacement coordinate	18
ξ_λ	real displacement coordinate associated with Wave λ	20
$\underset{\sim}{\xi}_\lambda$	complex displacement coordinate associated with Wave λ	20
$\hat{\xi}_\lambda(r,z,t)$	slowly varying part of $\underset{\sim}{\xi}_\lambda$	20
ρ_s	surface charge density	135
σ_λ	constant associated with coupled mode equation for Wave λ	21
φ	scalar potential	2
$\varphi(z)$	axial potential profile	15
$\hat{\varphi}(r)$	radial potential profile	15
$\varphi_\ell(\underset{\sim}{r})$	ℓ-th order term in the expansion of φ into cylindrical waves	74

Symbol		Page where defined on first use
$\varphi_n(r)$	radial potential profile of mode with azimuthal wavenumber n	2
φ_r	potential of reference signal	49
$\varphi_0(r)$	radial DC potential profile	73
$\hat{\varphi}_\lambda(r,z,t)$	real potential associated with Wave λ . . .	20
$\underline{\varphi}_\lambda$	complex potential associated with Wave λ . .	20
χ	gain	27
ψ	function defined in Eq. (B.5)	127
ψ	potential amplitude factor inside column . .	15
$\hat{\psi}$	potential amplitude factor outside column .	16
$\psi_\lambda(z,t)$	slowly varying part of the potential for Wave λ	26
$\psi_{\lambda 0}$	initial amplitude of Wave λ	27
$\psi_\ell(r)$	r-varying part of $\varphi_\ell(\underline{r})$	74
$\psi_{\ell j}(r)$	linearly independent solutions of Eq. (5.17)	75
$\psi_{\lambda\ell}(r)$	r-varying part of the ℓ-th term in the expansion of the potential of Wave λ into cylindrical waves	89
$\psi_{3\ell j}(r)$	solutions of Eq. (5.64)	90
ω	angular frequency	2
ω_c	electron cyclotron frequency	3
ω_R	resonant plasma frequency	2
ω_0	electron plasma frequency	2
$\langle\omega_0^2\rangle$	average of ω_0^2	82

Symbol		Page where defined on first use
	(3) Subscripts	
i,j	components of a vector	19
λ	quantity corresponding to Wave λ	20
α,β,γ	quantity corresponding to Wave α, β, γ . . .	20
s,i or p	quantity of the signal, idler or pump wave	26
ℓ	component varying as exp $j\ell\theta$	73

ACKNOWLEDGMENTS

I want to express my gratitude to my research adviser, Professor Frederick W. Crawford, for suggesting and guiding this research, and for his help in editing this thesis; Dr. Kenneth J. Harker for his comments on this manuscript as well as the many discussions which helped further my understanding of plasma physics; and Professor Peter A. Sturrock for reading the manuscript.

I also want to thank the staff of Stanford Electronics Laboratories for their help throughout this work. Special thanks go to the Tube Laboratory staff for their expert technical assistance; to the staff of the Drafting Department; to Gary McDonough, for his help in administrative matters; to Jane Johnston, for her infinite patience in expertly typing the many revisions of this work; to Larry Wigton, for his help in programming the results of Chapters II and IV. My fellow students, too numerous to mention individually, also deserve my gratitude for their help and support by the many discussions that we had over the years that I spent at Stanford.

Finally, I thank my wife, Lyndie, for her patience and her support during the course of this work. She has provided me with understanding and encouragement during times of hard work and difficulties. I am happy to share with her the joy of completing this thesis.

Chapter I

INTRODUCTION

In the past few years, the nonlinear properties of plasmas have been the subject of a rapidly increasing number of studies. The success of the linear plasma theory in predicting the observed small-signal properties of plasma waves has encouraged its extension to the nonlinear coupling of waves among themselves or with resonant particles.[1] Extensive use has been made of the coupled-mode theories familiar in microwave electronics[2] and in nonlinear optics.[3] So far, there have been few experimental results on nonlinear properties of plasma waves compared to the large number of theoretical studies on the subject. This does not necessarily mean that nonlinear effects are difficult to produce experimentally in plasmas, but it is often difficult to drive some particular modes into the nonlinear regime without perturbing the plasma appreciably or exciting other modes than the ones desired. Another difficulty is caused by factors like loss and fluctuations which can modify profoundly the nonlinear behavior of the system, as we shall see in Chapter III.

In what follows, we shall present theoretical and experimental studies of some nonlinear properties of electron plasma waves on a plasma column. In the linear regime these modes have been studied in two different ways: as longitudinal electron plasma waves propagating along the axis of a plasma column, and as resonances of a plasma column irradiated by an electromagnetic wave. These resonances are actually the long-wavelength cutoffs of electron plasma waves propagating along the axis.[4] Since the two aspects of the problem have been studied more or less independently, we shall review them separately.

1.1 Electron Plasma Waves in Bounded Plasmas

1.1.1 Linear Regime

The linear properties of electron plasma waves in bounded systems have been studied for over thirty years. In 1939, Ramo[5] and Hahn[6] showed that a circular waveguide containing an electron beam could guide waves propagating with a phase velocity smaller than the velocity

of light at frequencies below the cutoff frequency of the empty waveguide. These modes were called "space charge" or "slow" waves. They were also found in stationary plasmas placed in an infinite or zero magnetic field.[7] Exploiting the fact that slow waves have a phase velocity, v_p, smaller than the velocity of light, Trivelpiece and Gould[8] found an approximate solution for slow waves propagating on a cold plasma column in an arbitrary magnetic field by assuming that the speed of light is infinite. This assumption, called the "quasistatic approximation", implies that the electric field of the waves is essentially static, and hence derivable from a scalar potential: $\underline{E} = -\nabla\varphi$. The quasistatic theory for slow waves on a plasma column in infinite and zero magnetic fields will be reviewed in detail in Chapter II and IV, respectively. In order to facilitate the review of the work done on slow waves, we will state here without proof some results of the theory for slow waves on a plasma column in the presence of an arbitrary static magnetic field B_0.

The slow wave solutions form an infinite set of cylindrical waves of the form $\varphi_n(r)\exp j(\omega t-kz-n\theta)$, where the space variables refer to a cylindrical coordinate system having its z axis along the axis of the plasma column, and where ω is the angular frequency of the waves, k is their propagation constant, and n, an integer between $-\infty$ and $+\infty$, is their azimuthal wavenumber. The exact form of $\varphi_n(r)$ depends on the axial magnetic field and on the radial inhomogeneity. In the absence of a magnetic field, $\varphi_n(r) = I_n(kr)$, where $I_n(kr)$ is the modified Bessel function of the first kind. In this case, the waves can propagate only if the plasma column is immediately surrounded by a dielectric region. The dispersion characteristics for slow waves propagating on a plasma column of radius a surrounded by an infinite dielectric are shown in Fig. 1.1 for $n = 0$, 1 and 2. The angular frequency, ω, is normalized to the resonant plasma frequency, $\omega_R\left[= \omega_0/(1+\epsilon_g)^{1/2}\right]$, where ϵ_g is the relative permittivity of the surrounding dielectric, and ω_0 is the electron plasma frequency. All the modes have a resonance $(k \to \infty)$, and the azimuthally varying modes have a cutoff $(k = 0)$, at $\omega = \omega_R$. These cutoffs yield the multipolar "resonances" which will be studied in Chapters V and VI.

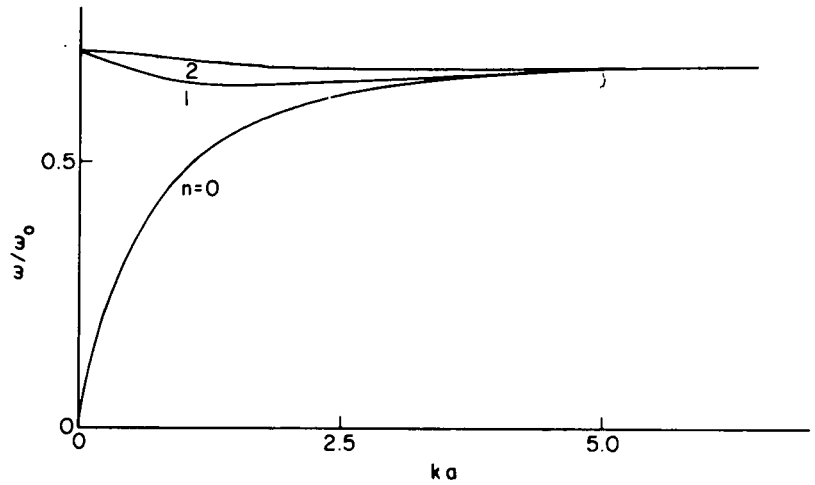

Fig. 1.1 Slow wave dispersion characteristics for $\omega_c = 0$: column of radius a surrounded by a vacuum.

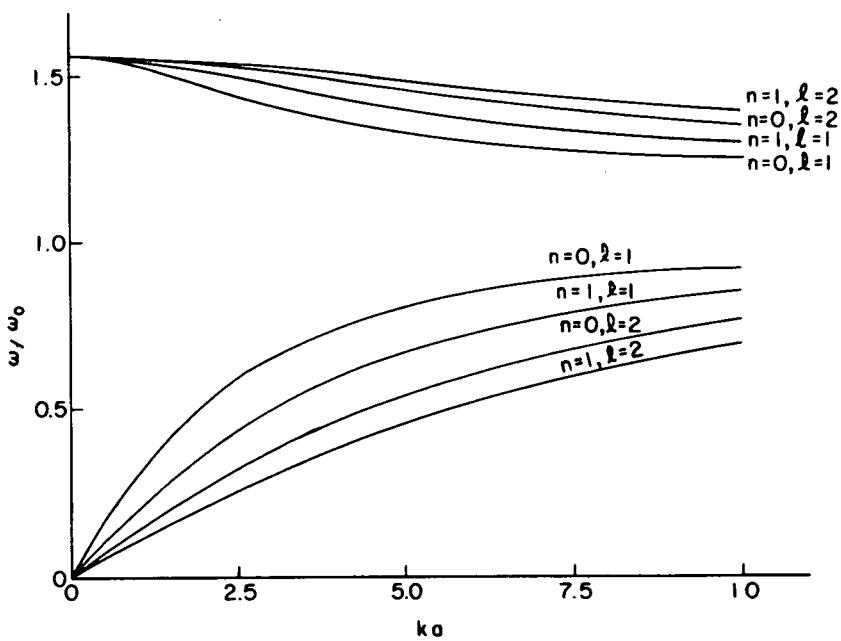

Fig. 1.2 Slow wave dispersion characteristics for $\omega_c = 1.2\ \omega_0$: column of radius a surrounded by metal.

As seen from Fig. 1.1, the phase velocity, v_p, and the group velocity, v_g, of the waves can be in the same or in opposite directions. In the former case, the wave is called "forward", and in the latter case "backward". When a magnetic field is present, $\varphi_n(r) = J_n(\beta r)$, where $J_n(\beta r)$ is the Bessel function of the first kind and β is an effective wavenumber proportional to k, and depending also on ω_0, ω, and on the cyclotron frequency ω_c. For each n, there can be an infinite number of radial modes labelled with the radial wavenumber $\ell \geq 1$, where ℓ is an integer. These modes differ from each other by the radial potential variations in the column. The dispersion characteristics for the (n,ℓ) combinations $(0,1)$, $(0,2)$, $(1,1)$ and $(1,2)$ are presented in Fig. 1.2 for slow waves propagating in a circular waveguide filled with a uniform plasma, and for a ratio $\omega_c/\omega_0 = 1.2$. Two passbands can exist in this case. When $\omega < \omega_0$, a forward wave can propagate and, for $\omega_c \leq \omega \leq (\omega_0^2 + \omega_c^2)^{1/2}$, a backward wave is predicted. In the simple geometry considered here, the frequencies ω_0 and ω_c can be interchanged without changing the dispersion characteristics.

After 1960, a large number of papers were published on theoretical slow wave characteristics. Some of these solved special cases of slow wave propagation without using the quasistatic approximation.[9,10] It was found that the full electromagnetic treatment did not improve very much the results of the quasistatic theory when $v_p \ll c$. This is not the case, however, for the $n \neq 0$ modes in the absence of a magnetic field,[10] and nonquasistatic, $n = 1$ slow waves were observed in the laboratory.[11] The $n = 1$ dispersion characteristics measurements obtained by Carlisle[12] did not extend to the nonquasistatic part of the dispersion characteristics, but they showed very well the backward character of the $n = 1$ mode in the absence of a magnetic field.

Three aspects of the experiments reported in the early sixties did not correspond to the theoretical predictions: the difficulty in obtaining measurements of waves in the upper passband in the presence of a magnetic field; the discrepancy between the attenuation predicted from electron-neutral collisions and the damping measured experimentally, and the absence of measurements of the higher order modes in the presence of a

magnetic field. These difficultes pointed to the inadequacies of the cold, uniform plasma model used up to that point. The first effect was shown to come from radial inhomogeneity.[13,14] When spatial nonuniformity is introduced in the cold plasma theory, the electric field becomes infinite at the point in space where the wave frequency is equal to the local plasma frequency.[15] The singularity is removed when finite electron temperature or finite collision frequencies are taken into account. It was shown[14] that collisional damping in the resonance region could account for the strong wave damping observed in measurements of the dispersion characteristics of the upper passband in the presence of a magnetic field.[8,16] The second effect can be explained by Landau damping in the sheath, when there is no magnetic field.[17] In the presence of a magnetic field, Landau damping in the body of the column was shown to account for the observed attenuation of the $n = 0$, $\ell = 1$ mode in the lower passband.[18] It should be noted that there is no enhanced collisional damping due to the radial density gradient in this case.[14] The fact that the higher order modes have never been observed, as far as the author knows, in experiments limited to the linear regime has not been resolved clearly. It has been said that the lowest order mode would be preferentially excited because the Landau damping of the slow waves in a magnetic field is inversely proportional to the phase velocity of the waves.[18] This question will be discussed further in Chapter III in relation to our experiments.

The importance of including electron temperature effects in slow wave theories was emphasized by some of the theories of Tonks-Dattner resonances which will be reviewed in Section 1.2. This work showed that some additional resonances observed experimentally, but not predicted by the cold plasma theory, could be accounted for by introducing electron thermal motions. These resonances are the cutoffs of slow propagating modes.[4] This set of waves has been investigated theoretically by means of pressure theory in order to find the slow waves associated with the Tonks-Dattner resonances of a warm uniform plasma column in the absence of a static magnetic field.[19] The corresponding problem in a nonuniform plasma has been solved in slab[20] and cylindrical geometries.[4,21] Some of these slow modes were observed experimentally.[4,21] Finally, various

slow wave problems have been solved using the Vlasov equation;[22] since we shall be concerned mainly with slow waves in a cold plasma, we shall not consider them further.

1.1.2 Nonlinear regime

The study of nonlinear effects in plasmas has been undertaken in many different ways. A very general and elegant approach has been to define a Lagrangian or Hamiltonian density for the system under study, and then to use the techniques of classical mechanics with suitable adaptations to derive the nonlinear properties of plasmas.[23-27] These methods can be used to treat the coupling of any number of waves. Various versions of the coupled mode analysis[2] have also been used to study the nonlinear coupling of waves in plasmas. We shall restrict ourselves to three-wave interactions. In order to obtain appreciable coupling between the waves, the following relations must be satisfied at least approximately

$$\omega_1 + \omega_2 = \omega_3 , \qquad k_1 + k_2 = k_3 , \tag{1.1}$$

where ω_i and k_i are the frequency and propagation constant of Wave i. When ω_3 is the largest frequency, k_3 is the largest wavenumber, and Wave 3 has a much larger amplitude than Waves 1 and 2, parametric amplification is obtained.[2] Wave 3 is called the pump and Waves 1 and 2 are called signal and idler. Both the signal and the idler can grow exponentially in a lossless system.

In 1960, Kino used a normal mode expansion to derive a theory for parametric amplification in plasmas and electron beams.[28] Although this theory described the coupling of slow waves on an electron beam or a plasma column in either an infinite or zero magnetic field in terms of the electric field, numerical results were not obtained. Paik[29] pointed out later that the nonlinear surface current had been neglected in Kino's theory, but his own analysis only accounted for axial surface currents in the small-ka limit. The theory presented in Chapter IV is derived from a Lagrangian formulation which includes all the current components. A slow wave parametric amplifier was built using the $n = 0$ mode on a

plasma column without a magnetic field.[28,30] As can be seen from Fig. 1.1, this mode is non-dispersive only for small frequencies. In practice, the synchronism conditions, given by Eq. (1.1), could be satisfied only approximately. This led to marginal growth rates.

Pérulli and his co-workers[31] obtained a plasma column in a strong magnetic field ($\omega_0 \ll \omega_c$) by letting the plasma produced in a Penning source diffuse through a small hole into a 64 cm long metal vacuum chamber of square cross-section. They took advantage of the numerous branches of the dispersion relation for slow waves on a column in a magnetic field, and observed the decay of a strong excited wave into pairs of waves which, together with the excited wave, satisfied the synchronism conditions approximately. The three interacting waves were on two or three branches of the dispersion characteristics. They also obtained parametric amplification by exciting a pump and a signal, and observing the growth of the signal and the idler. The growth rates measured experimentally differed by about 30% from those calculated from theory. Their theoretical model, however, was a metal waveguide completely filled with plasma,whereas the plasma column used in their experiment was a nonuniform column of about 0.8-1.0 cm in radius located in the center of their 14 cm square metal vacuum chamber. The same theoretical model was considered by Spithas and Manheimer, with the same result.

Some experiments on coupling of electromagnetic waves with slow waves and ion-acoustic waves were reported recently.[33] The electromagnetic waves were excited in a cavity surrounding part of the plasma column of a Q-machine, and the slow waves were excited and detected outside the cavity. Interactions of two electromagnetic waves and one slow wave; one electromagnetic and two slow waves, and two electromagnetic waves and one ion-acoustic wave, were observed.

1.2 Resonances of a Plasma Column

1.2.1 Linear Regime

In 1931, Tonks predicted that a uniform cylindrical plasma placed in a dipolar RF field should exhibit a resonance when the angular frequency of the RF signal is equal to $\omega_0/2^{1/2}$.[34] He observed this

dipole resonance, and also some extra resonances not explained by the theory. Herlofson also predicted the existence of the dipole resonance in an analysis of resonant scattering from meteor trails.[35] Dattner made an extensive study of the resonances in laboratory plasmas, and found that the number of extra resonances observed depended on the plasma column dimensions, the plasma parameters, and the incident frequency.[36] Since a comprehensive survey of the work done on the resonances of a plasma column up to 1968 has been published in a book by Vandenplas,[37] we need only present a brief review of the main developments in this field.

The extra resonances, now called "Tonks-Dattner resonances", were first thought to result from the radial inhomogeneity of the plasma columns used in experiments.[38,39] However, these theories, developed for a cold nonuniform plasma column, did not predict the Tonks-Dattner resonances and presented some serious theoretical problems when the RF signal has a frequency equal to the local plasma frequency at some point in the column; at this point the equivalent permittivity vanishes, leading to infinite electric fields.[15]

The inclusion of the electron temperature was the next improvement to the theoretical model. Instead of integrating the system of equations composed of the Vlasov equation, and of Maxwell's equations, Gould used the quasistatic approximation, $\underset{\sim}{E} = -\nabla\varphi$, and velocity moments of the Vlasov equation to calculate the resonant frequencies of a uniform plasma column.[40] He kept only the first two moments, i.e. the continuity equation,

$$\nabla\cdot(N\underset{\sim}{v}) + \frac{\partial N}{\partial t} = 0 \ , \qquad (1.1)$$

and the equation of motion,

$$m_e N \frac{d\underset{\sim}{v}}{dt} = - Ne\nabla\varphi - \nabla p \ , \qquad (1.2)$$

where e and m_e are the electronic charge and mass; N, $\underset{\sim}{v}$ and p are respectively the electron density, velocity and pressure. The electron pressure was assumed to obey an adiabatic law with respect to

small perturbations. A series of resonances at frequencies higher than ω_0 were obtained in addition to the dipole resonance at $\omega_0/2^{1/2}$. The Tonks-Dattner resonances were then interpreted as standing waves formed by electron pressure waves reflected back and forth across the plasma column.

Unfortunately, the spacing between the resonant frequencies predicted by this theory did not agree with the experimental results. It was suggested[41-43] that the nonuniformity of the plasma could explain the spacing of the observed resonances; electron waves could then be trapped between the wall and their cutoff point in the plasma,[43] and the phase shift of the wave would vary along its path according to the local wavenumber. A series of attempts to include the effect of the radial electron density profile (see Ref. 37, p. 131) finally led to a theory by Parker, Nickel and Gould[44] which agreed very well with the experimental results. The electron density profile used in this theory was computed from the Tonks-Langmuir theory of the positive column.[45]

While the theory developed by Parker and his co-workers was very successful in predicting the resonance frequencies of a plasma column, it also had some serious shortcomings. First, it did not include damping effects. Second, because the solution was obtained by means of the numerical integration of a differential equation, it did not provide too much insight into what was happening. Third, the limit of low temperatures could not be obtained because of numerical difficulties.

The absence of a damping mechanism caused the amplitude of the resonances to be infinite. Electron-neutral collisions were introduced in a study of the warm plasma capacitor,[37] but they could not account for the observed damping of the dipole resonance.[46] Radiation effects had been shown previously to account for the major part of the damping of the dipole resonance in the cold plasma limit.[47] A study using the first two moments of the Vlasov equation,and Maxwell's equations without the quasistatic approximation, has been completed recently for a plasma column with a parabolic electron density profile,[48] and shows that the radiation damping is indeed important in determining the amplitude of the dipole resonance. The Tonks-Dattner resonances are affected to a

much smaller degree by radiation effects. The effect of Landau damping on the resonances has been demonstrated by integration of the Vlasov equation along particle orbits.[49,50] The apparent limit in the series of resonances observed experimentally[36] was shown to be caused by the Landau damping of the wave as it penetrates into the region of almost uniform electron density close to the axis of the column.

Instead of relying only on numerical integration, as was done in Refs.49 and 50, Baldwin[51] found an approximate solution to the Tonks-Dattner resonance problem by obtaining solutions valid at different radii and coupling them at the point where $\omega = \omega_0(r)$. This analysis shows that electron plasma waves are excited at the resonance radius, and propagate towards the plasma wall. Close to the wall, the wave is Landau damped by resonant electrons which then stream towards the sheath, where they are reflected. On their way back to the center of the column, they re-excite a plasma wave which travels inwards. This theory provided mechanisms confirming the physical picture of Tonks-Dattner resonances as the result of electron plasma waves trapped between the wall and the resonance radius. The low-temperature limit of the theory was tested experimentally in an afterglow plasma, and satisfactory agreement was obtained, considering the assumptions made in the theory, and the experimental difficulties involved.[52]

Dorman obtained a low temperature expansion of the Vlasov equation in one dimension and compared it to the corresponding version of pressure theory.[53] He found a very good agreement between the resonance frequencies predicted by the two theories at low temperature. Finally, Miura and Barston developed a singular asymptotic analysis in the small parameter λ_D/L, where λ_D is the electronic Debye length, and L is a characteristic dimension of the discharge.[54] The analysis was applied to one-dimensional versions of the pressure theory, and of Dorman's theory, and good agreement was found between the singular expansion and the various theories. Because of the expansion parameter, the small temperature limit was accessible. This contrasts with pressure theory, where the limit $T \to 0$ cannot be obtained numerically due to the singularity at $T = 0$ in the equations.

1.2.2 Nonlinear Regime

Nonlinear effects induced by an increase in the power of the incident wave have been examined in various power limits. At power levels below approximately 0.1W, harmonic generation and wave mixing have been observed by Stern.[55] One interesting feature of these experiments, performed with a plasma column in a waveguide, was the absence of measurable second harmonic signal at frequencies other than the linear resonance frequencies. In the case of wave mixing, both incident waves had to excite a resonance at the same discharge current in order for the mixed signal to be measurable. A cold plasma analysis was used by Messiaen and Vandenplas[56] to obtain the nonlinear scattered power from a uniform plasma cylinder irradiated by two incident plane waves. This theory included the effect of a glass tube around the plasma and the interaction of the different terms in the expansion of each incident wave into an infinite set of cylindrical waves. The calculations of nonlinear scattering amplitudes presented, however, included only the effect of the dipole term. Some experimental results of forward scattering at the second harmonic of a strong incident wave were presented, and agreement with theory within an order of magnitude was claimed.

Some observations of possible nonlinear scattering from meteor trails[57] suggested the inclusion of the nonlinear resonances of a plasma column in a program of space-related plasma studies in progress at Stanford. A nonlinear theory using the quasistatic approximation showed[58] that a uniform plasma column excited by a strong dipolar signal should produce a second harmonic signal having a quadrupolar radiation pattern with the maximum power radiated at $\pi/4$, $3\pi/4$, $5\pi/4$ and $7\pi/4$ with respect to the direction of the incident wave. This fact was recognized and observed by Yen and McDermott,[59] but the second harmonic signals produced in their experiments did not occur at the linear resonance frequencies, as they did in Stern's experiment.[55] No explanation was given for this discrepancy. It should be noted that both Stern[55] and Vandenplas[56] observed forward scattering in their experiments. Some preliminary nonlinear scattering experiments at Stanford yielded a dipolar instead of a quadrupolar radiation pattern.[60] When the transverse component of

the Earth's magnetic field was cancelled, however, the radiation pattern became predominantly quadrupolar, as far as could be determined from the measurement over 90° reported in Ref. 60.

The quasistatic, uniform cold plasma model used at first[58] was extended in two ways. First, the effect of radial inhomogeneity was included in the quasistatic limit.[61] Since a cold plasma was considered, it was necessary to restrict the computations to frequencies higher than the plasma frequency at the center of the column, in order to avoid the singular behavior of the potential at the point where the incident frequency is equal to the plasma frequency. A warm plasma analysis removes this singularity and will be developed in Chapter V. Second, the full set of Maxwell's equations was solved[62] for scattering from a cold uniform plasma column irradiated by a plane wave in order to include radiation effects more properly in the theory. Contrary to what was thought previously,[56] it was shown that it was necessary to include all the terms up to the quadrupole term in the cylindrical wave expansion of the incident plane wave in order to obtain all the lowest order terms for the second harmonic radiation, even in the long-wavelength limit ($ka \ll 1$).

1.3 Outline of this Work

This thesis consists of two parts. The first problem to be studied is the nonlinear coupling of slow waves on a plasma column. Chapter II is devoted to the case of a plasma column in an infinite magnetic field. After a brief review of linear theory, the coupled mode equations for three-wave coupling are derived using the Lagrangian description of a cold plasma. These equations are then solved for the special cases of parametric amplification and mode conversion. The effects of wave damping and of a departure from synchronism due to the dispersion of the interacting waves are considered. Chapter III presents experimental results of mode conversion in the presence of loss. In Chapter IV, nonlinear coupling of slow waves in the absence of a magnetic field is examined and the coupled mode equations are derived using the Lagrangian density of a cold plasma.

In the second part of the thesis, nonlinear scattering from a plasma column is considered. In Chapter V, a warm plasma model is used to obtain the nonlinear scattering from a nonuniform plasma column illuminated by a large amplitude plane wave. Numerical results for the nonlinear scattering amplitude are presented for selected values of electron temperature and frequency. Chapter VI is devoted to some experimental results of nonlinear scattering. The effects of the Earth's magnetic field, and of the rotational asymmetry of the column on the radiation pattern at the second harmonic of the incident wave, are examined.

Chapter II

SLOW WAVES ON A PLASMA COLUMN: INFINITE MAGNETIC FIELD

This chapter is devoted to the study of nonlinear coupling of slow waves on a cold plasma column in the presence of an infinite static magnetic field. The ions are assumed to have infinite mass. The static magnetic field is aligned parallel to the axis of the plasma column. Two geometries are considered: a column of radius a surrounded either by metal or dielectric. The second geometry is more appropriate to the experiments which will be considered in Chapter III, but the first one results in simpler calculations, and has been used in previous work.[31,32]

The linear solution for slow waves on a plasma column is obtained in Section 2.1 using the quasistatic approximation, $\underset{\sim}{E} = -\nabla\varphi$. This linear solution is then used in the driving terms of the nonlinear coupled mode equations for three-wave interaction which are derived in Section 2.2.1. The Lagrangian formalism[23-25,27] is a very elegant method of obtaining the coupled mode equations. We use such a formulation developed by Galloway and Crawford.[25] The coupled mode equations are solved for parametric amplification in Section 2.2.3, and the bandwidth of the interaction is studied in Section 2.2.4. Mode conversion is considered in Section 2.2.5. In both cases, the effects of loss and departure from synchronism are included.

2.1 Linear Regime

A cold electron plasma is described by the following equations: the equation of motion,

$$m_e \frac{d\underset{\sim}{v}}{dt} = e\left(\underset{\sim}{E} + \underset{\sim}{v}\times\underset{\sim}{B}\right), \tag{2.1}$$

the continuity equation,

$$\frac{\partial N}{\partial t} + \nabla\cdot(N\underset{\sim}{v}) = 0 , \tag{2.2}$$

and Maxwell's equations,

$$\nabla \times \underset{\sim}{H} = \underset{\sim}{J} + \epsilon_0 \frac{\partial \underset{\sim}{E}}{\partial t} , \quad \nabla \cdot \underset{\sim}{E} = \frac{Ne}{\epsilon_0} , \quad \nabla \cdot \underset{\sim}{B} = 0 , \quad \nabla \times \underset{\sim}{E} = - \frac{\partial \underset{\sim}{B}}{\partial t} \tag{2.3}$$

The quasistatic approximation, $\underset{\sim}{E} = - \nabla \varphi$, can be used in Eqs. (2.1)-(2.3) which, to first order in perturbations, reduce to

$$m_e \frac{\partial v_z}{\partial t} = - e \frac{\partial \varphi}{\partial z} , \tag{2.4}$$

$$\frac{\partial n}{\partial t} + N_0 \frac{\partial v_z}{\partial z} = 0 , \qquad \nabla^2 \varphi = - \frac{ne}{\epsilon_0} , \tag{2.5}$$

$$(\nabla \times \underset{\sim}{H})_z = N_0 e v_z - \epsilon_0 \frac{\partial}{\partial t} (\nabla \varphi)_z , \tag{2.6}$$

where N_0 and n are, respectively, the DC and RF perturbation electron densities, and v_z is the only nonzero component of the velocity in the presence of an infinite magnetic field in the z-direction. It can be seen from Eq. (2.6) that $\underset{\sim}{H} \neq 0$ in the quasistatic approximation, in which the velocity of light is considered to be infinite.

An infinitely long plasma column of radius a , with its axis in the direction of the static magnetic field, can sustain cylindrical waves having a potential of the form

$$\varphi(\underset{\sim}{r},t) = \hat{\varphi}(r) \exp j(\omega t - kz - n\theta) , \tag{2.7}$$

where k is the propagation constant of the wave; n is its azimuthal wavenumber, and $\hat{\varphi}(r)$ is its radial potential profile. The coordinates r , θ and z refer to a cylindrical coordinate system with its z-axis along the axis of the plasma column. Equations (2.4)-(2.7) can be combined and the resulting equation for $\hat{\varphi}(r)$ is

$$\frac{1}{r} \frac{\partial}{\partial r} \left(r \frac{\partial \hat{\varphi}}{\partial r} \right) + \left(\beta^2 - \frac{n^2}{r^2} \right) \hat{\varphi} = 0 , \quad \beta^2 = k^2 \left(\frac{\omega_0^2}{\omega^2} - 1 \right) , \quad 0 \leq r \leq a. \tag{2.8}$$

The solution of this equation is

$$\hat{\varphi}(r) = \psi \, J_n(\beta r) , \qquad 0 \leq r \leq a, \tag{2.9}$$

where $J_n(\beta r)$ is the Bessel function of order n .

Plasma column surrounded by metal: In this case, the boundary condition is $\hat{\varphi}(a) = 0$, which yields the following dispersion relation for the waves,

$$\beta^2 a^2 = k^2 a^2 \left(\frac{\omega_0^2}{\omega^2} - 1 \right) = \alpha_{n\ell}^2 , \qquad (2.10)$$

where $\alpha_{n\ell}$ is the ℓ^{th} nonzero root of $J_n(\beta r) = 0$. For each azimuthal wavenumber n , there exists an infinite number of branches of the dispersion relation (2.10) labelled by their radial wavenumber ℓ . The dispersion characteristics for the branches with (n,ℓ) given by (0,1), (0,2), (1,1) and (1,2) are shown in Fig. 2.1. All the branches of the dispersion relation (2.10) have a resonance $(k \to \infty)$ when $\omega \to \omega_0$.

Plasma column surrounded by an infinite dielectric: In this case, the potential can extend outside the plasma, and Laplace's equation must hold for $r \geq a$

$$\frac{1}{r} \frac{\partial}{\partial r} \left(r \frac{\partial \hat{\varphi}}{\partial r} \right) - \left(k^2 + \frac{n^2}{r^2} \right) \hat{\varphi} = 0 , \qquad a \leq r. \qquad (2.11)$$

The solution of this equation is

$$\hat{\varphi}(r) = \hat{\psi} \; K_n(kr) , \qquad a \leq r , \qquad (2.12)$$

where $K_n(kr)$ is the modified Bessel function of order n .

The dispersion relation is obtained by requiring continuity of the potential, and of the radial electric displacement, at $r = a$:

$$\beta \frac{J_n'(\beta a)}{J_n(\beta a)} - \epsilon_g k \frac{K_n'(ka)}{K_n(ka)} = 0 . \qquad (2.13)$$

The constant $\hat{\psi}$ in Eq. (2.12) can be expressed as a function of ψ , the amplitude factor of the potential inside the plasma,

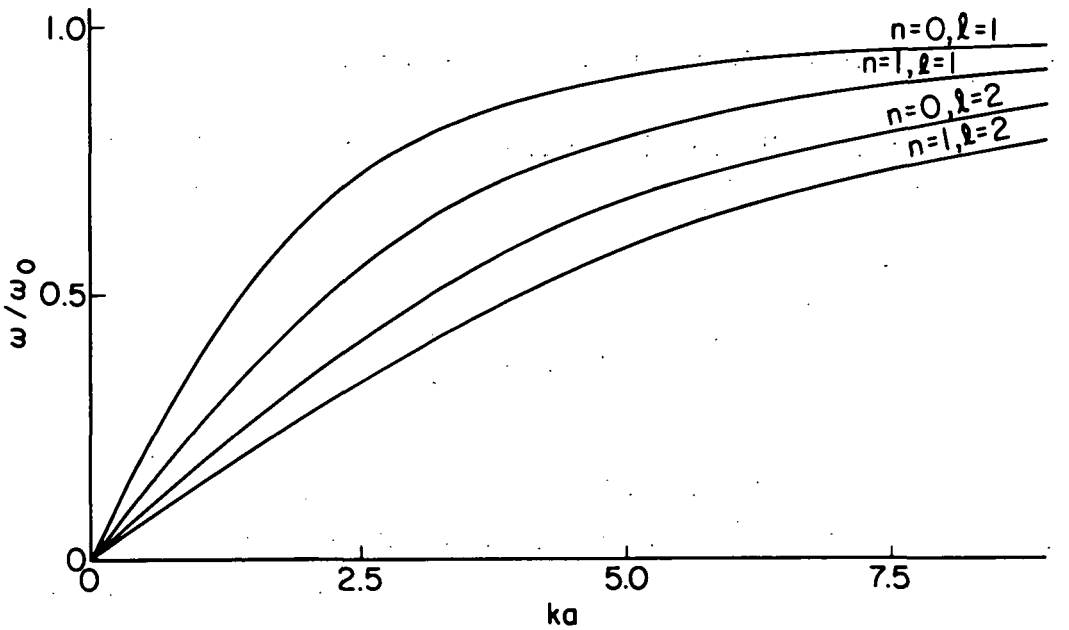

(a)

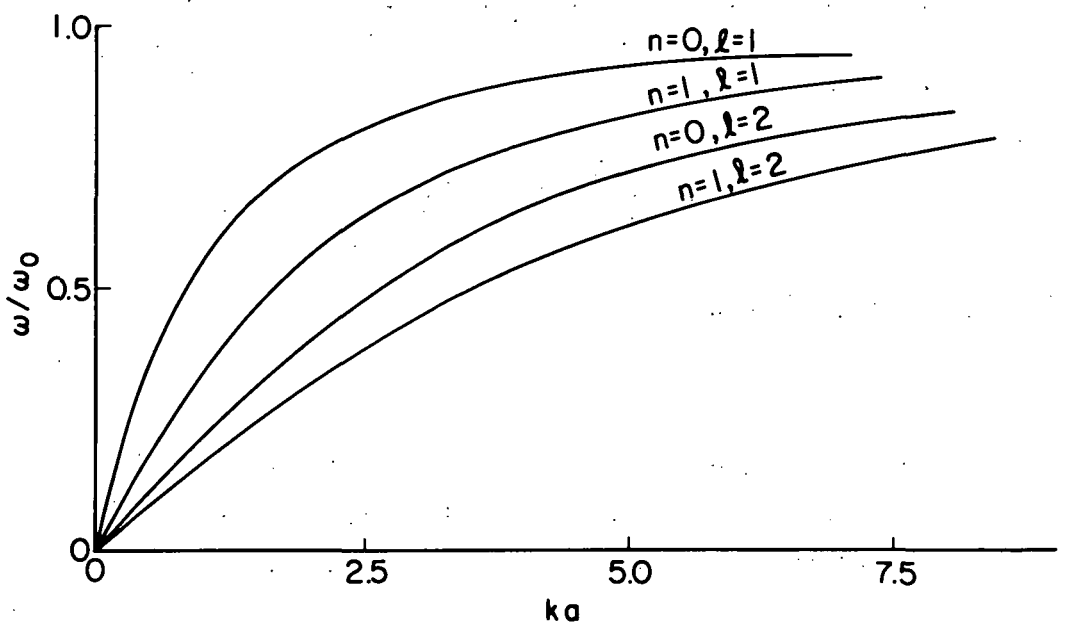

(b)

Fig. 2.1 Slow wave dispersion characteristics for $\omega_c \to \infty$: (a) column surrounded by metal; (b) column surrounded by vacuum.

$$\hat{\psi} = \psi \frac{J_n(\beta a)}{K_n(ka)} . \qquad (2.14)$$

The dispersion relation of Eq. (2.13) has an infinite number of branches for each n, all of which have a resonance at $\omega = \omega_0$, as in the case of a plasma-filled metal tube. The dispersion characteristics for four of the lower-order branches of Eq. (2.13) are shown in Fig. 2.1 for $\epsilon_g = 1$. In this case, the radial wavenumber ℓ is attached to the ℓ^{th} root of Eq. (2.13) for a given n.

2.2 Nonlinear Regime

2.2.1 Derivation of the Coupled Mode Equations

The coupled mode equations for nonlinear coupling of three slow waves can be derived directly by expanding Eqs. (2.1)-(2.3) up to second order in the perturbations.[30,31] An alternate method of obtaining the coupled mode equations uses an adaptation of the Lagrangian formulation of classical mechanics to wave propagation in a continuous medium. It has been shown that, for a system which can be described by a Lagrangian density $\mathcal{L}$, the coupled mode equations can be obtained from an expansion of $\mathcal{L}$ in powers of small perturbations of the generalized coordinates around their equilibrium positions.[25] This can usually be accomplished with simpler algebra than in the direct method. We will apply the formulation of the Lagrangian method developed in Ref. 25 to the slow wave problem.

In the quasistatic approximation, the Lagrangian density for a cold electron plasma in an infinite magnetic field is[25]

$$\mathcal{L}(\underline{\xi},\varphi,\underline{r},t) = N_0(r)\left[\frac{1}{2} m_e \dot{\underline{\xi}}^2 + e\varphi(\underline{r}+\underline{\xi})\right] + \frac{\epsilon}{2}[\nabla\varphi]^2 , \qquad (2.15)$$

where the displacement, $\underline{\xi}$, and the potential, φ, are the generalized coordinates of the problem, $\dot{\underline{\xi}}$ is the total time derivative of $\underline{\xi}$, $N_0(\underline{r})$ is the unperturbed electron density, and $\epsilon = \epsilon_0$ for the plasma and $\epsilon_g\epsilon_0$ for the surrounding dielectric regions. In the case of a bounded plasma, $\mathcal{L}$ reduces to the Lagrangian density for an electrostatic field in the regions where $N_0(\underline{r})$ vanishes. From $\mathcal{L}$, we can define a

Hamiltonian density, which can be written exclusively as a function of the generalized coordinates and their time derivatives,[25]

$$\mathcal{H}(\underset{\sim}{\xi},\varphi,\underset{\sim}{r},t) = \sum_i \frac{\partial \mathcal{L}}{\partial \dot{\xi}_i} \dot{\xi}_i + \frac{\partial \mathcal{L}}{\partial \dot{\varphi}} \dot{\varphi} - \mathcal{L} \quad . \tag{2.16}$$

The evolution of $\mathcal{H}$ is given by the following generalized energy conservation equation[25]

$$\frac{d\mathcal{H}}{dt} + \sum_j \frac{d\mathcal{F}_j}{dx_j} = - \frac{\partial \mathcal{L}}{\partial t} \quad , \tag{2.17}$$

where $\underset{\sim}{\mathcal{F}}$ is the generalized energy-flux vector. Its j^{th} spatial component is

$$\mathcal{F}_j = \sum_i \frac{\partial \mathcal{L}}{\partial\left(\frac{\partial \xi_i}{\partial x_j}\right)} \dot{\xi}_i + \frac{\partial \mathcal{L}}{\partial\left(\frac{\partial \varphi}{\partial x_j}\right)} \dot{\varphi} \quad . \tag{2.18}$$

In these equations, d/dt is the total time derivative; $\partial/\partial t$ is the partial time derivative; $\partial/\partial\alpha$ is the partial derivative with respect to quantity α, and $\partial/\partial x_j$ is the partial derivative with respect to component x_j of the space vector $\underset{\sim}{x}$. If $\mathcal{L}$ does not depend on time explicitly, the Hamiltonian density is also the energy density.

In order to apply the equations of Lagrangian mechanics to wave coupling, $\mathcal{L}$ is expanded around the equilibrium positions of the generalized coordinates $\underset{\sim}{\xi}$ and φ, and the terms are collected according to the order of the products of $\underset{\sim}{\xi}$, φ and their derivatives. This yields an expansion of the form

$$\mathcal{L} = \mathcal{L}_0 + \mathcal{L}_1 + \mathcal{L}_2 + \mathcal{L}_3 + \ldots \quad . \tag{2.19}$$

It has been shown that the terms $\mathcal{L}_0$ and $\mathcal{L}_1$ do not contribute to the wave motion because they only contain the equilibrium solutions,[25] while $\mathcal{L}_2$ and $\mathcal{L}_n$ generate the linear wave properties and the n-wave coupling, respectively. The three wave coupling that we shall study requires the

terms $\mathcal{L}_2$ and $\mathcal{L}_3$ in the expansion of $\mathcal{L}$. For a cold electron plasma in an infinite magnetic field, they are

$$\mathcal{L}_2 = N_0(r)\left[\frac{m_e}{2}\dot{\xi}^2 + e\,\xi\,\frac{\partial\varphi}{\partial z}\right] + \frac{\epsilon}{2}\left[\left(\frac{\partial\varphi}{\partial r}\right)^2 + \left(\frac{1}{r}\frac{\partial\varphi}{\partial\theta}\right)^2 + \left(\frac{\partial\varphi}{\partial z}\right)^2\right], \quad (2.20)$$

$$\mathcal{L}_3 = \frac{1}{2}N_0(r)\,e\,\xi^2\frac{\partial^2\varphi}{\partial z^2}, \quad (2.21)$$

where ξ is the displacement in the z direction.

The three interacting waves are characterized by their frequencies ω_α, ω_β and ω_γ, their propagation constants k_α, k_β and k_γ, and by their generalized coordinates, which are written as

$$\xi_\lambda = \frac{\underline{\xi}_\lambda + \underline{\xi}^*_\lambda}{2}, \quad \varphi_\lambda = \frac{\underline{\varphi}_\lambda + \underline{\varphi}^*_\lambda}{2}, \quad \lambda = \alpha, \beta, \gamma, \quad (2.22)$$

where

$$\underline{\varphi}_\lambda = \hat{\varphi}_\lambda(r,z,t)\exp j(\omega t - kz - n\theta), \quad (2.23)$$

$$\underline{\xi}_\lambda = \hat{\xi}_\lambda(r,z,t)\exp j(\omega t - kz - n\theta). \quad (2.24)$$

The only difference between Eq. (2.23) and Eq. (2.7) is the introduction of a space and time dependence in the amplitude factor of the potential. In order that the theory developed in Ref. 25 be valid, the amplitude variation in time and space must be small over a period and a wavelength of the wave. Equations (2.22)-(2.24) can be substituted in Eq. (2.20) and (2.21), and $\mathcal{L}_2$ and $\mathcal{L}_3$ can be averaged over a period and a wavelength of the wave. If the following synchronism conditions are satisfied at least approximately,

$$\omega_\alpha = \omega_\beta + \omega_\gamma, \quad k_\alpha = k_\beta + k_\gamma, \quad n_\alpha = n_\beta + n_\gamma, \quad (2.25)$$

$\mathcal{L}_3$ will be nonzero. In this case, it can be shown that the second-order generalized energy density for Wave λ is given by[25]

$$\mathcal{E}_{\lambda 2} = \overline{\mathcal{H}_2(\xi_\lambda, \varphi_\lambda, \underline{r}, t)} \quad , \tag{2.26}$$

and the third-order generalized energy density, called the coupling energy density, is[25]

$$\mathcal{E}_{c3} = \overline{\mathcal{L}_3\left(\sum_\lambda \xi_\lambda, \sum_\lambda \varphi_\lambda, \underline{r}, t\right)} \quad , \tag{2.27}$$

where the bar over $\mathcal{H}_2$ and $\mathcal{L}_3$ indicates that the average defined earlier has been performed. When Wave λ has a noninfinite group velocity, $v_{g\lambda}$, the energy conservation equation [Eq. (2.17)] becomes

$$\frac{\sigma_\lambda}{\omega_\lambda}\left(\frac{\partial}{\partial t} + \underline{v}_{g\lambda} \cdot \nabla\right) \mathcal{E}_{\lambda 2} = \mathcal{E}_{c3} \quad , \qquad \lambda = \alpha, \beta, \gamma, \tag{2.28}$$

where $-\sigma_\alpha = \sigma_\beta = \sigma_\gamma = 1$. Since the energy in slow waves on a plasma column propagates only in the z direction, the generalized energy densities $\mathcal{E}_{\lambda 2}$ and $\mathcal{E}_{c3}$ can be integrated over a plane perpendicular to the direction of the wave. Equation (2.28) then becomes

$$\frac{\sigma_\lambda}{\omega_\lambda}\left(\frac{\partial}{\partial t} + v_{g\lambda}\frac{\partial}{\partial z}\right) e_\lambda = e_c \quad , \qquad \lambda = \alpha, \beta, \gamma \quad , \tag{2.29}$$

where

$$e_\lambda = \iint \mathcal{E}_{\lambda 2}\, d^2r \quad , \qquad e_c = \iint \mathcal{E}_{c3}\, d^2r \quad . \tag{2.30}$$

The energy density for Wave λ can be calculated from the Lagrangian density using Eqs. (2.23) and (2.24) for the generalized coordinates. The result is

$$\epsilon_\lambda = \frac{1}{4}\iint\left\{N_0(r)\left[m_e\dot{\underline{\xi}}_\lambda\,\dot{\underline{\xi}}_\lambda^* - e\left(\underline{\xi}_\lambda\frac{\partial\underline{\varphi}_\lambda^*}{\partial z} + \underline{\xi}_\lambda^*\frac{\partial\underline{\varphi}_\lambda}{\partial z}\right)\right]\right.$$

$$\left. - \epsilon\left[\left(\frac{\partial\underline{\varphi}_\lambda}{\partial r}\right)\left(\frac{\partial\underline{\varphi}_\lambda^*}{\partial r}\right) + \frac{1}{r^2}\left(\frac{\partial\underline{\varphi}_\lambda}{\partial\theta}\right)\left(\frac{\partial\underline{\varphi}_\lambda^*}{\partial\theta}\right) + \left(\frac{\partial\underline{\varphi}_\lambda}{\partial z}\right)\left(\frac{\partial\underline{\varphi}_\lambda^*}{\partial z}\right)\right]\right\} d^2r \ . \tag{2.31}$$

The coupling energy density is given by

$$e_c = \frac{je}{8}\iint N_0(r)\left[\underline{\xi}_\alpha^*\,\underline{\xi}_\beta\frac{\partial^2\underline{\varphi}_\gamma}{\partial z^2} + \underline{\xi}_\alpha^*\,\underline{\xi}_\gamma\frac{\partial^2\underline{\varphi}_\beta}{\partial z^2} + \underline{\xi}_\beta\,\underline{\xi}_\gamma\frac{\partial^2\underline{\varphi}_\alpha^*}{\partial z^2}\right] d^2r + (\text{c.c.}) \ , \tag{2.32}$$

where (c.c.) denotes the complex conjugate of the first term in Eq. (2.32). The quantities introduced in Eqs. (2.23) and (2.24) can be substituted in Eqs. (2.31) and (2.32), which become, after the angular integration is performed,

$$e_\lambda = \frac{\pi}{2}\int_0^\infty\left\{N_0(r)\left[m_e\omega_\lambda^2\,\hat{\xi}_\lambda\hat{\xi}_\lambda^* - j\,k_\lambda e\,(\hat{\xi}_\lambda\hat{\varphi}_\lambda^* - \hat{\xi}_\lambda^*\,\hat{\varphi}_\lambda)\right]\right.$$

$$\left. - \epsilon\left[\left(\frac{\partial\hat{\varphi}_\lambda}{\partial r}\right)\left(\frac{\partial\hat{\varphi}_\lambda^*}{\partial r}\right) + \left(\frac{n_\ell^2}{r^2} + k_\lambda^2\right)\hat{\varphi}_\lambda\hat{\varphi}_\lambda^*\right]\right\} r\,dr \ , \tag{2.33}$$

$$e_c = -\frac{je\pi}{4}\int_0^\infty N_0(r)\left[k_\gamma^2\,\hat{\xi}_\alpha^*\,\hat{\xi}_\beta\hat{\varphi}_\lambda + k_\beta^2\,\hat{\xi}_\alpha^*\,\hat{\xi}_\gamma\hat{\varphi}_\beta + k_\alpha^2\,\hat{\xi}_\beta\hat{\xi}_\gamma\hat{\varphi}_\alpha^*\right] r\,dr + (\text{c.c.}) \ . \tag{2.34}$$

The linear solutions must now be substituted in Eqs. (2.33) and (2.34), with $\hat{\xi}_\lambda$ obtained by integrating Eq. (2.4) twice with respect to time. The energy densities become

$$e_\lambda = \frac{\pi}{2}\int_0^\infty \left\{ 3\epsilon_0\, \omega_0^2(r)\, \frac{k_\lambda^2}{\omega_\lambda^2}\, \hat{\varphi}_\lambda \hat{\varphi}^*_\lambda - \epsilon \left[\left(\frac{\partial \hat{\varphi}_\lambda}{\partial r}\right)\left(\frac{\partial \hat{\varphi}^*_\lambda}{\partial r}\right) + \left(\frac{n_\lambda^2}{r^2} + k_\lambda^2\right) \right] \hat{\varphi}_\lambda \hat{\varphi}^*_\lambda \right\} r\, dr \ , \tag{2.35}$$

$$e_c = \frac{j\pi}{4}\, \epsilon_0\, C_{\alpha\beta\gamma} \int_0^\infty \omega_0^2(r) \hat{\varphi}^*_\alpha\, \hat{\varphi}_\beta \hat{\varphi}_\gamma\, r\, dr + (c.c.) \ , \tag{2.36}$$

where

$$C_{\alpha\beta\gamma} = k_\alpha k_\beta k_\gamma \left[\frac{k_\alpha}{\omega_\beta^2 \omega_\gamma^2} - \frac{k_\beta}{\omega_\alpha^2 \omega_\gamma^2} - \frac{k_\gamma}{\omega_\alpha^2 \omega_\beta^2} \right] \ . \tag{2.37}$$

Plasma column surrounded by metal: The radial potential profile for Wave λ is given by Eq. (2.9). The wave energy density becomes

$$e_\lambda = \pi\epsilon_0 \left\{ \frac{\omega_0^2 k_\lambda^2}{\omega_\lambda^2} \int_0^a J_{n\lambda}^2(\beta_\lambda r) r\, dr \right.$$

$$\left. - \frac{1}{2} \int_0^a \left[\left(\frac{\partial J_{n\lambda}}{\partial r}\right)^2 + \left(\frac{n_\lambda^2}{r^2} - \beta_\lambda^2\right) J_{n\lambda}^2 \right] r\, dr \right\} \psi_\lambda \psi^*_\lambda \ . \tag{2.38}$$

Integrating by parts gives

$$\int_0^a \left(\frac{\partial J_{n\lambda}}{\partial r}\right)^2 r\, dr = r J_{n\lambda}(\beta_\lambda r)\, \frac{\partial J_{m\lambda}}{\partial r} \Bigg|_0^a - \int_0^a J_{n\lambda}(\beta_\lambda r)\, \frac{\partial}{\partial r}\left(r\, \frac{\partial J_{n\lambda}}{\partial r} \right) dr \ . \tag{2.39}$$

The first term on the RHS vanishes at both limits, and the second term combines with the last term of Eq. (2.38) to give Bessel's equation. We are left with

$$e_\lambda = \pi\epsilon_0 \omega_0^2\, \frac{k_\lambda^2}{\omega_\lambda^2}\, A_\lambda \psi_\lambda \psi^*_\lambda \ , \tag{2.40}$$

where

$$A_\lambda = \int_0^a J_{n\lambda}^2(\beta_\lambda r)\ r\ dr = \frac{a^2 J_n'^2(\beta_\lambda)}{2} . \qquad (2.41)$$

The coupling energy is

$$e_c = \frac{j\epsilon_0\omega_0^2\pi}{4}\frac{e}{m_e} I_{\alpha\beta\gamma}\left[\psi_\alpha^*\psi_\beta\psi_\gamma - \psi_\alpha\psi_\beta^*\psi_\gamma^*\right], \qquad (2.42)$$

where

$$I_{\alpha\beta\gamma} = C_{\alpha\beta\gamma}\int_0^a J_{n\alpha}(\beta_\alpha r)\ J_{n\beta}(\beta_\beta r)\ J_{n\gamma}(\beta_\gamma r)\ \ r\ dr . \qquad (2.43)$$

Plasma column surrounded by dielectric: The linear solutions are

$$\hat{\varphi}_\lambda(r) = \begin{cases} \psi_\lambda\ J_{n\lambda}(\beta_\lambda r) , & r \le a , \\ \psi_\lambda\ \dfrac{J_{n\lambda}(\beta_\lambda a)}{K_{n\lambda}(k_\lambda a)}\ K_{n\lambda}(k_\lambda r) , & r \ge a , \end{cases} \qquad (2.44)$$

$$\hat{\xi}_\lambda(r) = \begin{cases} j\dfrac{e}{m_e}\dfrac{k_\lambda}{\omega_\lambda^2}\hat{\varphi}_\lambda(r) , & r \le a , \\ 0 , & r \ge a . \end{cases} \qquad (2.45)$$

The energy densities will now be calculated. The integrals have to be separated into two parts: from 0 to a , and from a to ∞ . The wave energy density is

$$e_\lambda = \pi\epsilon_0 \left\{ k_\lambda^2 \frac{\omega_0^2}{\omega_\lambda^2} \int_0^a J_{n\lambda}^2(\beta_\lambda r) - \frac{1}{2}\int_0^a \left[\left(\frac{\partial J_{n\lambda}}{\partial r}\right)^2 + \left(\frac{n_\lambda^2}{r^2} - \beta_\lambda^2\right) J_{n\lambda}^2(\beta_\lambda r) \right] r\, dr \right.$$

$$\left. - \frac{\epsilon_g}{2} \frac{J_{n\lambda}^2(\beta a)}{K_{n\lambda}^2(k_\lambda a)} \int_a^\infty \left[\left(\frac{\partial K_{n\lambda}}{\partial r}\right)^2 + \left(\frac{n_\lambda^2}{r^2} + k_\lambda^2\right) K_{n\lambda}^2(k_\lambda r) \right] r\, dr \right\} \psi_\lambda \psi_\lambda^* \ . \qquad (2.46)$$

An integration by parts of the terms $(\partial J_{n\lambda}/\partial r)^2$ and $(\partial K_{n\lambda}/\partial r)^2$ gives a Bessel equation and a modified Bessel equation, in the integral, but the integrated terms are non-zero in this case. We have

$$e_\lambda = \pi\epsilon_0 \left[k_\lambda^2 \frac{\omega_0^2}{\omega_\lambda^2} \int_0^a J_{n\lambda}^2(\beta_\lambda r)\, r\, dr - \frac{a}{2} J_{n\lambda}(\beta_\lambda a) \left.\frac{\partial J_{n\lambda}}{\partial r}\right|_{r=a} \right.$$

$$\left. + \epsilon_g \frac{a}{2} \frac{J_{n\lambda}^2(\beta_\lambda a)}{K_{n\lambda}(k_\lambda a)} \left.\frac{\partial K_{n\lambda}}{\partial r}\right|_{r=a} \right] \psi_\lambda \psi_\lambda^* \ . \qquad (2.47)$$

The last two terms of Eq. (2.47) form the linear dispersion relation of the problem. The wave energy reduces to Eq. (2.40) with

$$A_\lambda = \int_0^a J_{n\ell}^2(\beta_\lambda r) r\, dr = \frac{1}{2\beta_\lambda^2} \left[k_\lambda^2 a^2 \frac{K_n'(k_\lambda a)}{K_n^2(k_\lambda a)} + \beta_\lambda^2 a^2 - n_\lambda^2 \right] J_{n\lambda}^2(\beta_\lambda a) \ . \qquad (2.48)$$

The coupling energy, e_c, is still given by Eq. (2.42).

The energy conservation equation for Wave λ can now be written for both of the cases considered as

$$\frac{\sigma_\lambda}{\omega_\lambda} \psi_\lambda^* \left(\frac{\partial}{\partial t} + v_{g\lambda} \frac{\partial}{\partial z}\right) \psi_\lambda + (c.c.) = - \frac{je}{4m_e} \frac{\omega_\lambda^2}{k_\lambda^2} \frac{I_{\alpha\beta\gamma}}{A_\lambda} \psi_\alpha \psi^*_\beta \psi^*_\gamma + (c.c.)$$

$$\lambda = \alpha, \beta, \gamma \ . \qquad (2.49)$$

The coupled mode equations can be obtained from Eq. (2.49) by matching each term in the LHS with the term of the RHS corresponding to the same exponential behavior. For example, the coupled mode equation for Wave α is

$$\left(\frac{\partial}{\partial t} + v_{g\alpha}\frac{\partial}{\partial z}\right)\psi_\alpha = -\frac{je}{4m_e}\frac{\omega_\alpha^3}{k_\alpha^2}\frac{I_{\alpha\beta\gamma}}{A_\alpha}\psi_\beta\psi_\gamma \ . \qquad (2.50)$$

2.2.2 Solution of the Coupled Mode Equations

The coupled mode equations can be solved analytically when either $\partial\psi_\lambda/\partial z$ or $\partial\psi_\lambda/\partial t = 0$. Solutions are obtained in terms of elliptic integrals,[1,3] and indicate that the three waves exchange some or all of their energy periodically, depending on their initial relative amplitudes. The problem is simplified considerably when one of the waves has a much larger amplitude than the other waves. Since the RHS of the coupled mode equation for this pump only contains a product of two relatively small quantities, namely the amplitudes of the other waves, the amplitude of the pump can be considered to be constant.

When the pump has a higher frequency than the other two waves, the coupled mode equations are

$$\frac{\partial\psi_s}{\partial t} + v_{gs}\frac{\partial\psi_s}{\partial z} = -jF_s\psi_p\psi^*_i \ , \qquad (2.51)$$

$$\frac{\partial\psi_i}{\partial t} + v_{gi}\frac{\partial\psi_i}{\partial z} = -jF_i\psi_p\psi^*_s \ , \qquad (2.52)$$

$$F_\lambda = \frac{e}{4m_e}\frac{\omega_\lambda^3}{k_\lambda^2}\frac{I_{\alpha\beta\gamma}}{A_\lambda} \ , \qquad \lambda = s,i \ , \qquad (2.53)$$

where the subscripts p, s and i refer to the pump, signal and idler, respectively. It is necessary to perform a stability analysis in order to determine if the nonlinear coupling leads to a stable or unstable situation, and if unstable, to an absolute or convective instability. It is useful to write the amplitude variations as

$$\psi_s = \psi_{s0} \exp\left\{j\left[\left(\omega_r + j\omega_j\right)t - \left(k_r + jk_j\right)\right]\right\}z \quad , \tag{2.54}$$

$$\psi_i = \psi_{i0} \exp\left\{j\left(-\omega_r + j\omega_j\right)t - \left(-k_r + jk_j\right)z \quad , \right. \tag{2.55}$$

where $\psi_{\lambda 0}$ is a constant amplitude factor. The signs in front of ω_r and k_r are chosen in such a way as to preserve synchronism. The following dispersion relation can be obtained from Eqs. (2.51)-(2.55):

$$\left(k - \frac{\omega}{v_{gs}}\right)\left(k - \frac{\omega}{v_{gi}}\right) = -\chi^2 \quad , \tag{2.56}$$

where $\omega = \omega_r + j\omega_j$, $k = k_r + jk_j$, $\chi^2 = \frac{F_s F_i}{v_{gs} v_{gi}}|\psi_p|^2$. (2.57)

According to Briggs[63] and Cassedy,[64] there is convective instability, i.e. wave growth in space, when all the waves have their group velocities in the same direction. The solutions of Eqs. (2.51) and (2.52) are

$$\psi_\lambda = a_\lambda \exp(\chi z) + b_\lambda \exp(-\chi z) \quad , \quad \lambda = s,i \ , \tag{2.58}$$

where a_λ and b_λ are constants determined by the initial conditions. A typical application of this type of coupling is the parametric amplifier[2] which makes use of the interaction between a pump, a signal to be amplified, and an idler created in the interaction. If the signal has an amplitude ψ_{s0} and the idler has zero amplitude at $z = 0$, their respective amplitudes ψ_s and ψ_i as a function of distance are given by

$$\psi_s = \psi_{s0} \cosh \chi z \quad , \quad \psi_i = \psi^*_{s0} \sinh \chi z \ . \tag{2.59}$$

When the pump is one of the lower frequency waves, the coupled mode equations for the other two waves are

$$\frac{\partial \psi_i}{\partial t} + v_{gs} \frac{\partial \psi_s}{\partial z} = - jF_s \psi_p \psi_i \ , \tag{2.60}$$

$$\frac{\partial \psi_i}{\partial t} + v_{gi} \frac{\partial \psi_i}{\partial z} = - jF_i \psi_p^* \psi_s \ . \tag{2.61}$$

In this case, the amplitude variations must be written as

$$\psi_\lambda = \psi_{\lambda 0} \exp j(\omega t - kz) \ , \qquad \lambda = s,i. \tag{2.62}$$

The dispersion relation,

$$\left(k - \frac{\omega}{v_{gs}}\right)\left(k - \frac{\omega}{v_{gi}}\right) = \chi^2 \ , \tag{2.63}$$

leads to a stable situation for $v_{g\lambda} > 0$. Since time averaging can be performed in an experiment, we need only consider variations in space. The solutions of Eqs. (2.60) and (2.61) are, in this case,

$$\psi_\lambda = a_\lambda \exp(j\chi z) + b_\lambda \exp(-j\chi z) \ , \qquad \lambda = s,i. \tag{2.64}$$

If only the pump and the signal are present at $z = 0$, we obtain

$$\psi_s = \psi_{s0} \cos \chi z \ , \qquad \psi_i = \psi_{s0} \sin \chi z \ , \tag{2.65}$$

showing that the signal and the idler exchange their energy periodically.

2.2.3 Parametric Amplification

Since the coupled mode equations were obtained by assuming that the synchronism conditions were satisfied exactly, it is necessary to determine for what values of the frequencies and wavenumbers synchronism can be achieved in any particular case. Examination of the dispersion curves of Fig. 2.1 shows that, except for a small region near the origin, the synchronism conditions cannot be satisfied using only one branch of the dispersion relation. This is always the case when the slope of the dispersion characteristics varies monotonically. It is possible, however, to use more than one branch to obtain synchronism

over a wide range of parameters. Some combinations of the four branches of the dispersion relations shown in Fig. 2.1 are displayed in Fig. 2.2 for a metal tube filled with a uniform plasma, and Fig. 2.3 for a uniform plasma column surrounded by a vacuum ($\epsilon_g = 1$). The parameter ranges over which synchronism is possible are indicated by the heavy line portion of the characteristics. A typical interaction is shown in each case by means of a parallelogram formed by joining the origin and the points on the characteristics representing the interacting waves. The combinations shown in Figs. 2.2 and 2.3 do not exhaust all of the possibilities since there is an infinite number of curves to choose from in order to obtain synchronism. They represent some of the most likely candidates for obtaining an interaction, however, because they involve the lowest order modes, which should be the easiest to excite experimentally.

The growth rate, or gain, of the waves is given by

$$\chi = \left[\frac{F_s F_i}{v_{gs} v_{gi}}\right]^{1/2} |\psi_p| \qquad \text{neper/unit length.} \tag{2.66}$$

It is convenient to define Γ, the gain in dB per unit length,

$$\Gamma = 8.69\chi = \frac{\Gamma_n |\psi_p|}{N_0 a^3}, \tag{2.67}$$

where

$$\Gamma_N = 8.69\, N_0 a^3 \left[\frac{F_s F_i}{v_{gs} v_{gi}}\right]^{1/2}. \tag{2.68}$$

We shall refer to Γ_N as the normalized gain factor, because it can be expressed as a function of the normalized variables $(\omega_\lambda/\omega_0)$ and $(k_\lambda a)$. Hence, it is the same for any plasma column subject to a specific set of boundary conditions. Computations of Γ_N for the cases of nonlinear interaction shown in Figs. 2.2 and 2.3 are presented in Fig. 2.4, for a plasma-filled metal tube, and in Fig. 2.5, for a plasma column surrounded by an infinite dielectric. Curves of the frequencies and wavenumber at

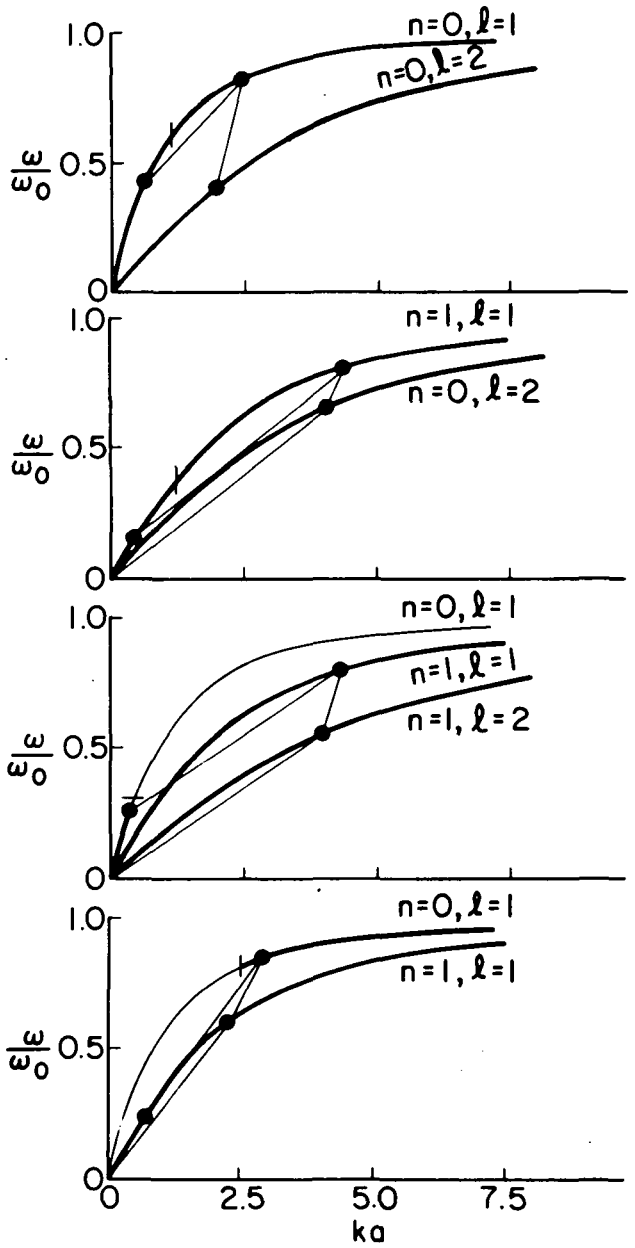

Fig. 2.2 Synchronism conditions and dispersion characteristics for $\omega_c \to \infty$: column surrounded by metal.

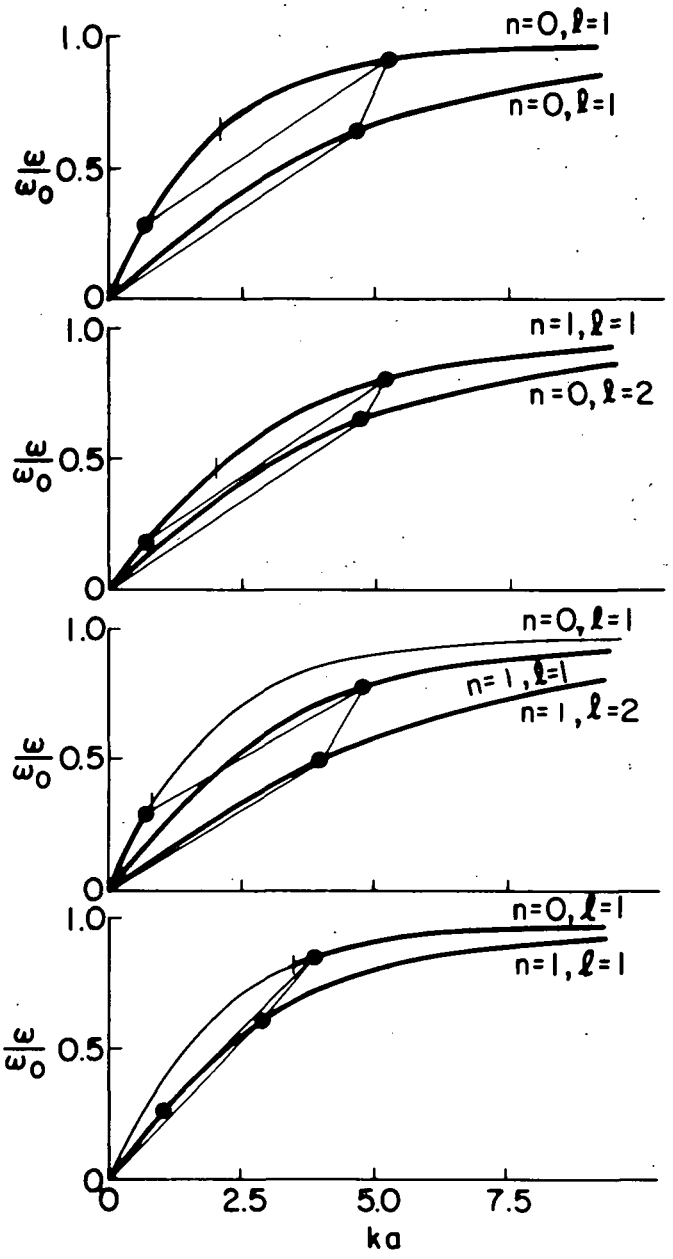

Fig. 2.3 Synchronism conditions and dispersion characteristics for $\omega_c \to \infty$: column surrounded by dielectric.

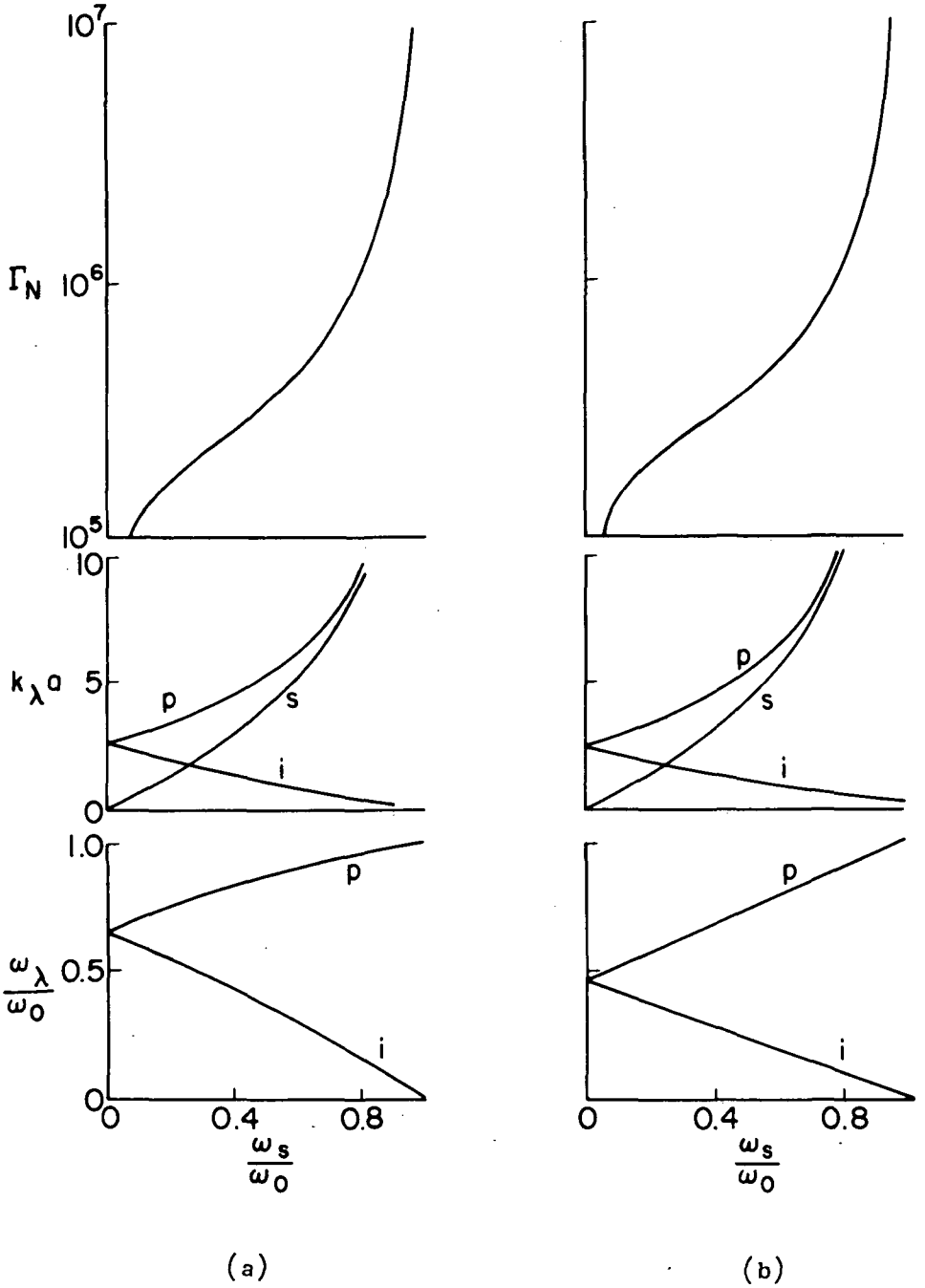

Fig. 2.4 Synchronism conditions and normalized gain factor for $\omega_c \to \infty$: column surrounded by metal.
(a) $n_p = 0$, $\ell_p = 1$; $n_s = 0$, $\ell_s = 2$; $n_i = 0$, $\ell_i = 1$;
(b) $n_p = 1$, $\ell_p = 1$; $n_s = 0$, $\ell_s = 2$; $n_i = 1$, $\ell_i = 1$.

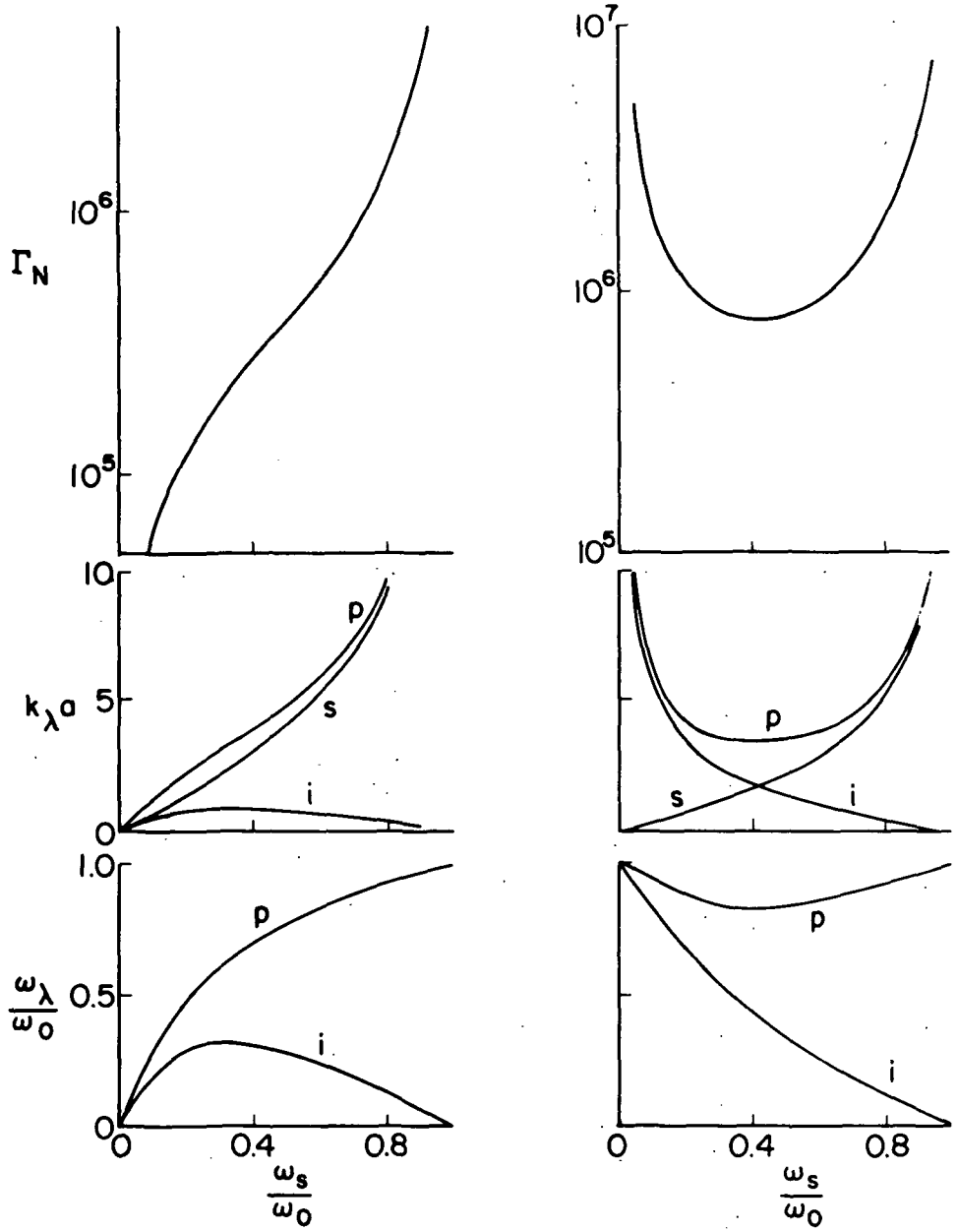

(c) (d)

Fig. 2.4 (Cont.)

(c) $n_p=1$, $\ell_p=1$; $n_s=1$, $\ell_s=2$; $n_i=0$, $\ell_i=1$;

(d) $n_p=0$, $\ell_p=1$; $n_s=1$, $\ell_s=1$; $n_i=1$, $\ell_i=-1$.

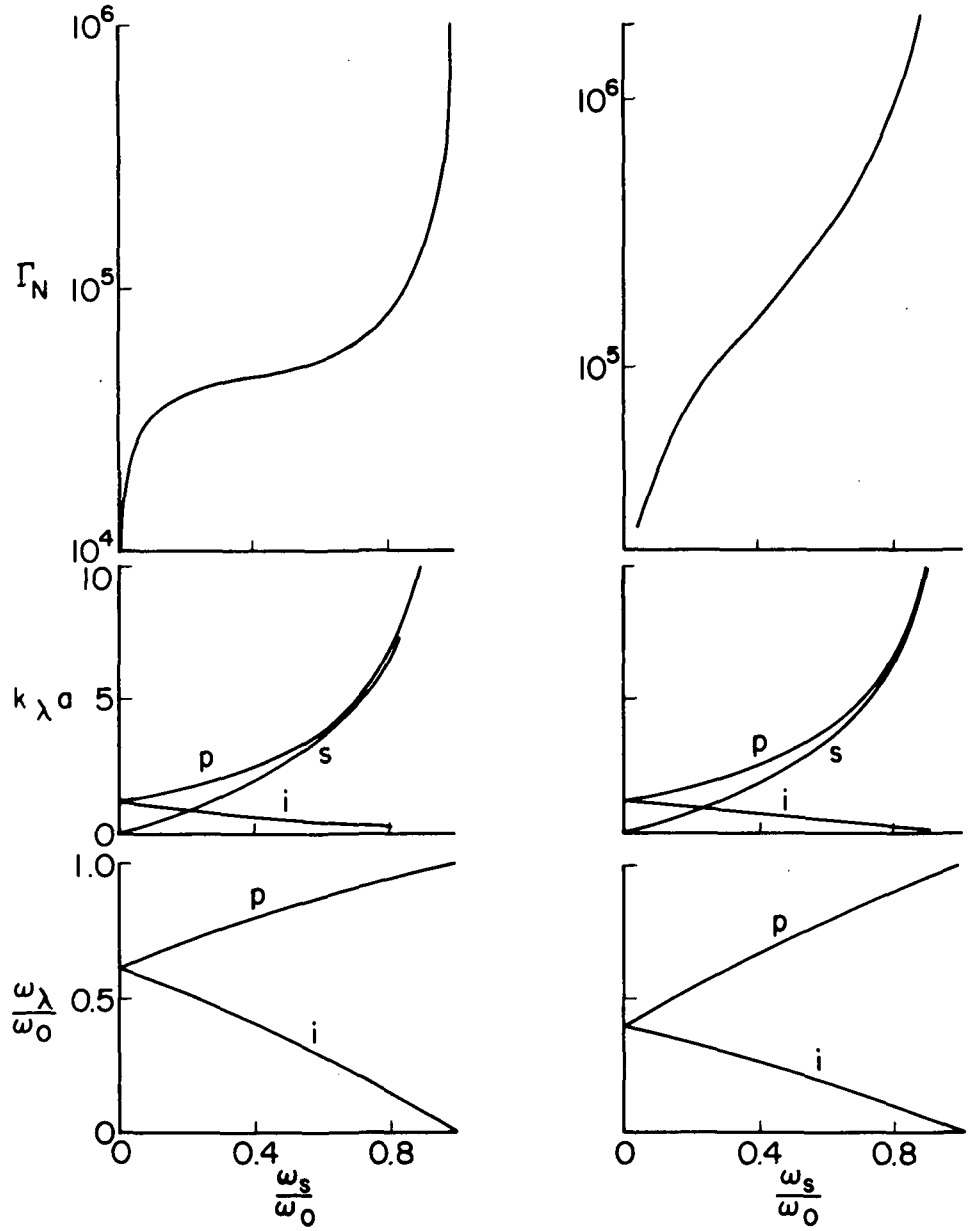

Fig. 2.5 Synchronism conditions and normalized gain factor for $\omega_c \to \infty$: column surrounded by vacuum.

(a) $n_p=0$, $\ell_p=1$; $n_s=0$, $\ell_s=2$; $n_i=0$, $\ell_i=1$;

(b) $n_p=1$, $\ell_p=1$; $n_s=0$, $\ell_s=2$; $n_i=1$, $\ell_i=1$;

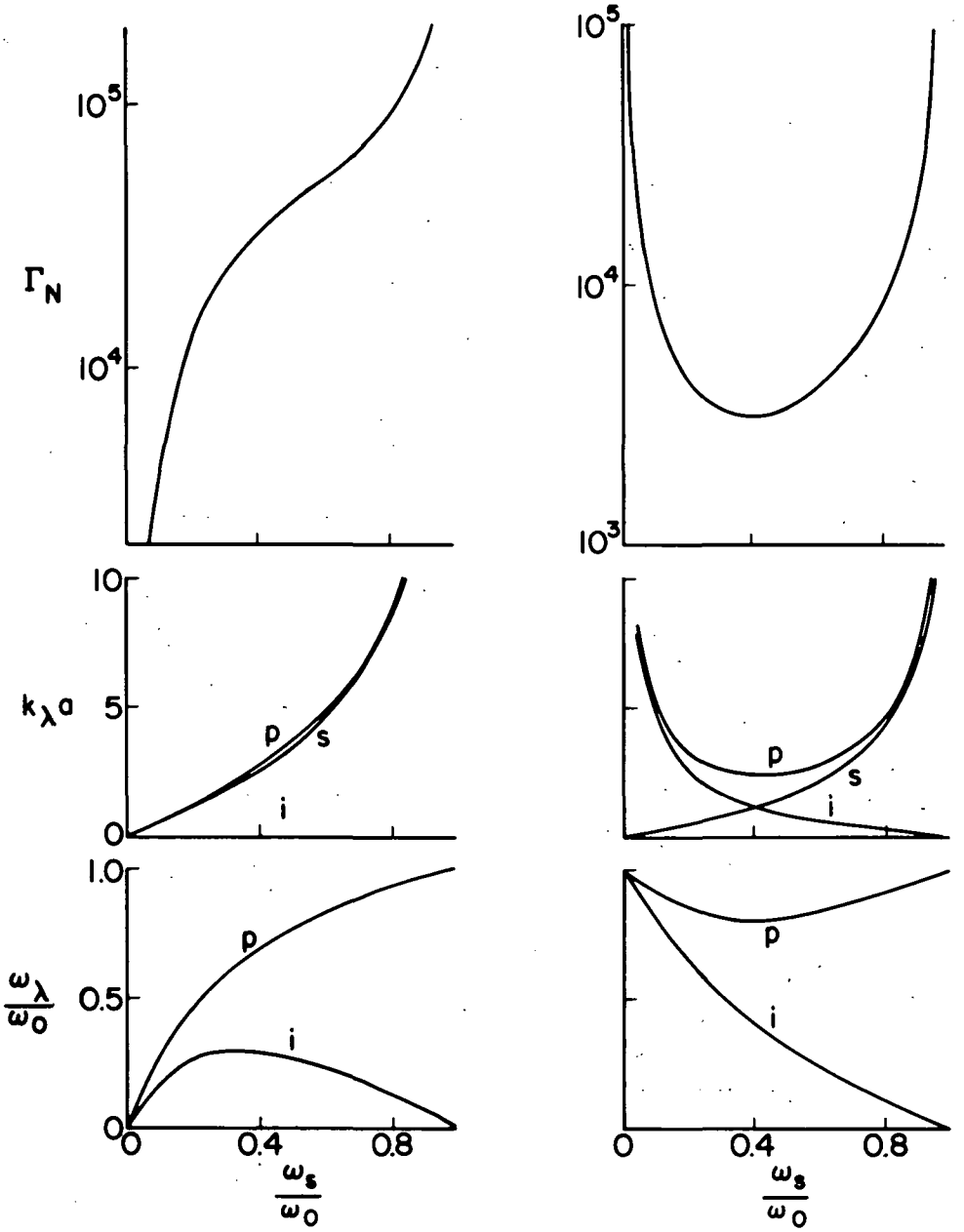

(c) (d)

Fig. 2.5 (Cont.)

(c) $n_p=1$, $\ell_p=1$; $n_s=1$, $\ell_s=2$; $n_i=0$, $\ell_i=1$;

(d) $n_p=0$, $\ell_p=1$; $n_s=1$, $\ell_s=1$; $n_i=1$, $\ell_i=-1$.

synchronism are presented in the same figures. For a plasma column of radius $a = 0.4$ cm and electron density $N_0 = 10^8/cm^3$, the gain Γ is

$$\Gamma = 1.6 \times 10^{-8} \Gamma_N |\psi_p| \text{ dB/m} \tag{2.69}$$

when Γ_N is expressed in MKS units. If a value of 10^5 is taken for Γ_N, a gain of a fraction of a dB/cm can be achieved with a pump potential of the order of a few volts. A survey of the results shown in Fig. 2.4 and 2.5 indicates that the chosen value of Γ_N is conservative.

One must bear in mind that the present theory does not take into account the effect of losses, which become important when the group velocity of the waves is small. It can be seen from Figs. 2.4 and 2.5 that at least one of the waves has a frequency close to the plasma frequency when the gain factor is large. The dispersion curves of Fig. 2.1 show that the group velocity decreases with frequency.

2.2.4 Bandwidth of the Interaction

An important characteristic of parametric interaction is its bandwidth. If an experiment is to be performed, it is important that the interaction have a bandwidth wide enough not to be affected significantly by small departures from synchronism. For example, if two waves with frequencies ω_p and ω_s are excited, a third wave is produced with $\omega_i = \omega_p \pm \omega_s$. The wavenumbers k_s, k_i, and k_p can be obtained from the linear dispersion relations (2.10) or (2.13). In general, the wavenumbers do not satisfy a synchronism condition, but we can write

$$\Delta k = k_p - k_s - k_i \tag{2.70}$$

The coupled mode equations can be written as

$$\frac{\partial \psi_s}{\partial z} + \alpha_s \psi_s = - j \frac{F_s}{v_{gs}} \psi_p \psi_i^* \exp j\Delta kz , \tag{2.71}$$

$$\frac{\partial \psi_i}{\partial z} + \alpha_i \psi_s = - j \frac{F_i}{v_{gi}} \psi_p \psi_s^* \exp j\Delta kz , \tag{2.72}$$

where α_s and α_i are linear phenomenological loss factors. The equation for ψ_s is

$$\frac{\partial^2 \psi_s}{\partial z^2} + (\alpha_s + \alpha_i - j\Delta k) \frac{\partial \psi_s}{\partial z} - \left[\chi^2 - \alpha_s(\alpha_i - j\Delta k)\right]\psi_s = 0 \quad . \tag{2.73}$$

The solution for ψ_s is

$$\psi_s = a_s \exp p_{s+} z + b_s \exp p_{s-} z \quad , \tag{2.74}$$

$$p_{s\pm} = -\frac{1}{2}(\alpha_s + \alpha_i - j\Delta k) \pm \left[\frac{1}{4}(a_s - \alpha_i)^2 + \frac{j}{2}(\alpha_s - \alpha_i)\Delta k + \chi^2 - \frac{\Delta k^2}{4}\right]^{1/2} \quad . \tag{2.75}$$

We may obtain ψ_i from Eqs. (2.73)-(2.75) by interchanging s and i .

In a lossless system, $p_{s\pm}$ reduce to

$$p_{s\pm} = j\frac{\Delta k}{2} \pm \left[\chi^2 - \frac{\Delta k^2}{4}\right]^{1/2} \quad . \tag{2.76}$$

Usually, a parametric amplifier uses a fixed frequency pump, and the bandwidth of the nonlinear coupling determines the range of frequencies over which the signal can be amplified. Exponential growth of the signal occurs when p_{s+} has a positive real part. In the case of a lossless system, the gain is

$$\Gamma = 8.69 \ \mathrm{Re}\left[\chi^2 - \frac{\Delta k^2}{4}\right]^{1/2} \ \mathrm{dB/m} \quad . \tag{2.77}$$

In Fig. 2.6, we show curves of the gain Γ at a fixed pump frequency as a function of the signal frequency for some of the mode combinations considered in Fig. 2.3. The combination of the (1,1), (1,2) and (0,1) branches of the dispersion relation is not shown in Fig. 2.6 because it leads to a bandwidth of the order of 0.01 ω/ω_0 , which is too small to be of practical interest. The effect of loss on the gain is shown as a broken curve in Fig. 2.6, for $\omega_p/\omega_0 = 0.65$, in the case of the

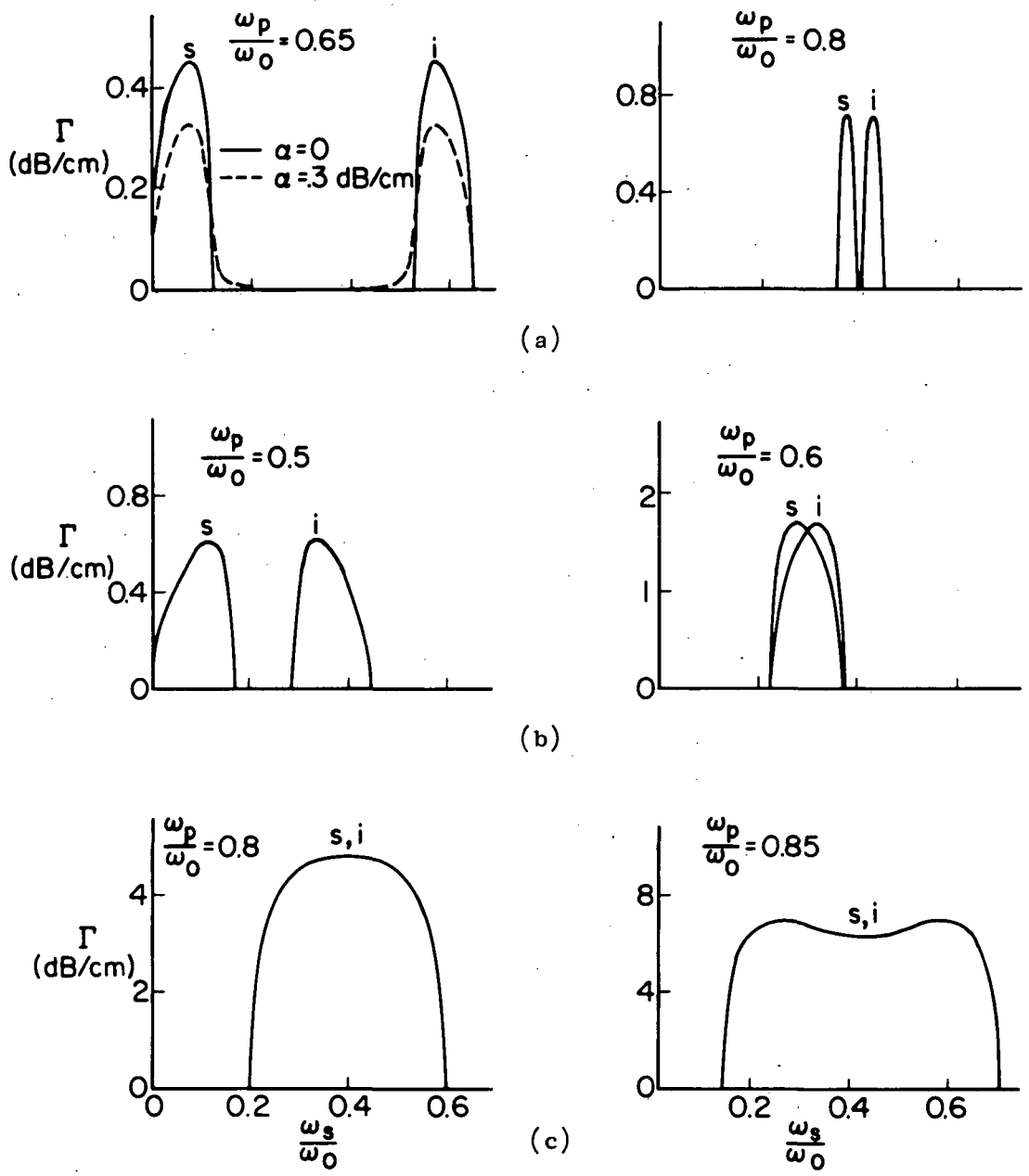

Fig. 2.6 Gain as a function of signal frequency at fixed pump frequency for $\omega_c \to \infty$: a=0.4 cm, $N_0=10^8/cm^3$, ψ_p=1V.

(a) $n_p=0$, $\ell_p=1$; $n_s=0$, $\ell_s=2$; $n_i=0$, $\ell_i=1$;

(b) $n_p=1$, $\ell_p=1$; $n_s=0$, $\ell_s=2$; $n_i=1$, $\ell_i=1$;

(c) $n_p=0$, $\ell_p=1$; $n_s=1$, $\ell_s=1$; $n_i=1$, $\ell_i=-1$.

(0,1), (0,2), (0,1) interaction. A loss rate $\alpha = 0.3$ dB/cm has been chosen arbitrarily for either the signal or the idler. There is a decrease in the maximum gain and a small increase in the bandwidth.

2.2.5 Mode Conversion

Since the group velocity of slow waves on a plasma column decreases with increasing frequency, the highest frequency wave present in the nonlinear interaction is damped more rapidly than the other waves and may prove to be unsuitable to be used as a pump. This has been our own experience, as reported in Chapter III. Consequently, one of the lower frequency waves, which can be excited at a high enough level, is chosen as the pump, and is assumed to be undamped. The signal, at the highest frequency, and the idler are attenuated in the linear regime. The coupled mode equations can be written in the following way, including the effect of a departure from synchronism, Δk , defined by Eq. (2.70),

$$\frac{\partial \psi_s}{\partial z} + \alpha_s \psi_s = - \frac{jF_s}{v_{gs}} \psi_p \psi_i \exp(j\Delta k\, z) , \qquad (2.78)$$

$$\frac{\partial \psi_i}{\partial z} + \alpha_i \psi_i = - \frac{jF_i}{v_{gi}} \psi_p^* \psi_s \exp(-j\Delta k\, z) . \qquad (2.79)$$

The equation for ψ_s is

$$\frac{\partial^2 \psi_s}{\partial z^2} + (\alpha_s + \alpha_i - j\Delta k) \frac{\partial \psi_s}{\partial z} + \left[\chi^2 + \alpha_s(\alpha_i - j\Delta k)\right] \psi_s = 0, \qquad (2.80)$$

and has the solution

$$\psi_s = a_s \exp p_{s+} z + b_s \exp p_{s-} z , \qquad (2.81)$$

with

$$p_{s+} = - \frac{1}{2} (\alpha_s + \alpha_i - j\Delta k) \pm \frac{1}{2} \left[(\alpha_s - \alpha_i + j\Delta k)^2 - 4\chi^2\right]^{1/2} . \qquad (2.82)$$

The equations for ψ_i can be obtained by interchanging s and i, and replacing Δk by $-\Delta k$, in Eqs. (2.80)-(2.82). The boundary conditions $\psi_s(0) = \psi_{s0}$ and $\psi_i = 0$ allow the constants to be evaluated as

$$a_s = \left[\frac{p_{s-}+\alpha_s}{p_{s-}-p_{s+}}\right]\psi_{s0} \quad , \qquad b_s = -\left[\frac{p_{s+}+\alpha_s}{p_{s-}-p_{s+}}\right]\psi_{s0} \quad ,$$

$$a_i = -j\,\frac{F_i\,\psi_p^*}{v_{gi}}\,\frac{\psi_{s0}}{(p_{i-}-p_{i+})} \quad , \qquad b_i = -a_i \quad . \tag{2.83}$$

The behavior of the solutions obtained in this section is rather difficult to predict, in view of the large number of parameters present in the solution, and we do not intend to survey all of the various possibilities. We simply show in Fig. 2.7 a set of curves for ψ_s and ψ_i corresponding to an experimental situation to be discussed further in Chapter III. The main features of these curves are typical of our experimental results obtained with a heavily damped signal. The position of the maximum in the idler power depends mainly on Δk.

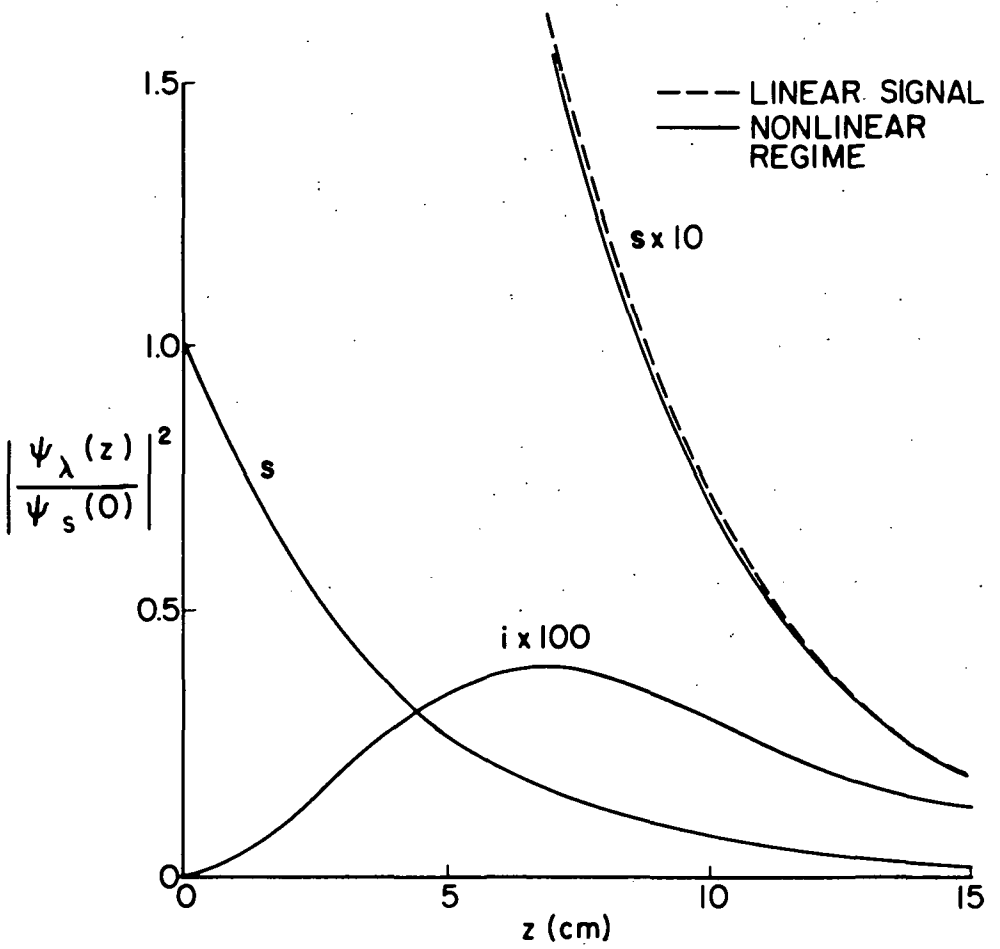

Fig. 2.7 Axial power variation for mode conversion for $\omega_c \to \infty$: column surrounded by vacuum. $\omega_p/\omega_0=0.517$, $\psi_p=9.5V$, $n_p=0$, $\ell_p=1$; $\omega_s/\omega_0=0.794$, $\alpha_s=-.13/cm$, $n_s=0$, $\ell_s=1$; $\omega_i/\omega_0=0.277$, $\alpha_i=0.01/cm$, $n_i=0$, $\ell_i=2$.

Chapter III

NONLINEAR INTERACTIONS OF SLOW WAVES ON A PLASMA COLUMN IN A STRONG MAGNETIC FIELD: EXPERIMENTS

The aim of the experiments described in this chapter was to investigate nonlinear interactions of slow waves on a plasma column in a strong magnetic field under conditions approaching those treated theoretically in Chapter II. Some demonstrations of parametric amplification under such conditions have been reported by Pérulli and his co-workers.[31] Their experiments were performed in a low density ($N_0 \approx 5 \times 10^8/cm$) xenon discharge of radius $a \approx 0.8$ cm in a strong magnetic field ($B_0 = 2.25$ kG). Landau damping introduced a threshold for the onset of the amplification, as predicted by the theory. In our experiments, wave damping prevented the observation of parametric amplification, but mode conversion was obtained.

3.1 Experimental Set-up

Some preliminary experiments aimed at studying the linear properties of slow waves were performed on the positive column of a hot cathode helium discharge placed in a magnetic field of 300 G, at electron densities of the order of $5 \times 10^9/cm^3$. The $n = 0$, $\ell = 1$ branch of the dispersion relation was obtained with the double ring couplers shown in Fig. 3.1. No other branch of the dispersion relation could be obtained, however, even with the dipolar couplers shown in Fig. 3.1. As mentioned in Chapter I, to our knowledge, nobody has succeeded in measuring, in the linear regime, the higher order branches of the dispersion relation for slow waves in the presence of a magnetic field.

A different set-up was used for the rest of the experiments. The reasons for the change were the following. First, computations of the gain, Γ, given by Eq. (2.67), showed the necessity of using a discharge with electron densities of a few times $10^8/cm^3$ in order to obtain measurable amplification. Second, it was necessary to use as strong a magnetic field as possible in order to approximate the theory with an infinite magnetic field. The positive column used in the preliminary experiments became unstable for magnetic fields larger than 300 G.

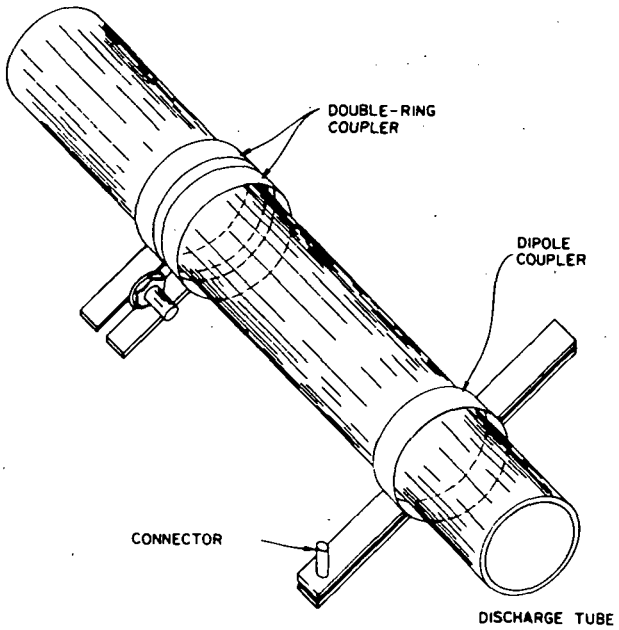

FIG. 3.1. Double ring and dipole couplers.

Third, a discharge with low background gas pressure was desirable, in order to lower collisional losses, and to avoid supplementary ionization by the RF signals used in the experiments. The system which was chosen to satisfy these requirements is shown schematically in Fig. 3.2.

3.1.1 Magnetic Field System

The magnetic field, produced by 14 coils positioned as shown in Fig. 3.2, was uniform to better than 1% over a length of about 55 cm between the third and twelfth coils. Fields of up to 5.0 kG could be obtained with this system but most of the experiments were performed with a magnetic field of 1.4 kG, which produced optimum results.

3.1.2 Plasma Source

The plasma source, shown in Fig. 3.3, was an argon reflex discharge placed at one end of the discharge tube. The plasma created in the source diffused into the central part of the tube through a hole 0.95 cm in diameter. Typically, the source was operated with 600 V on the central electrode. The discharge current was 100 mA at a pressure of 2×10^{-4} Torr.

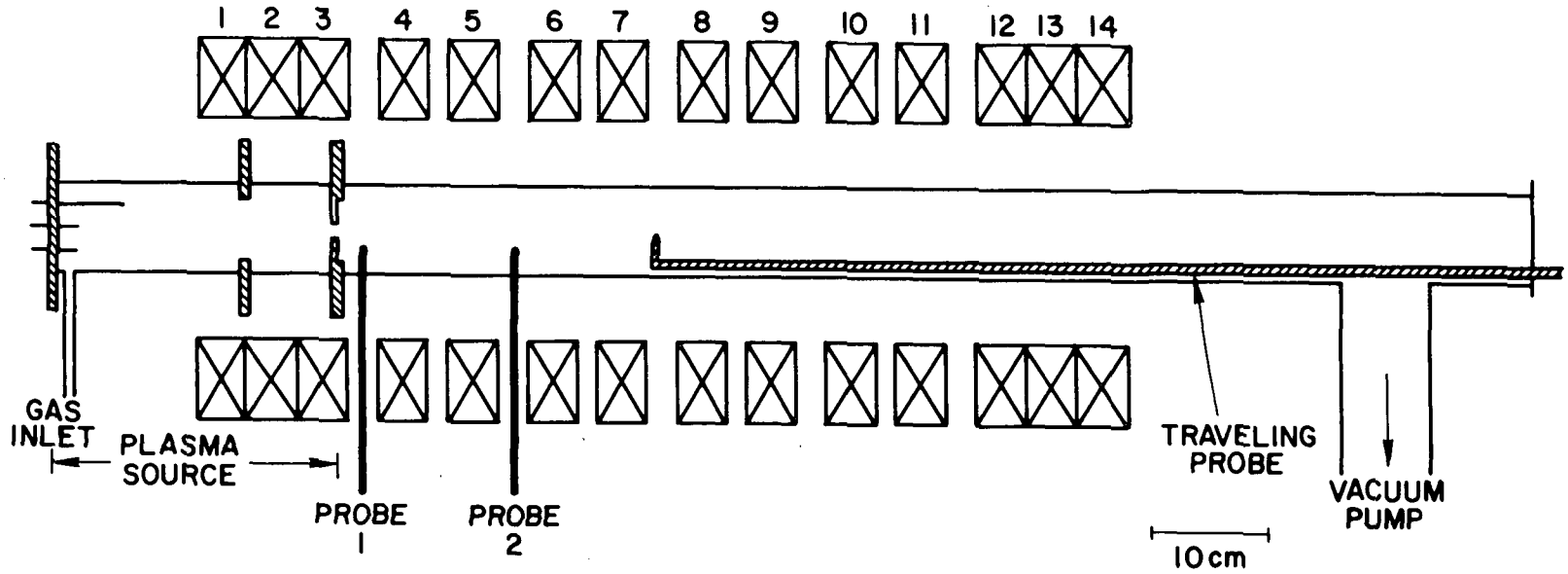

Fig. 3.2 Experimental set-up.

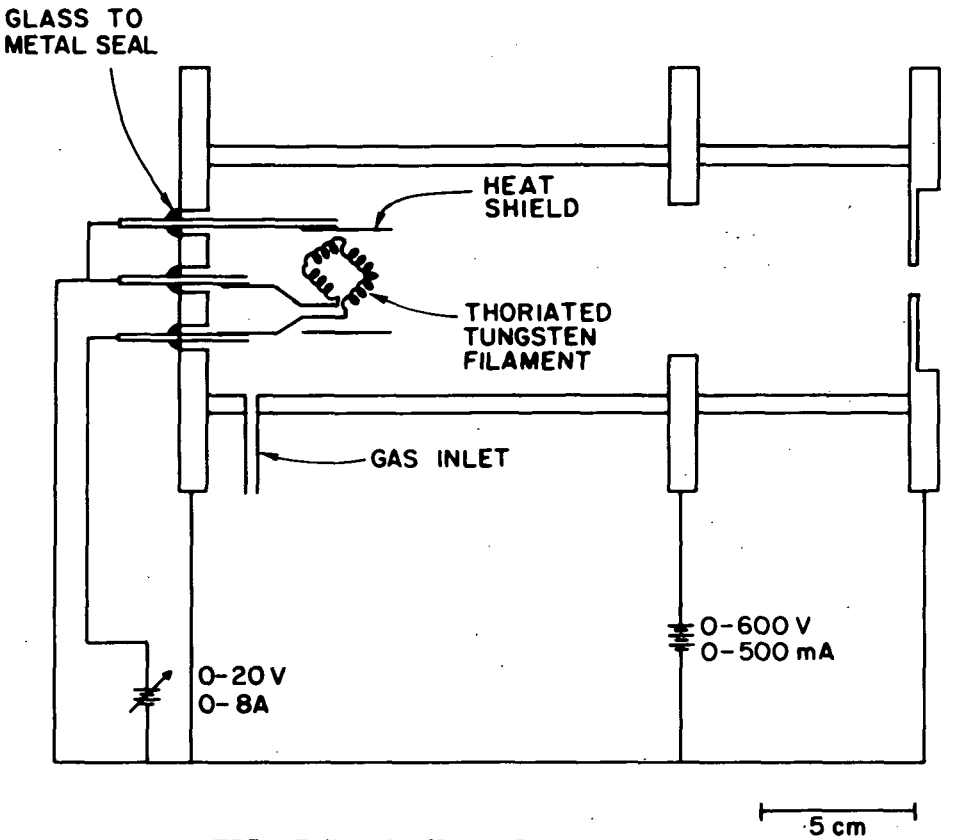

FIG. 3.3. Reflex plasma source.

3.1.3 Plasma Column

The radial electron density profile of the plasma column produced by diffusion out of the source along the magnetic field lines was measured at Probe 2 using a spherical Langmuir probe 0.104 cm in diameter. A sketch of this probe is shown in Fig. 3.4. The interpretation of Langmuir probe measurements in a low density plasma, or in the presence of a strong magnetic field, is always difficult. In the former case, it has been shown that the simple theories of Langmuir are not valid when λ_D is comparable to the probe radius.[65] In the presence of a strong magnetic field, the Larmor radius of the electrons is usually much smaller than the probe dimensions and the electron collection region of the probe characteristics is not usable to obtain electron density. The ion collection regime has been studied, in the absence of a magnetic field, by Allen, Boyd and Reynolds[66] in the case of cold ions. Laframboise[67] has computed the ion collection current for a Maxwellian ion distribution and presented his results, as well as those of Allen

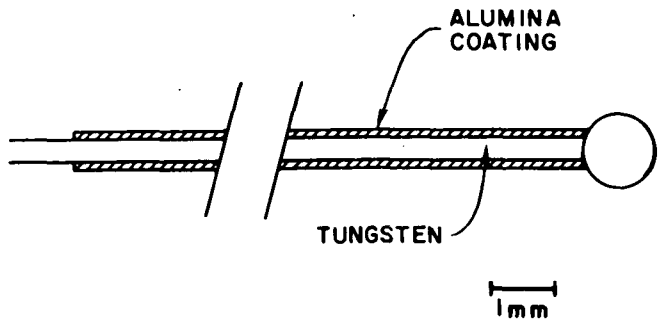

FIG. 3.4 Spherical Langmuir probe.

et al.,[66] in a form readily usable to interpret experimental results. In the presence of a magnetic field, the ion collection part of the probe characteristics should be usable as long as the ion Larmor radius is much larger than the probe radius. Some electron density measurements in a Q-machine, reported by Chen, Etiévant and Mosher,[68] showed very good agreement with Laframboise's theory down to $10^8/cm^3$ at 1.5 kG. In contrast to a Q-machine, in which the ions and the electrons are roughly at the same temperature, the ion temperature should be much smaller than the electron temperature in our discharge. Consequently, the Allen, Boyd and Reynolds theory was used to interpret our probe measurements.

The measured radial electron density profile is shown in Fig. 3.5. The axial density profile was measured by using the traveling probe shown in Fig. 3.6. Since this probe was designed primarily as an RF coaxial probe, no attempt was made to measure the electron density from the probe characteristics. Instead, the ion saturation current collected by the probe when biased at -50 V with respect to the exit electrode of the plasma source was measured as a function of distance parallel to the axis of the column. The ion saturation current was found to decrease linearly as a function of distance away from the source and was down by about 40% at the end of the probe travel, between the tenth and the eleventh coils.

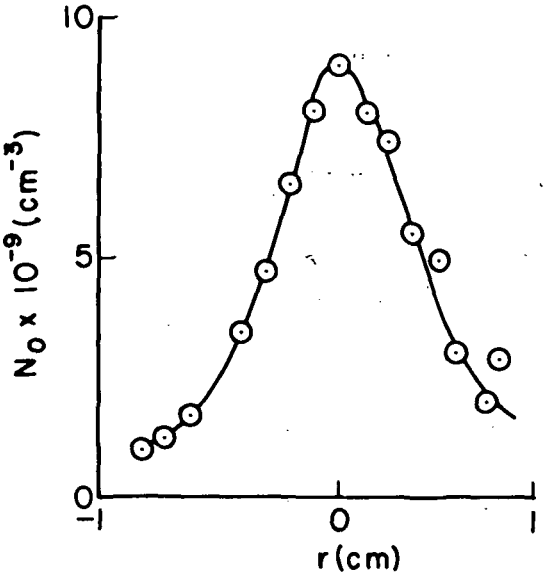

Fig. 3.5 Radial electron density profile.

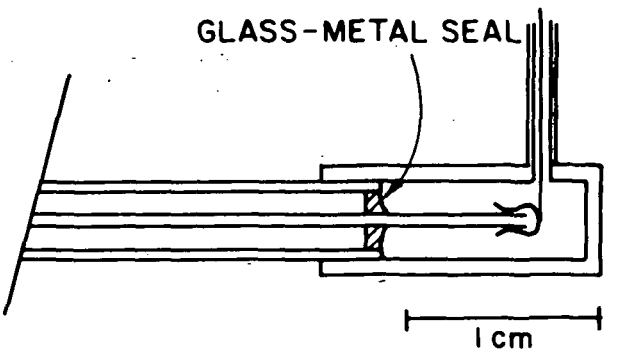

Fig. 3.6 Travelling RF probe.

3.1.4 RF System

A block diagram of the RF system is shown in Fig. 3.7. The waves were excited by means of coaxial probes. These probes, shown in Fig. 3.8, reflected between 85 and 92% of the input power, depending on the frequency. The presence of the plasma did not affect the reflection coefficient of the probes. The traveling probe shown in Fig. 3.6 was used to measure the wave potential as a function of distance in the axial direction.

The receiver could be used either as a square-law detector, or as an interferometer. In the latter case, the signal from the traveling probe was added to a much stronger reference signal through a hybrid junction. The reference signal came from a sample of the signal fed into the exciting probe, for measurements involving one wave, or by mixing a sample of each signal, for nonlinear interaction experiments. The output of the receiver, V , was then proportional to

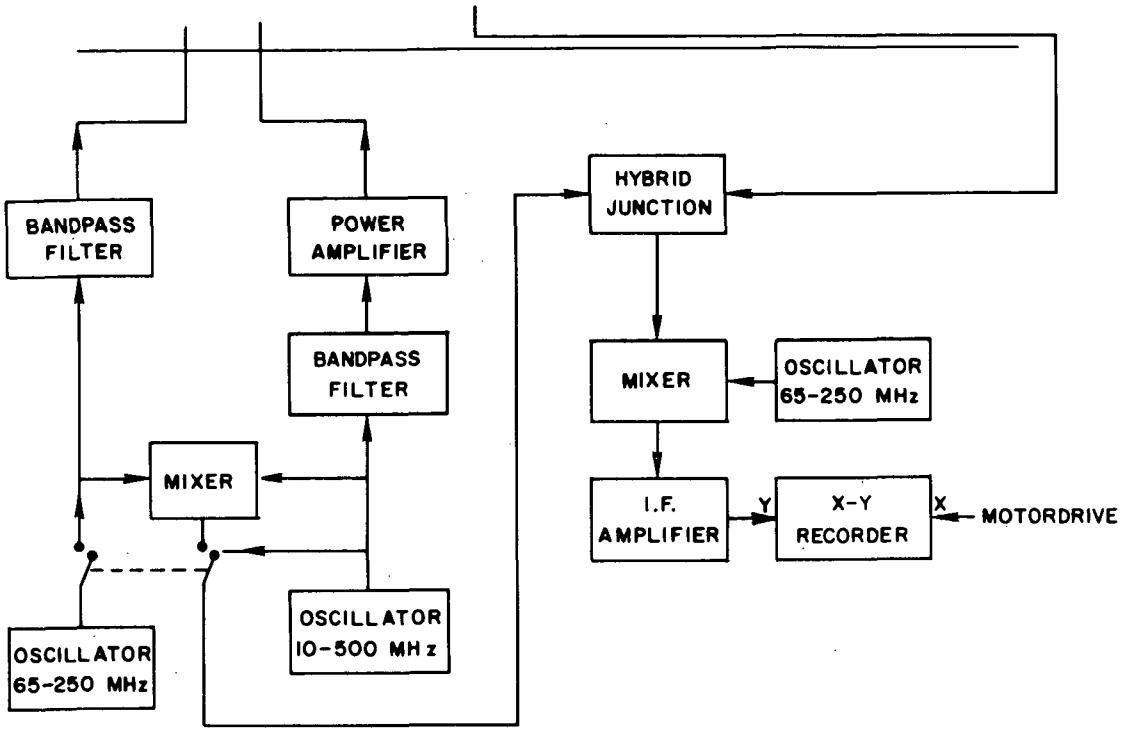

Fig. 3.7 RF system.

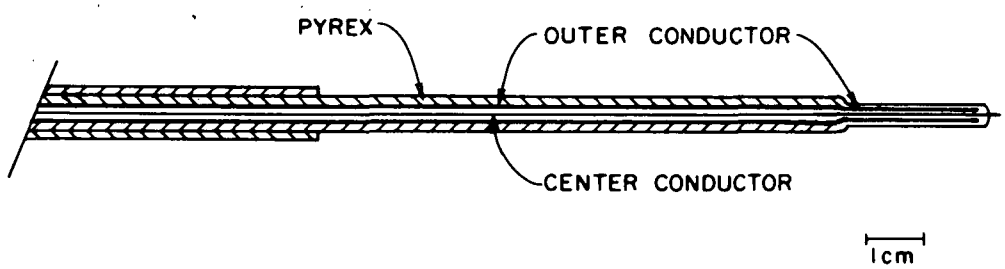

Fig. 3.8 Coaxial RF probe.

$$V = C\left\{\varphi_r^2 + \varphi^2(z) + 2\varphi_r\varphi(z)\cos[\alpha_r - \alpha(z)]\right\}$$

$$\simeq C\left\{\varphi_r^2 + 2\varphi_r\varphi(z)\cos[\alpha_r - \alpha(z)]\right\}, \qquad \varphi_r \gg \varphi(z)\ , \qquad (3.1)$$

where φ_r and α_r are the amplitude and phase of the reference signal, and $\varphi(z)$ and $\alpha(z)$ are the amplitude and phase of the signal from the traveling probe. In the nonlinear interaction experiments, each fixed probe was isolated from the mixer producing the reference signal by a bandpass filter, to prevent the mixed signal from reaching the plasma. The receiver permitted the detection of signals down to -95 dBm. A thermo-electric power meter was used to perform the absolute power measurements.

3.2 Experiments on Small Signal Theory

The dispersion characteristics of the $n = 0$, $\ell = 1$ branch of the dispersion relation were obtained from interference curves produced as described in Section 3.1.4. The waveforms obtained at frequencies of 100 MHz or less showed a complicated structure which could be due to the excitation of more than one mode. An example of the interference measurements is shown in Fig. 3.9. These waveforms were Fourier analyzed on the computer. Unfortunately, the shortness of the column, the attenuation of some of the modes involved, and the wavelength variations due to the axial electron density gradient, caused the results to be inconclusive; the secondary peaks generated by a Fourier analysis over a finite distance could not usually be separated clearly from those produced by the higher order modes. Figure 3.10 shows the Fourier analysis of the waveform of Fig. 3.9. The first maximum in Fig. 3.10 was interpreted as an $n = 0$, $\ell = 1$ wave, and the remaining peaks were rejected as spurious. It was possible to measure approximately the wavelength of a second mode in Fig. 3.9, since the region from $z = 20$ to $z = 35$ cm contained some short wavelength oscillations. This could also be done on interference curves obtained at some other frequencies. At frequencies higher than 150 MHz, the damping of the wave was measured from curves of the axial power variation for the $n = 0$, $\ell = 1$ mode.

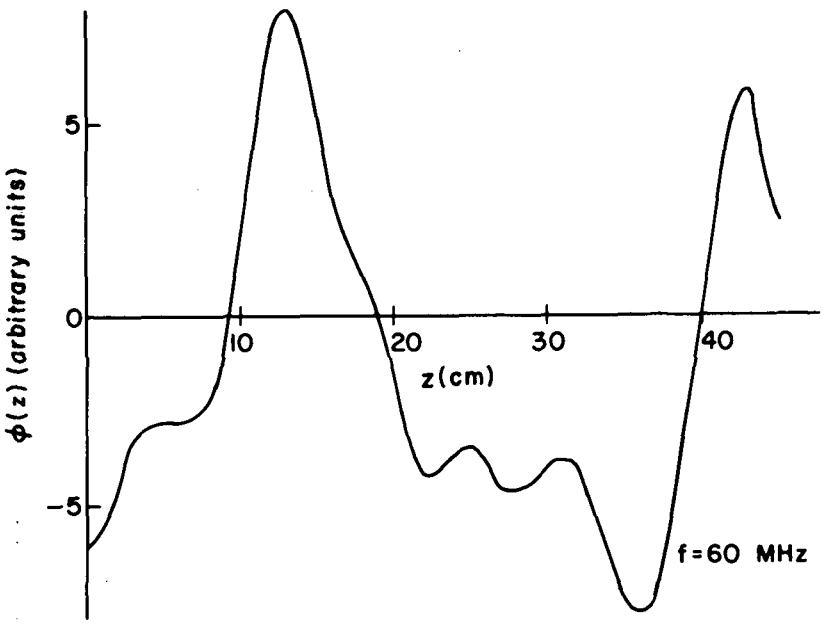

Fig. 3.9 Axial potential profile.

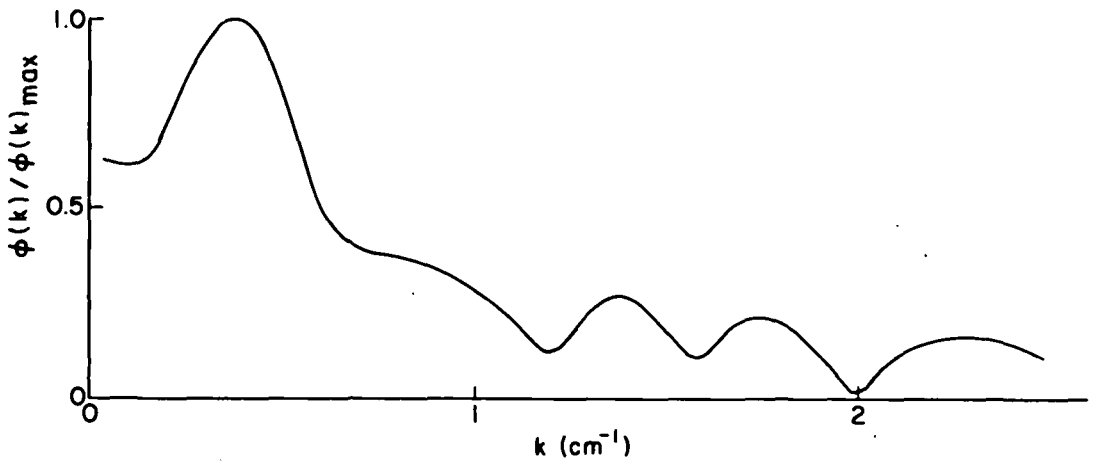

Fig. 3.10 Fourier analysis of curve of Fig. 3.9.

The experimental points obtained for the $n = 0$, $\ell = 1$ mode were fitted to the corresponding branch of the dispersion relation for slow waves on a plasma column surrounded by vacuum. The plasma frequency and the column radius giving the best fit were 290 MHz and 0.65 cm. These values were then used to plot all the experimental dispersion results as a function of the dimensionless variables ka and ω/ω_0. Figure 3.11 shows theoretical dispersion curves and all the experimental points, including those obtained in the nonlinear regime, as described in Section 3.3. The plasma frequency at the center of the column, as determined from the probe measurements, was 270 MHz. Many factors can explain the discrepancy between the plasma frequency calculated from the measured electron density, and that obtained from the fit of the dispersion characteristics. The short wavelengths, and the heavy loss present at the higher frequencies (220-240 MHz), introduced errors of at least 10% in the wavenumbers obtained from the slow wave propagation measurements. The electron density calculated from the slow wave measurements should be the average density of the radially inhomogeneous column,[8] although in the present case the discrepancy is in the wrong direction to be accounted for by inhomogeneity. It was difficult to assess the uncertainty in the probe measurements due to the magnetic field, and to the perturbation introduced by the stem of the spherical probe.

At this point, it is appropriate to discuss the adequacy of the cold uniform plasma model used in the theory, since the experimental results presented in this section were obtained on a warm nonuniform plasma column. While there is no doubt that a warm nonuniform plasma model would be superior, it was seen in the review of previous work presented in Chapter I that the cold plasma theory predicted many of the features of the experimental results of slow wave propagation. In particular, the electron density measurements obtained by Trivelpiece[8] showed very good agreement between slow wave propagation and cavity perturbation measurements. The main feature of our experimental results not accounted for by the cold plasma column was the wave damping. The collisional damping was about 100 times too small to account

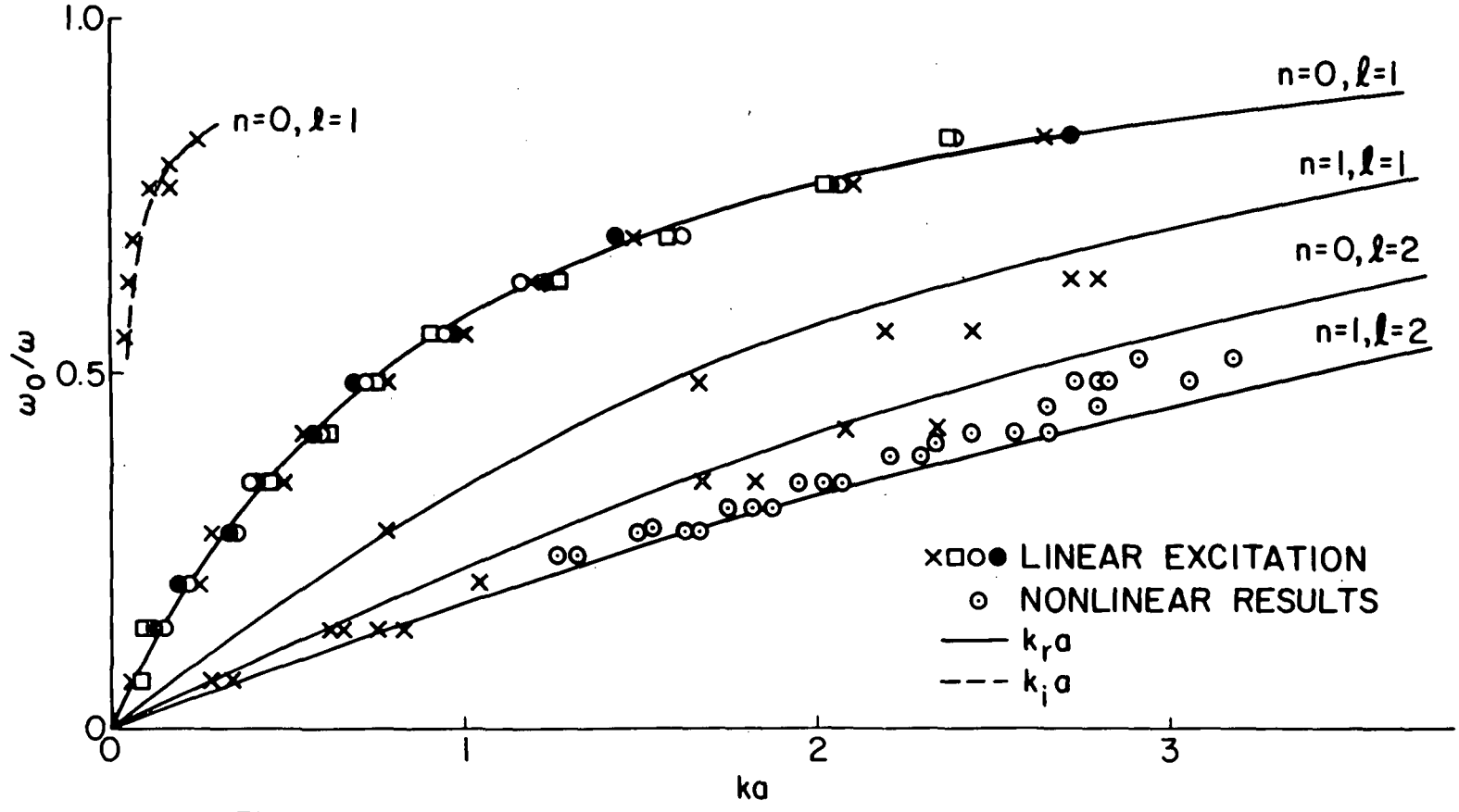

Fig. 3.11 Fit of the experimental dispersion measurements to the theoretical dispersion characteristics.

for the observed loss. While this was not checked with a suitable theory, it was suspected that the wave damping was due to Landau damping.[18] We have assumed that the cold plasma model can be considered acceptable for our purposes, provided the fitted discharge parameters are used in the theory.

3.3 Experiments on Nonlinear Interactions

At the onset of the present research on nonlinear interactions of slow waves, two types of experiments were envisioned. In the first, a single strong excited wave would decay into a spectrum of lower frequency waves growing out of the noise. The curves of Fig. 2.3 show the ranges of frequency over which some of the possible decay interactions can occur. In the second type of experiment, two excited waves, a pump and a signal, would interact nonlinearly and create an idler. Parametric amplification or mode conversion would be obtained, depending on the relative frequencies of the pump and the signal. While it is not essential to measure all the interacting modes in the linear regime for nonlinear interactions to occur, the properties of the waves observed in the linear regime can suggest whether some or all of the possible nonlinear coupling experiments can be realized. As can be seen from the results of Section 3.2, there was no strong evidence that modes other than $n = 0$, $\ell = 1$ could be excited at appreciable levels. This seemed to indicate that any excited wave would probably belong to the $n = 0$, $\ell = 1$ branch of the dispersion relation. Linear damping, which was found to be very severe at the higher frequencies, proved to be very important in determining the course actually taken by our nonlinear slow wave experiments.

The decay of a strong excited wave could not be observed in our set-up. This was due to the fact that the wave could not be excited at a high enough level in the plasma, due to the weak coupling between the probe and the plasma, and the damping of the waves in the plasma. For the same reason, parametric amplification could not be observed: the highest frequency wave could not be excited strongly enough to act as a pump.

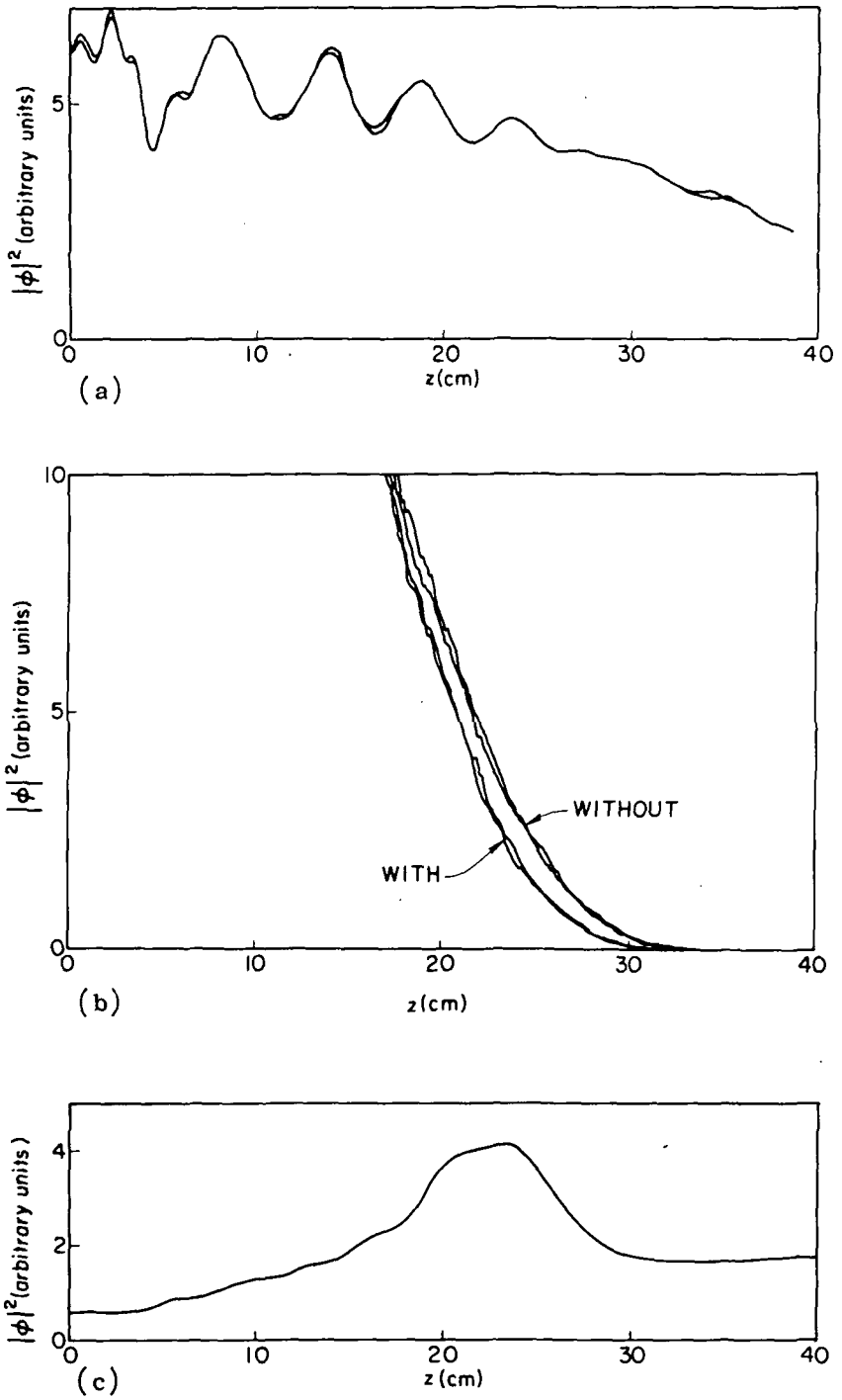

Fig. 3.12 Axial power profile in mode conversion. (a) 150 MHz; (b) 230 MHz; (c) 80 MHz.

Even with the foregoing difficulties, observations of mode conversion remained as a possible nonlinear interaction experiment. A typical set of curves obtained in such an experiment are shown in Fig. 3.12. In this particular experiment, a 150 MHz and a 230 MHz signal were fed respectively to Probes 1 and 2, either separately or together. The curves in Fig. 3.12 show the axial power variation received by the traveling probe at various frequencies. Probe 1 was positioned at - 11 cm and Probe 2, at +2 cm with respect to the starting position of the traveling probe. The almost identical curves of Fig. 3.12(a) demonstrate that the axial power variation observed at 150 MHz was the same whether the 230 MHz wave was excited or not. The axial power variation at 230 MHz, with and without the wave at 150 MHz, was also measured. The resulting curves, repeated twice in each case to evaluate the reproducibility of the measurements, are displayed in Fig. 3.12(b). The presence of the 150 MHz wave increased the damping rate of the 230 MHz wave. A third curve, given in Fig. 3.12(c), was recorded at 80 MHz, with both the 150 and 230 MHz waves excited simultaneously. It can be seen from Figs. 3.12(b) and (c) that the region where the 80 MHz wave was measured coincided with the region where the damping of the 230 MHz wave was increased, suggesting mode conversion between the signal and the idler. The wavenumber of the idler was obtained from the interferometric record shown in Fig. 3.13.

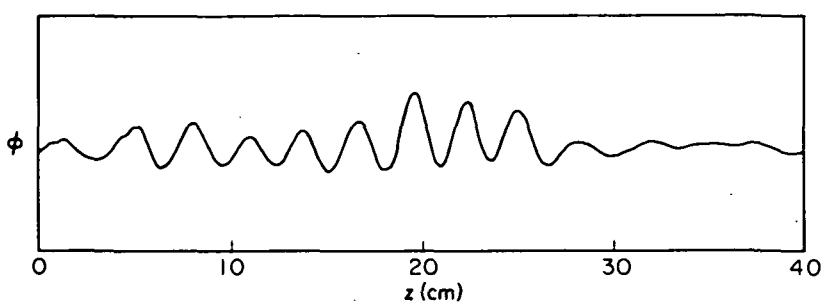

FIG. 3.13. Interferometer measurement for the conditions of Fig. 3.12(c).

The experimental curves of Fig. 3.12 show qualitative agreement with those of Fig. 2.7 obtained from the theory of Section 2.2.5. The experimental values of the frequencies, of the signal damping rate, and of the electron density were used in the calculation. The wave potential was estimated in the following way. It is shown in Appendix A that the power carried by a slow wave on a plasma column in an infinite magnetic field surrounded by vacuum can be expressed as

$$P = aN_0^{1/2} P_N |\psi|^2 , \qquad (3.2)$$

where P_N is a normalized power coefficient independent of the column parameters given by

$$P_N = \frac{\pi e}{2} \left(\frac{\epsilon_0}{m}\right)^{1/2} ka \frac{\omega_0}{\omega} J_n^2 (\beta a) . \qquad (3.3)$$

A curve of P_N as a function of ω/ω_0 is presented in Fig. 3.14 for the $n = 0$, $\ell = 1$ branch of the dispersion relation. Taking into account the reflection coefficient of the probe, the power transmitted through the exciting probe was measured as 17.5 mW. Assuming that the power was divided into slow waves propagating in both directions, the value of ψ obtained from Eq. (3.2) was 9.5V.

The main difference between the theoretical curves of Fig. 2.7 and the experimental curves of Fig. 3.12, is the position of the maximum in the axial power variation for the idler. One of the reasons for the discrepancy stems from the difference between the theoretical and the experimental values of the idler wavenumber. Since the pump and the signal are on the branch of the dispersion relation which has been fitted to the theoretical dispersion curve for $\ell = 0$, $n = 1$, the theoretical and experimental values of their wavenumbers are the same, and the departure from synchronism ($a\Delta k$), which is 0.243 in the theory and -0.104 in the experiment, comes from the idler. Another possible cause of error comes from the difficulty in defining the point $z = 0$ for the start of the interaction, because of disturbances of the plasma itself due to the excitation of the signal. These perturbations could

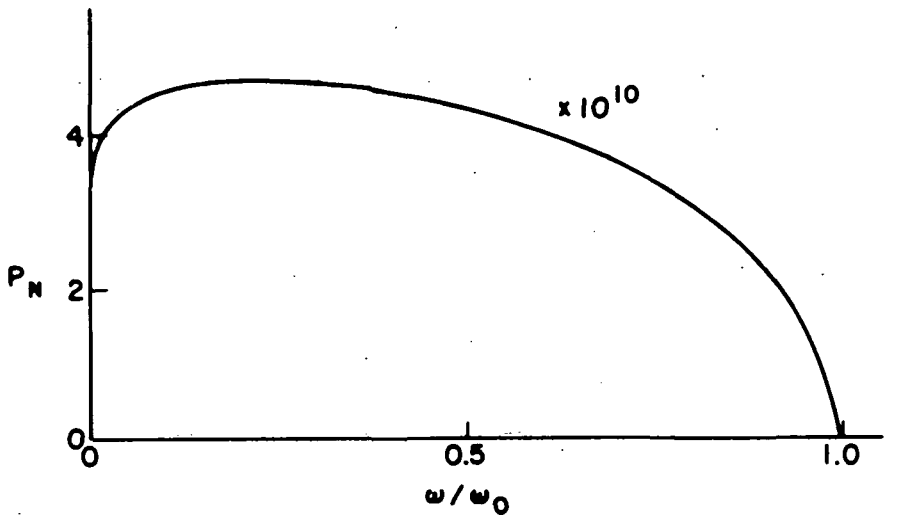

Fig. 3.14 Normalized power coefficient.

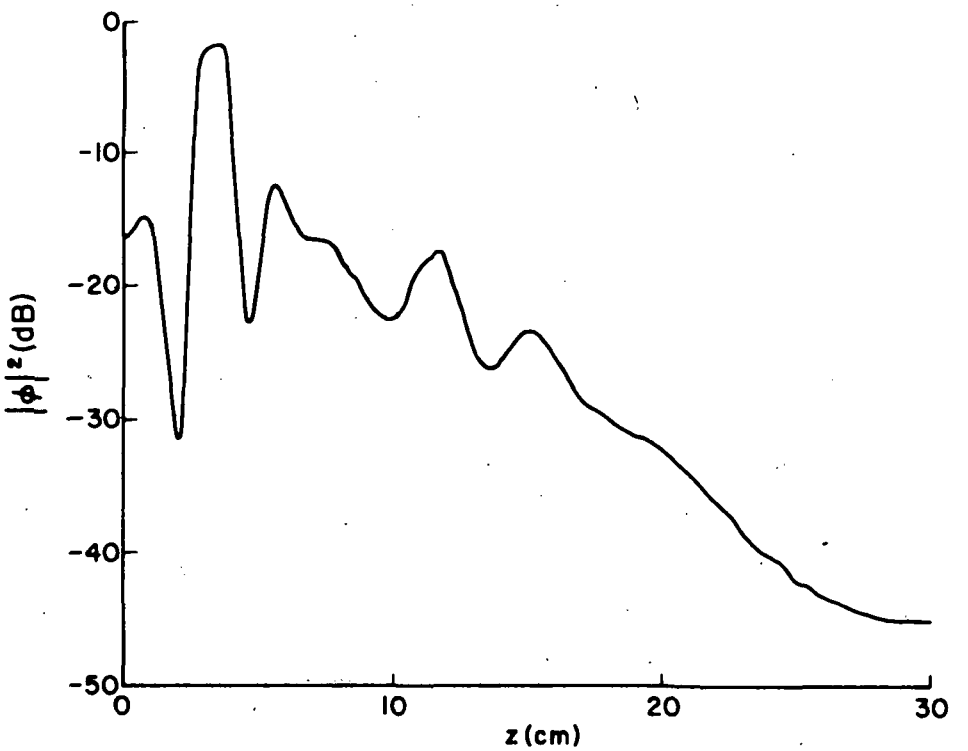

Fig. 3.15 Axial power profile for 220 MHz wave propagating alone.

be seen in the experimental curves as irregular spatial oscillations in the axial power curves, close to the exciting probe, as illustrated in Fig. 3.15. Finally, the pump power was not exactly constant, as required by the theory. Since the damping rate of the pump, as seen in Fig. 3.12(a), was smaller than the rate of change of the signal and the idler, it could be neglected in this particular experiment.

The measurements that we have just described were typical of all of the energy exchange measurements that we obtained. A summary of four series of measurements performed at a fixed signal frequency is presented in Fig. 3.16, which shows the dispersion characteristics measured for the pump, the signal and the idler. The lower two frequencies involved in a given interaction are indicated by the same number on the curves. It can be seen that the synchronism conditions are not even approximately satisfied in most of the cases. The points forming the experimental dispersion characteristic of the idler are also shown in Fig. 3.11 where they fall between the curves for the $n = 0$, $\ell = 2$ branches of the theoretical dispersion relation. It should be noted that these experimental points were plotted on the dimensionless graph of Fig. 3.11 using the values of a and ω_0 obtained from the best fit for the linear measurements.

The influence of Δk on the solutions, which was considered one of the main reasons for the discrepancy between the theory and the experiments, was determined by recording the position of the maximum in the idler curve as a function of Δk. This is shown in Fig. 3.17. The distance of the maximum, z_m, was measured from Probe 2, on which the signal was injected. A similar curve, given in Fig. 3.18, was obtained from Eq. (2.81) so as to show that the same trends could be predicted theoretically. The potential ψ_p was taken as 9.5 V, and the idler damping was chosen arbitrarily as 0.03 neper/cm, since the position of the maximum was found to depend weakly on this parameter.

The main difference between the theoretical and the experimental curves of Fig. 3.17 and 3.18 is the absence of experimental results when $\Delta k > 0$. The dispersion characteristics of Fig. 3.16 indicate that $\Delta k > 0$ would be obtained for pump frequencies higher than

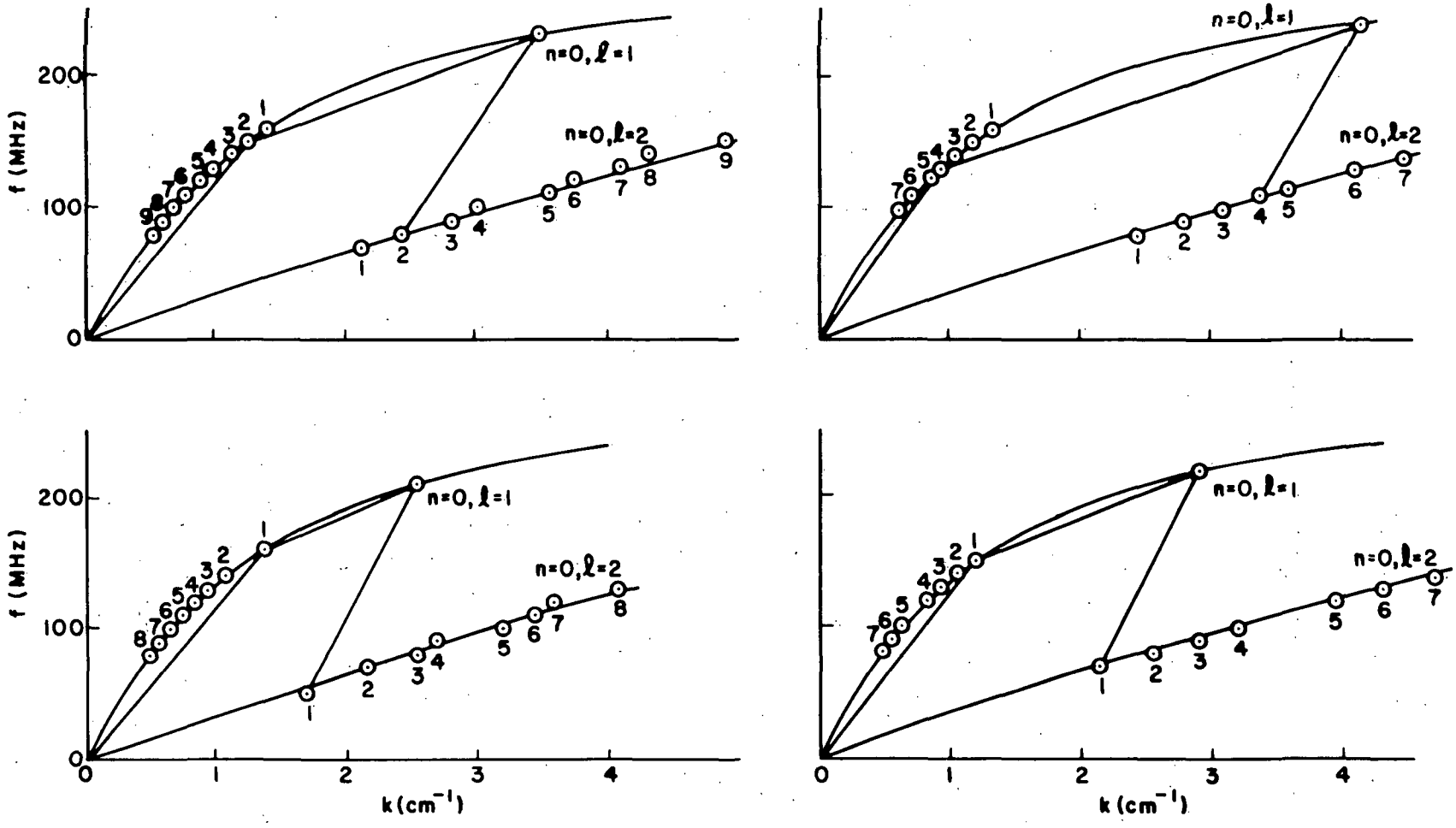

Fig. 3.16 Measurements of nonlinear coupling.

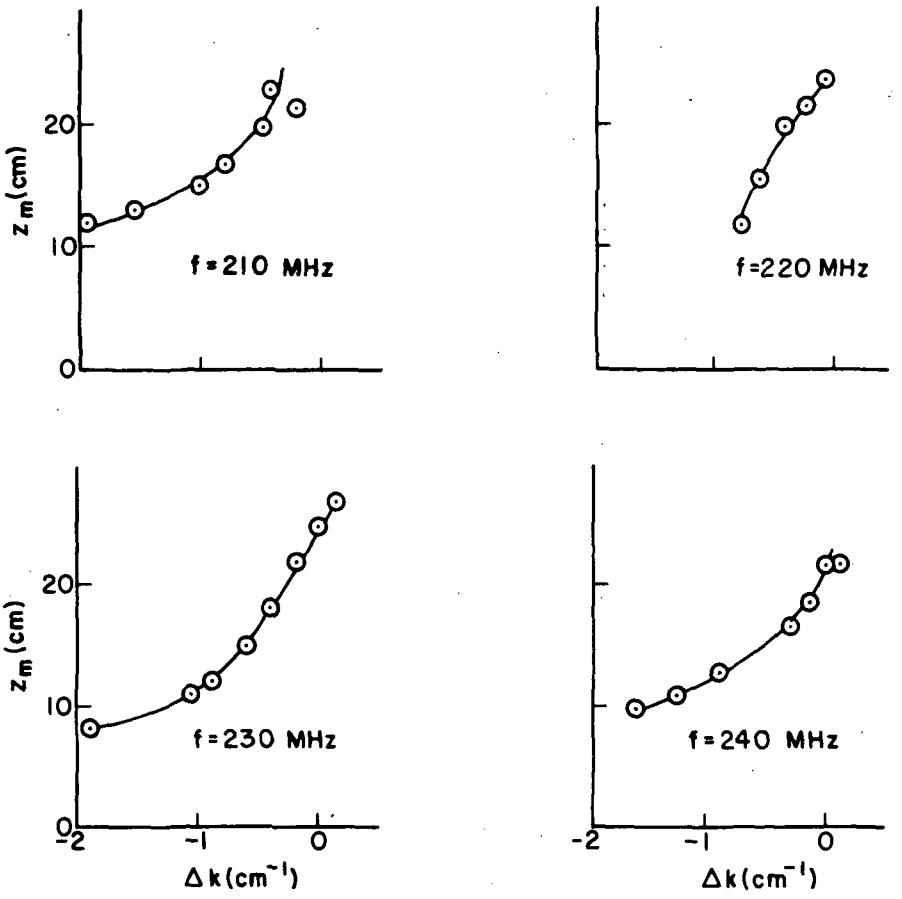

Fig. 3.17 Position of maximum in idler power curve: experiment.

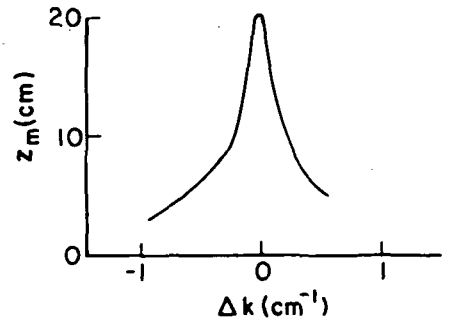

Fig. 3.18 Position of maximum in idler power curve: theory.

160 MHz($\omega/\omega_0 > 0.55$). The wave damping, already 0.5 dB/cm at 160 MHz, and increasing rapidly at higher frequencies, was probably the cause for the absence of measurements at frequencies higher than 160 MHz.

Chapter IV

SLOW WAVES ON A PLASMA COLUMN: NO MAGNETIC FIELD

Some of the linear properties of slow waves propagating on a plasma column in the absence of a static magnetic field were mentioned without proof in Chapter I. In Section 4.1, the linear properties of slow waves on a uniform plasma column surrounded by an infinite dielectric are reviewed in detail. Slow wave propagation can also be obtained on a plasma column surrounded by a combination of dielectric regions,[8] possibly bounded by a metal tube, but they are not considered here. As will be seen later, there cannot be any slow wave propagation in a metal tube completely filled with plasma in the absence of a static magnetic field. The nonlinear interaction of slow waves is studied in Section 4.2. The coupled mode equations are derived from a Lagrangian density, as in Section 2.2.1, and are solved for the case of parametric amplification.

4.1 Linear Regime

The relevant basic equations are obtained from Eq. (2.1)-(2.3), by using the quasistatic approximation and setting the DC magnetic field equal to zero. To first order in small perturbations, we obtain the equation of motion,

$$m_e \frac{\partial \underset{\sim}{v}}{\partial t} = - e\nabla\varphi \ , \tag{4.1}$$

the continuity equation,

$$\frac{\partial n}{\partial t} + N_0 \nabla \cdot \underset{\sim}{v} = 0 \ , \tag{4.2}$$

and Maxwell's equations,

$$\nabla \times \underset{\sim}{H} = N_0 e \underset{\sim}{v} - \epsilon_0 \frac{\partial}{\partial t} (\nabla\varphi) \ , \qquad \nabla^2\varphi = - \frac{ne}{\epsilon_0} \ . \tag{4.3}$$

For cylindrical waves of the form

$$\varphi(\underset{\sim}{r},t) = \hat{\varphi}(r) \exp \ j(\omega t - kz - n\theta) \ , \tag{4.4}$$

Equations (4.1)-(4.3) can be combined to yield

$$\left(1 - \frac{\omega_0^2}{\omega^2}\right)\left[\frac{1}{r}\frac{\partial}{\partial r}\left(r\frac{\partial\hat{\varphi}}{\partial r}\right) - \left(\frac{n^2}{r^2} + k^2\right)\hat{\varphi}\right] = 0 , \qquad r \le a. \quad (4.5)$$

The radial potential profile in the plasma column is given by

$$\hat{\varphi}(r) = \psi\, I_n(kr) , \qquad r \le a, \quad (4.6)$$

where $I_n(kr)$ is a modified Bessel function of the first kind. Since $\hat{\varphi}(r)$ is monotonically increasing, it is impossible to match the boundary condition at a metal surface at $r = a$ except for $\psi = 0$. This precludes slow wave propagation in a metal tube completely filled with plasma when there is no DC magnetic field. The potential φ satisfies Laplace's equation both outside and inside the plasma column. Outside, the potential profile is

$$\hat{\varphi}(r) = \hat{\psi}\, K_n(kr) , \qquad r \ge a. \quad (4.7)$$

The dispersion relation is obtained by requiring that the potential and the radial displacement be continuous at the boundary. These conditions yield

$$\hat{\psi} = \psi \frac{I_n'(ka)}{I_n(ka)} , \qquad \left(1 - \frac{\omega_0^2}{\omega^2}\right)\frac{I_n'(ka)}{I_n(ka)} - \epsilon_g \frac{K_n'(ka)}{K_n(ka)} = 0 . \quad (4.8)$$

In contrast to the infinite magnetic field case, there is only one root of the dispersion relation for each n. The dispersion characteristics for the $n = 0$, 1 and 2 modes are shown in Fig. 1.1. For large ka, the dispersion relation becomes

$$ka\left[\frac{\omega_0^2}{\omega^2} - 1 + \epsilon_g\right] = 0 , \quad (4.9)$$

and all the branches of the dispersion relation have a resonance ($k \to \infty$)

with $\omega = \omega_0/(1 + \epsilon_g)^{1/2}$. The small-ka limit of the dispersion relation is given by

$$1 - \frac{\omega_0^2}{\omega^2} = \begin{cases} -\dfrac{2\epsilon_g}{(ka)^2 |\ell n\ ka|} , & n = 0 , \\ -\epsilon_g & n \neq 0 . \end{cases} \tag{4.10}$$

The group velocities $(d\omega/dk)$ for $ka \approx 0$ are

$$[v_g]_{ka \approx 0} \approx \begin{cases} a\omega_0 \dfrac{|\ell n\ ka|^{1/2}}{\epsilon_g} , & n = 0 , \\ 0 , & n \neq 0 . \end{cases} \tag{4.11}$$

This equation indicates that, for $n = 0$, the group velocity is very large near the origin.

4.2 Nonlinear Regime

4.2.1 Derivation of the Coupled Mode Equations

The coupled mode equations are obtained in the same way as for slow waves in the presence of an infinite magnetic field. The notation from Chapter II will be used. In the present case, the second and third order parts of the Lagrangian densities are

$$\mathcal{L}_2 = N_0(r) \left[\frac{m_e}{2} \dot{\underline{\xi}} \cdot \dot{\underline{\xi}} + e\ (\underline{\xi} \cdot \nabla\varphi) \right] + \frac{\epsilon}{2} (\nabla\varphi)^2 , \tag{4.12}$$

$$\mathcal{L}_3 = \frac{1}{2} e\ N_0(r)\ \underline{\xi} \cdot [(\underline{\xi} \cdot \nabla)\nabla\varphi] , \tag{4.13}$$

where the vectorial expression contained in $\mathcal{L}_3$ is to be evaluated in cartesian coordinates, and then transformed into cylindrical coordinates. This is necessary because there is no vector operator ∇ in cylindrical coordinates, whereas Equation (3.13) was obtained from the Taylor series expansion of $\mathcal{L}$ in cartesian coordinates by using

$$\nabla \equiv \frac{\partial}{\partial x} \underline{i} + \frac{\partial}{\partial y} \underline{j} + \frac{\partial}{\partial z} \underline{k} . \tag{4.14}$$

Introducing the generalized coordinates as

$$\underset{\sim}{\xi} = \frac{\underset{\sim}{\xi} + \underset{\sim}{\xi}^*}{2} \quad , \qquad \varphi = \frac{\varphi + \varphi^*}{2} \quad , \tag{4.15}$$

the wave energy density, e_λ , is derived from $\mathcal{L}_2$ according to Eq. (2.30). The result is

$$e_\lambda = \frac{1}{4}\iint \left\{ N_0(r)\left[m_e(\dot{\underset{\sim}{\xi}}\cdot\dot{\underset{\sim}{\xi}}) - e(\underset{\sim}{\xi}_\lambda\cdot\nabla_\perp\varphi_\lambda^* + \underset{\sim}{\xi}_\lambda^*\cdot\nabla_\perp\varphi_\lambda)\right] - \epsilon(\nabla_\perp\varphi_\lambda\cdot\nabla_\perp\varphi_\lambda^*)\right\} d^2r \ , \tag{4.16}$$

$$\lambda = \alpha,\beta,\gamma \ .$$

The equation of motion, Eq. (4.1), can be integrated twice with respect to time to obtain the displacement, $\underset{\sim}{\xi}_\lambda$, in the plasma as

$$\underset{\sim}{\xi}_\lambda = \frac{e}{m_e\omega_\lambda^2}\nabla_\perp\varphi_\lambda \quad , \qquad \lambda = \alpha,\beta,\gamma \ . \tag{4.17}$$

The wave energy can now be written as

$$e_\lambda = \frac{\epsilon_0}{4}\left(3\frac{\omega_0^2}{\omega_\lambda^2} - 1\right)\iint_P [\nabla_\perp\varphi_\lambda\cdot\nabla_\perp\varphi_\lambda^*]\, d^2r - \frac{\epsilon}{4}\iint_D [\nabla_\perp\varphi_\lambda\cdot\nabla_\perp\varphi_\lambda^*]\, d^2r, \lambda=\alpha,\beta,\gamma, \tag{4.18}$$

where the first integral is taken over the cross-section of the plasma in a plane perpendicular to the axis of the column, and the second integral is in the same plane, but outside the plasma column. The integrations in Eq. (4.18) are performed using the linear expressions for φ_λ given by Eq. (4.6) for the plasma, and by Eq. (4.7) for the dielectric, and give the wave energy density as

$$e_\lambda = \frac{\pi\epsilon_0}{2}\frac{\omega_0^2}{\omega_\lambda^2}\, k_\lambda a\, I_{n\lambda}(k_\lambda a) I'_{n\lambda}(k_\lambda a)\psi_\lambda\psi_\lambda^* \quad , \qquad \lambda = \alpha,\beta,\gamma \ . \tag{4.19}$$

It is interesting to note that the wave energy density is expressed as a surface term. In the cases studied in Chapter II, the wave energy

density given by Eq. (2.40) contained an integral over the cross-section of the plasma column. This stems from the fact that, for an infinite magnetic field, an RF charge density occurs in the volume of the plasma; if there is no magnetic field, the RF charge density is restricted to the surface of the column, since φ_λ satisfies Laplace's equation in the plasma.

The coupling energy is given by

$$\epsilon_c = \frac{jeN_0}{8} \iint_P \left\{ \underline{\xi}_\alpha^* \cdot [(\underline{\xi}_\beta \cdot \nabla)\nabla\varphi_\gamma] + \underline{\xi}_\alpha^* \cdot [(\underline{\xi}_\gamma \cdot \nabla)\nabla\varphi_\beta] + \underline{\xi}_\beta \cdot [(\underline{\xi}_\gamma \cdot \nabla)\nabla\varphi_\alpha^*] \right\} d^2r + (c.c.). \tag{4.20}$$

Using the expression for $\underline{\xi}_\lambda$ given by Eq. (4.17), this equation becomes

$$e_c = \frac{j\,\omega_0^2 e}{8m_e} \epsilon_0 \iint_P \left\{ \frac{\nabla\varphi_\beta}{\omega_\alpha^2 \omega_\beta^2} \cdot \left[(\nabla\varphi_\alpha^* \cdot \nabla)\nabla\varphi_\gamma\right] + \frac{\nabla\varphi_\gamma}{\omega_\alpha^2 \omega_\gamma^2} \cdot \left[(\nabla\varphi_\alpha^* \cdot \nabla)\nabla\varphi_\beta\right] + \frac{\nabla\varphi_\beta}{\omega_\beta^2 \omega_\gamma^2} \cdot \left[(\nabla\varphi_\gamma \cdot \nabla)\nabla\varphi_\alpha^*\right] \right\} d^2r + (c.c.) \quad . \tag{4.21}$$

It is shown in Appendix B that the coupling energy density can be written as

$$e_c = \frac{j\omega_0^2 e\epsilon_0}{4m_e \omega_\alpha^2} \left\{ \pi a \left[\frac{1}{\omega_\beta^2} \frac{\partial\varphi_\beta}{\partial r} (\nabla\varphi_\alpha^* \cdot \nabla\varphi_\gamma) + \frac{1}{\omega_\gamma^2} \frac{\partial\varphi_\gamma}{\partial r} (\nabla\varphi_\alpha^* \cdot \nabla\varphi_\beta) \right]_{r=a} \right.$$

$$+ \pi\Delta k \int_0^a \left[\frac{k_\beta}{\omega_\beta^2} \varphi_\beta (\nabla\varphi_\alpha^* \cdot \nabla\varphi_\gamma) + \frac{k_\gamma}{\omega_\gamma^2} (\nabla\varphi_\alpha^* \cdot \nabla\varphi_\beta) \right] r\, dr$$

$$\left. + \frac{1}{\omega_\beta \omega_\gamma} \iint_P \left[\nabla\varphi_\beta \cdot (\nabla\varphi_\gamma \cdot \nabla)\nabla\varphi_\alpha^* \right] d^2r \right\} + (c.c.) \,, \tag{4.22}$$

where

$$\Delta k = k_\alpha - k_\beta - k_\gamma \ . \tag{4.23}$$

It can be seen from the dispersion characteristics presented in Fig. 1.1 that the only way to satisfy the synchronism conditions, at least approximately, is by coupling three $n = 0$ waves with frequencies small enough to make use of the almost linear portion of the dispersion characteristic near the origin. In this case, the coupling energy density becomes, after substituting Eq. (4.6) in Eq. (4.22),

$$e_c = \frac{j\pi\omega_0^2 e\epsilon_0}{4m_e} C_{\alpha\beta\gamma} \ , \tag{4.24}$$

where

$$C_{\alpha\beta\gamma} = \frac{k_\alpha k_\beta k_\gamma}{\omega_\alpha^2} \Bigg\{ a \left[\left(\frac{1}{\omega_\beta^2} + \frac{1}{\omega_\gamma^2} \right) I_0'(k_\alpha a) I_0'(k_\beta a) I_0'(k_\gamma a) \right.$$

$$\left. + I_0(k_\alpha a) \left(\frac{1}{\omega_\beta^2} I_0'(k_\beta a) I_0(k_\gamma a) + \frac{1}{\omega_\gamma^2} I_0(k_\beta a) I_0'(k_\gamma a) \right) \right]$$

$$+ \int_0^a \left[\frac{2k_\alpha}{\omega_\beta \omega_\gamma} I_0''(k_\alpha r) I_0'(k_\beta r) I_0'(k_\gamma r) + \left(\frac{\Delta k}{\omega_\beta^2} + \frac{2k_\alpha}{\omega_\beta \omega_\gamma} \right) I_0'(k_\alpha r) I_0(k_\beta r) I_0'(k_\gamma r) \right.$$

$$+ \left(\frac{\Delta k}{\omega_\gamma^2} + \frac{2k_\alpha}{\omega_\beta \omega_\gamma} \right) I_0'(k_\alpha r) I_0'(k_\beta r) I_0(k_\gamma r)$$

$$\left. + \left(\frac{\Delta k}{\omega_\beta^2} + \frac{\Delta k}{\omega_\gamma^2} + \frac{2k_\alpha}{\omega_\beta \omega_\gamma} \right) I_0(k_\alpha r) I_0(k_\beta r) I_0(k_\gamma r) \right] r \, dr \Bigg\} + (c.c.) \ . \tag{4.25}$$

The modified Bessel functions on the RHS of Eq. (4.25) can be expanded in the small $k_\lambda a$ limit, and the result is

$$C_{\alpha\beta\gamma} = \frac{k_\alpha k_\beta k_\gamma}{2}\left\{\frac{k_\alpha}{\omega_\beta^2\omega_\gamma^2}\left[1 + \frac{a^2}{8}\left(k_\alpha^2 + k_\alpha(k_\beta + k_\gamma) + k_\beta^2 + k_\gamma^2\right)\right]\right.$$

$$- \frac{k_\beta}{\omega_\alpha^2\omega_\gamma^2}\left[1 + \frac{a^2}{8}\left(k_\beta^2 + k_\beta(k_\alpha - k_\gamma) + k_\alpha(k_\beta - k_\gamma) + k_\gamma^2\right)\right.$$

$$\left.\left. - \frac{k_\gamma}{\omega_\alpha^2\omega_\beta^2}\left[1 + \frac{a^2}{8}\left(k_\gamma^2 + k_\gamma(k_\alpha - k_\beta) + k_\alpha(k_\gamma - k_\beta) + k_\beta^2\right)\right] + \frac{k_\alpha k_\beta k_\gamma a^2}{\omega_\alpha^2\omega_\beta\omega_\gamma}\right\}\psi_\alpha^*\psi_\beta\psi_\gamma\right.$$

$$+ (c.c.) \quad . \qquad (4.26)$$

The energy conservation equations are given by

$$\frac{\sigma_\lambda}{\omega_\lambda}\left(\frac{\partial}{\partial t} + v_{g\lambda}\frac{\partial}{\partial z}\right)\psi_\lambda\psi_\lambda^* = \frac{-je}{2m_e}\omega_\lambda^2\frac{C_{\alpha\beta\gamma}}{G_\lambda}\psi_\alpha^*\psi_\beta\psi_\gamma + (c.c.) \ , \qquad (4.27)$$

where

$$G_\lambda = k_\lambda a I_0(k_\lambda a) I_0'(k_\lambda a) \simeq \frac{k_\lambda^2 a^2}{2}\left(1 + \frac{k_\lambda^2 a^2}{4}\right) \ . \qquad (4.28)$$

4.2.2 Parametric Amplification

It can be seen from Eq. (4.10) that the synchronism conditions cannot be satisfied exactly, even for small ka. It is consequently important to include Δk in the calculation of the gain, which is given by Eq. (2.77) as

$$\Gamma = 8.69\ \mathrm{Re}\left[\chi^2 - \frac{\Delta k^2}{4}\right]^{1/2} \ \mathrm{dB/m} \ . \qquad (4.29)$$

In the present case,

$$\chi^2 = \frac{F_s F_i}{v_{gs} v_{gi}}|\psi_p|^2 \ , \qquad (4.30)$$

where

$$F_\lambda = \frac{e}{2m_e} \omega_\lambda^3 \frac{C_{\alpha\beta\gamma}}{G_\lambda} \quad . \tag{4.31}$$

Figure 4.1 presents numerical values of Γ for a special case. Since χ is inversely proportional to v_{gs} and v_{gi}, the smaller the pump frequency, the smaller the gain. This explains the increase of Γ with the pump frequency, even though Δk is increasing at the same time, due to the curvature of the dispersion characteristics. In practice, the gain would be reduced by damping, which increases with frequency.

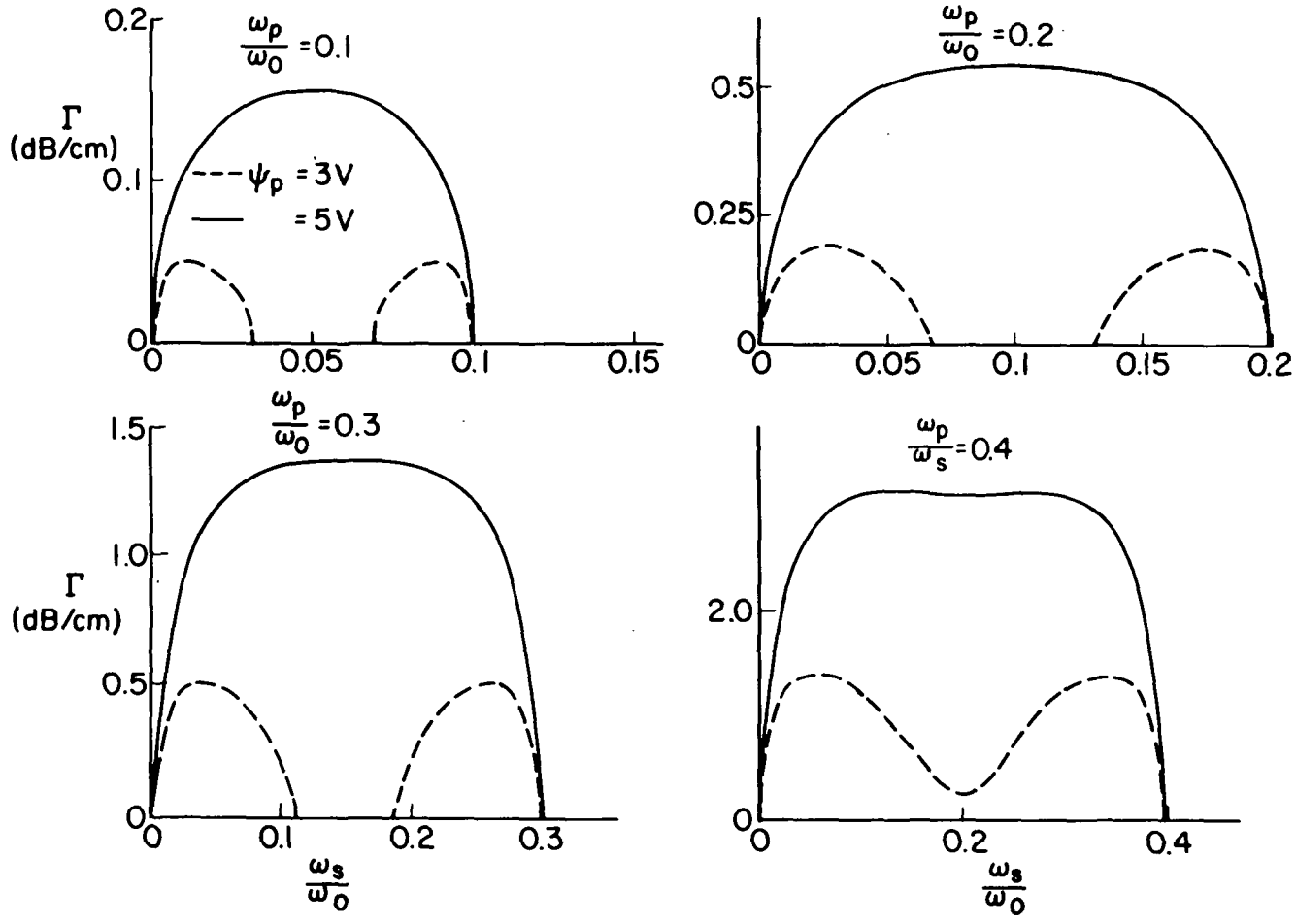

Fig. 4.1 Gain as a function of signal frequency at fixed pump frequency for $\omega_c = 0$: column surrounded by vacuum. a=0.4 cm; $N_0=10^8/cm^3$.

Chapter V

NONLINEAR SCATTERING FROM A PLASMA COLUMN

In this chapter, we shall use hydrodynamic plasma theory to study the resonances of a plasma column irradiated by a plane wave. In this model, the first two velocity moments of the Vlasov equation are kept, i.e. the continuity equation,

$$\nabla \cdot (N\underset{\sim}{v}) + \frac{\partial N}{\partial t} = 0 \ , \tag{5.1}$$

and the equation of motion,

$$m_e N \frac{d\underset{\sim}{v}}{dt} = Ne\underset{\sim}{E} - \nabla p - m_e \nu N\underset{\sim}{v} \ , \tag{5.2}$$

where ν is the effective momentum transfer collision frequency. Maxwell's equations, given in Eq. (2.3), are used to close the set of equations. Since the radius of the plasma column used in our experiments is much smaller than a free space wavelength, the quasistatic approximation can be used. The higher order multipoles in the expansion of the plane wave will be retained in the analysis; previous work has shown that some of the higher order terms contribute significantly to nonlinear scattering from a cold uniform plasma column, even in the small-ka limit.[62] It is also important to include in the theory a nonuniform static electron density profile, in order to obtain linear resonance frequencies which agree well with the experimental results.[44]

In Section 5.1.1, Eqs. (2.3), (5.1) and (5.2) are linearized in the quasistatic approximation, and a differential equation for the potential inside the plasma column is obtained for a parabolic electron density profile. The special case of a uniform plasma column, for which an analytical solution can be obtained, is considered in Section 5.1.2. Usually,[44] the solution for the potential inside the plasma column is matched to solutions of Laplace's equation outside. This approach neglects radiation effects, and yields infinite fields at resonance unless loss is introduced into the theory. Instead, we shall obtain the magnetic field, $\underline{H}$, inside the plasma column by use of the Maxwell equation

$$\nabla \times \underset{\sim}{H} = \underset{\sim}{J} + \epsilon_0 \frac{\partial \underset{\sim}{E}}{\partial t} , \qquad (5.3)$$

and match it to the solutions of the wave equation for $\underset{\sim}{H}$ outside the column. The power scattered by the column is obtained in Section 5.1.3, and numerical results are presented in Section 5.1.4.

Having obtained the linear solution of the problem, we consider the nonlinear mixing of two incident waves. Equations (2.3), (5.1) and (5.2) are expanded up to second order, to obtain the equations of the nonlinear problem. The nonlinear fields in the plasma column are obtained in Section 5.2.1, and are matched to the fields outside in Section 5.2.2. Numerical results for harmonic generation are presented in Section 5.2.3.

5.1 Linear Theory

We consider an infinitely long plasma column contained in a glass tube of relative permittivity ϵ_g. The geometry of the problem is illustrated in Fig. 5.1. The incoming wave sets up $\underset{\sim}{E}$ and $\underset{\sim}{H}$ fields

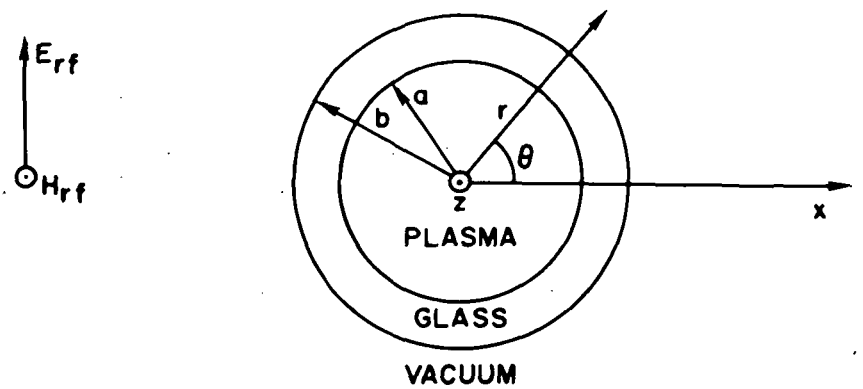

FIG. 5.1. Incoming wave, and plasma column surrounded by glass wall.

in the glass tube and plasma column, and some power is scattered. The r-dependence of the $\underset{\sim}{H}$ fields in the three regions formed by the plasma, the glass tube, and free space can be written as

$$H_z(\underline{r}) = \sum_{\ell=-\infty}^{+\infty} H_{z\ell}(\underline{r}) = H_0 \sum_{\ell=-\infty}^{+\infty} M_\ell \mathcal{H}_{z\ell}(r) \exp j\ell\theta \ , \qquad r \le a \ , \qquad (5.4)$$

$$H_z(\underline{r}) = H_0 \sum_{\ell=-\infty}^{+\infty} \left[B_\ell H_\ell^{(1)}(k_g r) + C_\ell H_\ell^{(2)}(k_g r) \right] \exp j\ell\theta \ , \qquad a \le r \le b \ , \qquad (5.5)$$

$$H_z(\underline{r}) = H_0 \sum_{\ell=-\infty}^{+\infty} \left[S_\ell H_\ell^{(2)}(kr) + j^{-\ell} J_\ell(kr) \right] \exp j\ell\theta \ , \qquad b \le r \ , \qquad (5.6)$$

where

$$k_g = \epsilon_g^{1/2} k \ , \qquad (5.7)$$

H_0 is the amplitude of the magnetic field of the incident wave, and $H_\ell^{(1)}$ and $H_\ell^{(2)}$ are the Hankel functions of the first and second kind; assuming time variation as exp $j\omega t$, they represent the r-dependence of ingoing and outgoing waves in a cylindrically symmetric source-free medium.

5.2.1 Potential Inside a Nonuniform Plasma Column

If the quasistatic approximation, $\underline{E} = -\nabla\varphi$, is used in Eqs. (2.3), (5.1) and (5.2), we have

$$\nabla\cdot(N\underline{v}) + \frac{\partial N}{\partial t} = 0 \ , \qquad m_e N \frac{d\underline{v}}{dt} = -Ne\nabla\varphi - \nabla p - m_e \nu N\underline{v} \ , \qquad (5.8)$$

$$\nabla\times\underline{H} = \underline{J} - \epsilon_0 \frac{\partial\nabla\varphi}{\partial t} \ , \qquad \nabla^2\varphi = -\frac{Ne}{\epsilon_0} \ . \qquad (5.9)$$

The static electron density profile will be expressed as $N_0 f(r)$, where N_0 is the electron density on the axis of the column. The static charge gradient is accompanied by a static potential profile, $\varphi_0(\underline{r})$, given by Boltzmann's law,

$$\nabla\varphi_0 = -\frac{\kappa T}{e}\frac{\nabla f}{f} \ . \qquad (5.10)$$

An adiabatic pressure law is used for the first order pressure term to truncate the series of moment equations.[37] The pressure becomes

$$p(\underset{\sim}{r},t) = [N_0 f(r) + \gamma\, n(\underset{\sim}{r},t)]\kappa T \ , \qquad (5.11)$$

where κ is the Boltzmann constant, T is the electron temperature and γ is the compression constant for the electron gas. For one-dimensional adiabatic compression, $\gamma = 3$. For time variations as exp $j\omega t$, Eq. (5.8) becomes, to first order,

$$N_0 \nabla\cdot(f\underset{\sim}{v}) = - j\omega n \ , \qquad (5.12)$$

$$jm_e N_0 \Gamma\omega f\underset{\sim}{v} = -eN_0 f\nabla\varphi + \kappa T \frac{\nabla f}{f} n - \gamma\kappa T\nabla n \ , \qquad (5.13)$$

where

$$\Gamma = 1 - j\nu/\omega \ . \qquad (5.14)$$

The equation for the potential is obtained by taking the divergence of Eq. (5.13), and then using Eq. (5.12) and Poisson's equation to eliminate n and $\underset{\sim}{v}$. The result is

$$\nabla^4\varphi - \frac{1}{\gamma}\nabla\cdot\left(\nabla^2\varphi\,\frac{\nabla f}{f}\right) + \frac{1}{\gamma\lambda_D^2}\left[\left(\frac{\Gamma\omega^2}{\omega_0^2} - f\right)\nabla^2\varphi - \nabla f\cdot\nabla\varphi\right] = 0 \ . \qquad (5.15)$$

The solution of Eq. (5.15) is of the form

$$\varphi(\underset{\sim}{r}) = \sum_{\ell=-\infty}^{+\infty} \varphi_\ell(\underset{\sim}{r}) = \sum_{\ell=-\infty}^{+\infty} \psi_\ell(r)\ \exp j\ell\theta \ , \qquad 0 \le r \le a. \qquad (5.16)$$

Substituting Eq. (5.16) in Eq. (5.15) yields

$$D_\ell \psi_\ell \equiv \left\{ \frac{\partial^4}{\partial r^4} + \left[\frac{2}{r} - \frac{f'}{\gamma f}\right]\frac{\partial^3}{\partial r^3} + \left[\frac{1}{\gamma\lambda_D^2}\left(\frac{\Gamma\omega^2}{\omega_0^2} - f\right) - \frac{(2\ell^2+1)}{r^2} - \frac{1}{\gamma}\left(\frac{f''}{f} - \frac{f'^2}{f^2}\right) - \frac{2f'}{\gamma r f}\right]\frac{\partial^2}{\partial r^2} \right.$$

$$+\left[\frac{(2\ell^2+1)}{r^3} - \frac{1}{\gamma r}\left(\frac{f''}{f} - \frac{f'^2}{f^2}\right) + \frac{\ell^2 f'}{\gamma r^2 f} + \frac{1}{\gamma\lambda_D^2 r}\left(\frac{\Gamma\omega^2}{\omega_0^2} - f\right) - \frac{f'}{\lambda_D^2\gamma}\right]\frac{\partial}{\partial r}$$

$$\left.+\left[\frac{\ell^2}{\gamma r^2}\left(\frac{f''}{f} - \frac{f'^2}{f^2}\right) - \frac{\ell^2 f'}{\gamma r^3 f} - \frac{\ell^2(4-\ell^2)}{r^4} - \frac{\ell^2}{\gamma r^2\lambda_D^2}\left(\frac{\Gamma\omega^2}{\omega_0^2} - f\right)\right]\right\}\psi_\ell = 0,$$

$$0 \le r \le a. \quad (5.17)$$

This fourth order differential equation has a regular singularity at $r = 0$. It is also singular when $f = 0$. In this work, a parabolic electron density profile will be used as an approximation of the profile of a positive column

$$f(r) = 1 - \alpha(r/a)^2, \qquad 0 \le r \le a. \quad (5.18)$$

It is usually recognized that $\alpha = 0.6$ gives a good approximation of the actual profile when $a/\lambda_D \to \infty$.[45] Since the zero of f occurs outside the range of integration, it does not have any effect on the solution.

A solution of Eq. (5.17) by the method of Frobenius is presented in Appendix C, and two linearly independent solutions are found which are regular at $r = 0$. The other two solutions are shown to be singular at $r = 0$. The two series solutions that are regular at $r = 0$, $\psi_{\ell 1}(r)$ and $\psi_{\ell 2}(r)$, are used to start the numerical integration of Eq. (5.17), and the potential, ψ_ℓ, can be written formally as

$$\psi_\ell(r) = H_0\left[M_\ell \psi_{\ell 1}(r) + P_\ell \psi_{\ell 2}(r)\right], \quad 0 \le r \le a. \quad (5.19)$$

The solution given by Eq. (5.19) contains two constants. One of these can be eliminated by requiring that the radial electron velocity vanish at $r = a$ since the plasma column is enclosed in a glass tube.

In an experimental plasma, a sheath at the plasma-glass boundary insures that this boundary condition is satisfied. The velocity can be obtained from Eq. (5.13), and becomes, after using Poisson's equation,

$$\underset{\sim}{v} = \frac{je}{m_e \Gamma \omega}\left[\nabla\varphi + \lambda_D^2 \frac{\nabla f}{f^2}\nabla^2\varphi - \gamma\frac{\lambda_D^2}{f}\nabla(\nabla^2\varphi)\right] . \tag{5.20}$$

After substituting Eqs. (5.16) and (5.19) in Eq. (5.20), the radial velocity can be set equal to zero. We obtain finally

$$\psi_\ell(r) = M_\ell H_0\left[\psi_{\ell 1}(r) - \frac{h_{\ell_1}(a)}{h_{\ell_2}(a)}\psi_{\ell 2}(r)\right] , \tag{5.21}$$

where

$$h_{\ell_j}(r) = -\gamma\psi'''_{\ell j} + \left[\frac{f'}{f} - \frac{\gamma}{r}\right]\psi''_{\ell j} + \left[\frac{f}{\lambda_D^2} + \frac{f'}{rf} + (\ell^2+1)\frac{\gamma}{r^2}\right]\psi'_{\ell j} - \ell^2\left[\frac{f'}{fr^2} + \frac{2\gamma}{r^3}\right]\psi_\ell . \tag{5.22}$$

We now write expressions for the variables $\underset{\sim}{v}$ and n which will be needed later,

$$\underset{\sim}{v}_\ell = \frac{je\lambda_D^2 H_0}{m_e\Gamma\omega f} M_\ell\left\{\left[h_{\ell 1}(r) - \frac{h_{\ell_1}(a)}{h_{\ell_2}(a)}h_{\ell 2}(r)\right]\underset{\sim}{i} + \frac{j\ell}{r}\left[g_{\ell 1}(r) - \frac{h_{\ell_1}(a)}{n_{\ell_2}(a)}g_{\ell 2}(r)\right]\underset{\sim}{j}\right\} \times \exp j\ell\theta , \tag{5.23}$$

where

$$g_{\ell_j}(r) = -\gamma\left(\psi''_{\ell j} + \frac{\psi'_{\ell j}}{r}\right) + \left(\frac{f}{\lambda_D^2} + \frac{\gamma\ell^2}{r^2}\right)\psi_{\ell j} , \tag{5.24}$$

and

$$n_\ell = -\frac{\epsilon_0}{e}\nabla^2\varphi_\ell = -\frac{\epsilon_0}{e}\left\{\psi''_\ell + \frac{\psi'_\ell}{r} - \frac{\ell^2}{r^2}\psi_\ell\right\}\exp j\ell\theta . \tag{5.25}$$

Finally, we must obtain the field $H_{z\ell}(\underset{\sim}{r})$ from the potential φ_ℓ ,

in order to match the solution in the plasma to the solution outside. To first order, the radial component of Eq. (5.3) is

$$\frac{1}{r}\frac{\partial H_{z\ell}}{\partial \theta} = N_0 e v_{\ell r} - j\omega\epsilon_0 \frac{\partial \varphi_\ell}{\partial r} . \qquad (5.26)$$

Since all the quantities on the RHS of Eq. (5.26) vary as exp $j\ell\theta$, we obtain

$$H_{z\ell}(\underline{r}) = H_0 \mathcal{H}_{z\ell}(r)\exp\, j\ell\theta = \frac{r}{j\ell}\left(N_0 e v_{\ell r} - j\omega\epsilon_0 \frac{\partial \varphi_\ell}{\partial r}\right), \quad |\ell| > 0 . \qquad (5.27)$$

The restriction put on ℓ comes from the fact that H_{z0} would be infinite according to Eq. (5.27). This means that the $\ell = 0$ solution cannot be obtained from the quasistatic approximation. It has been shown for a cold uniform plasma column that the terms with $\ell = 0$ do not contribute to the nonlinear scattering in the limit of a small column radius.[62] It is plausible to expect that the same thing happens in case of a warm plasma. To evaluate the $\ell = 0$ terms, it would be necessary to take the small radius limit of the solution obtained from the full electromagnetic treatment, which we have decided not to use because of its complexity.

5.1.2 Potential Inside a Uniform Plasma Column

In this case, an analytical solution for the potential can be obtained.[44] Equation (5.15) becomes

$$\nabla^2\left(\nabla^2 + k_p^2\right)\varphi = 0 , \qquad (5.28)$$

where

$$k_p^2 = \frac{1}{\gamma\lambda_D^2}\left(\frac{\Gamma\omega^2}{\omega_0^2} - 1\right) . \qquad (5.29)$$

The solutions of the two equations

$$\nabla^2\varphi = 0 , \qquad \left(\nabla^2 + k_p^2\right)\varphi = 0 , \qquad (5.30)$$

are also the solutions of Eq. (5.28). The potential given by Eq. (5.16) can be used in Eq. (5.30), and the following equations are obtained

$$\psi''_{\ell 1} + \frac{\psi'_{\ell 1}}{r} - \ell^2 \frac{\psi_{\ell 1}}{r^2} = 0 , \qquad \frac{1}{r}\frac{\partial}{\partial r}\left(r \frac{\partial \psi_{\ell 2}}{\partial r}\right) + \left(k_p^2 - \frac{\ell^2}{r^2}\right) \psi_{\ell 2} = 0 . \qquad (5.31)$$

Each of these two equations has two linearly independent solutions, one of which is singular at $r = 0$. Keeping only the regular solutions, $\psi_\ell(r)$ is

$$\psi_\ell(r) = H_0\left[M_\ell J_\ell(k_p r) + P_\ell r^{|\ell|}\right] , \qquad |\ell| \geq 1 . \qquad (5.32)$$

Requiring that the radial velocity vanish at $r = a$ yields

$$\psi_\ell(r) = M_\ell H_0 \left[J_\ell(k_p r) - \frac{\Gamma\omega^2}{\omega_0^2} k_p a \frac{J'_\ell(k_p a)}{|\ell|} \left(\frac{r}{a}\right)^{|\ell|} \right] . \qquad (5.33)$$

The velocity associated with the ℓ mode is

$$\underset{\sim}{v}_\ell(r) = - \frac{M_\ell H_0 k_p \omega_e}{j m_e \omega_0^2} \left\{ \left[J'_\ell(k_p r) - J'_\ell(k_p a) \left(\frac{r}{a}\right)^{|\ell|-1} \right] \underset{\sim}{i} \right.$$

$$\left. + j\ell \left[\frac{J_\ell(k_p r)}{k_p r} - \frac{J'_\ell(k_p a)}{|\ell|} \left(\frac{r}{a}\right)^{|\ell|-1} \right] \underset{\sim}{j} \right\} \exp j\ell\theta , \qquad (5.34)$$

and the electron density is

$$n_\ell = M_\ell H_0 \frac{\epsilon_0}{e} k_p^2 J_\ell(k_p r) \exp(j\ell\theta) . \qquad (5.35)$$

5.1.3 Scattered Power

The first step in calculating the scattered power is the matching of the tangential electric field, and of the radial displacement, at the interfaces. This determines the constants M_ℓ, B_ℓ, C_ℓ and S_ℓ in Eqs. (5.4)-(5.6). The boundary conditions on the electric

field, rather than the magnetic field, are used for convenience. The displacement in the plasma, including the polarization, can be obtained by writing Poisson's equation

$$\nabla \cdot \epsilon_0 \underset{\sim}{E} = ne \ , \tag{5.36}$$

and using the continuity equation, Eq. (5.12), to yield

$$\nabla \cdot \epsilon_0 \underset{\sim}{E} = j \frac{N_0 e}{\omega} \nabla \cdot (f\underset{\sim}{v}) \ . \tag{5.37}$$

The displacement can then be written as

$$\underset{\sim}{D} = \epsilon_0 \underset{\sim}{E} - j \frac{N_0 e}{\omega} f\underset{\sim}{v} \ . \tag{5.38}$$

Since the radial velocity is assumed to vanish at $r = a$, the radial displacement at the boundary is simply

$$D_r(a) = \epsilon_0 E_r(a) = - \epsilon_0 \varphi'(a) \ . \tag{5.39}$$

We obtain, as a function of the potential $\psi_\ell(a)$,

$$M_\ell = \frac{8\ell \ j^{-\ell}}{\pi^2 \epsilon_0 k^2 a^2 b \omega R_\ell \psi_\ell(a)} \ , \qquad B_\ell = \frac{2\epsilon_g^{1/2} F_{\ell 2} j^{-\ell+1}}{\pi k b R_\ell} \ ,$$

$$C_\ell = - \frac{2\epsilon_g^{1/2} F_{\ell 1} j^{-\ell+1}}{\pi k b R_\ell} \ , \qquad S_\ell = - \frac{j^{-\ell}}{R_\ell} \left[\epsilon_g^{1/2} V_\ell J_\ell'(kb) - V_\ell' J_\ell(kb) \right] \ , \tag{5.40}$$

where

$$R_\ell = \epsilon_g^{1/2} V_\ell H_\ell^{(2)'}(kb) - V_\ell' H_\ell^{(2)}(kb) \ , \tag{5.41}$$

$$F_{\ell j} = L_{n\ell} H_\ell^{(j)'}(k_g a) - \frac{\ell^2 \epsilon_g^{1/2}}{ka^2} H_\ell^{(j)}(k_g a) ,$$

$$L_{n\ell} = \frac{\psi_\ell'(a)}{\psi_\ell(a)} , \qquad V_\ell = F_{\ell 1} H_\ell^{(2)}(k_g b) - F_{\ell 2} H_\ell^{(1)}(k_g b) , \tag{5.42}$$

$$V_\ell' = F_{\ell 1} H_\ell^{(2)'}(k_g b) - F_{\ell 2} H_\ell^{(1)'}(k_g b) .$$

Since the exciting magnetic field term, $j^{-\ell} J_\ell(kr)$, is symmetrical with respect to an interchange between ℓ and $-\ell$, the scattered magnetic field must also be symmetrical. It is given by

$$H_{zs}(\underset{\sim}{r}) = 2H_0 \sum_{\ell=1}^{\infty} S_\ell H_\ell^{(2)}(kr) \cos \ell\theta , \tag{5.43}$$

while the scattered electric field is obtained from Eq. (5.3) as

$$E_{\theta s}(\underset{\sim}{r}) = \frac{2jkH_0}{\omega\epsilon_0} \sum_{\ell=1}^{\infty} S_\ell H_\ell^{(2)'}(kr) \cos \ell\theta . \tag{5.44}$$

If we use the convention $\bar{\underset{\sim}{A}} = \underset{\sim}{A} + \underset{\sim}{A}^*$, where $\bar{\underset{\sim}{A}}$ is a real field vector and $\underset{\sim}{A}$ is a complex vector of the form $\hat{\underset{\sim}{A}}(r) \exp j(\omega t - n\theta - kz)$, the incoming power is related to the magnetic field intensity by

$$P_i = 2 \mu_0 c H_0^2 , \tag{5.45}$$

where c is the velocity of light. The average scattered power is given by

$$P_s = E_\theta H_z^* + E_\theta^* H_z , \tag{5.46}$$

which becomes, after using Eqs. (5.43) and (5.44) for the fields,

$$P_s = \frac{4kH_0^2}{\omega\epsilon_0}\left\{ j\sum_{i=1}^{\infty}\sum_{\ell=1}^{\infty} S_i S_\ell^* \left[H_i^{(2)'}(kr) H_\ell^{(1)}(kr) - H_i^{(1)'}(kr)\, H_\ell^{(2)}(kr) \right] \right.$$
$$\left. \times \cos i\theta \cos \ell\theta \right\} . \qquad (5.47)$$

At distances such that $kr \gg 1$, the scattered power becomes

$$P_s = \frac{16}{\pi} \frac{c\,\mu_0 H_0^2}{kr} \left| \sum_{\ell=1}^{\infty} S_\ell \cos \ell\theta \right|^2 . \qquad (5.48)$$

5.1.4 Numerical Results

One of the main results of the linear scattering theory is the frequency spectrum of the resonances of a plasma column. A resonance occurs when $|R_\ell|$ reaches a minimum. In the absence of collisions, this occurs when

$$\epsilon_g^{1/2} V_\ell Y_\ell'(kb) - V_\ell' Y_\ell(kb) = 0 , \qquad (5.49)$$

as can be seen from Eq. (5.41). In this equation, $Y_\ell(kb)$ is the Bessel function of the second kind. It was shown in Appendix C that Eq. (5.17) can be written in terms of the dimensionless variable r/a , and of the dimensionless parameters a/λ_D and $\Gamma\omega^2/\omega_0^2$. It is then possible to transform Eq. (5.49) into

$$\frac{\psi'(1)}{\psi(1)} = -\frac{\ell^2 \epsilon_g^{1/2}}{ka} \left\{ \frac{p_\ell J_\ell(k_g a) - q_\ell Y_\ell(k_g a)}{p_\ell J_\ell'(k_g a) - q_\ell Y_\ell'(k_g a)} \right\} , \qquad (5.50)$$

where

$$p_\ell = \epsilon_g^{1/2} Y_\ell'(kb) Y_\ell(k_g b) - Y_\ell(kb) Y_\ell'(k_g b) , \qquad (5.51)$$

$$q_\ell = \epsilon_g^{1/2} Y_\ell'(kb) J_\ell(k_g b) - Y_\ell(kb) J_\ell'(k_g b) . \qquad (5.52)$$

In the small-ka limit, the RHS of Eq. (5.50) can be written as $-\ell\epsilon_{eff}$,

where ϵ_{eff} is an effective dielectric constant for the region outside the plasma.[44] The LHS of Eq. (5.50), given in terms of the variable r/a, depends only on the plasma parameters a/λ_D and $\Gamma\omega^2/\omega_0^2$. Curves of $\psi_1'(1)/\psi_1(1)$ vs $\omega^2/\langle\omega_0^2\rangle$ for a given ratio a/λ_D are shown in Fig. 5.2. It is convenient to use $\langle\omega_0^2\rangle$, the average value of ω_0^2 over the column, as the normalization factor for frequency. It can be seen from Fig. 5.2 that the curves for $\alpha = 0.0$ and $\alpha = 0.6$ are almost identical for $\omega^2/\langle\omega_0^2\rangle < 1.0$. This means that the dipole resonance depends only on the average properties of the column.

The resonant frequencies of a plasma column are usually measured by sweeping the discharge current and observing either the reflected or the absorbed power. We present in Fig. 5.3 some theoretical curves of the scattered power as a function of the electron density. The curves for T = 3 eV correspond to a mercury discharge while those for T = 8 eV are approximately valid for a low pressure argon discharge. The scattering amplitude from a cold uniform plasma column is also included in Fig. 5.3, for comparison. This model for linear and nonlinear scattering has been developed by Bruce et al.,[61] and is extended to Appendix D to include the effect of a glass tube. The dimensions are those of the tubes used in the experiments reported in Chapter VI. The values of ω and T were chosen to permit reasonable computing time and accuracy.

It is well known that numerical difficulties prevent the computation of the scattering amplitude for large a/λ_D, corresponding to small temperatures and/or large electron densities.[37,44,48] This comes about because one of the solutions of Eq. (5.17) varies very rapidly with radius for large a/λ_D. For example, one of the solutions of Eq. (5.28), for a uniform plasma column, is $J_\ell(k_p r)$. Since the main resonance occurs at $\omega < \omega_0$, k_p is purely imaginary in a collisionless plasma and can be written as $j\kappa_p$. If $\kappa_p a$ is large, the asymptotic form of the solution is $j^\ell \exp(\kappa_p r)/(2\pi\kappa_p r)^{1/2}$. With an incident frequency of 2.2 GHz and a column radius of 0.31 cm, $\kappa_p a$ is 30 for T = 8 eV ($a/\lambda_D = 62$), and 50 for T = 3 eV ($a/\lambda_D = 100$). Because of the exponential nature of the solution, a relatively small change in electron temperature produces a change of about 10^8 in $J_\ell(k_p a)$. Our experience has been that the

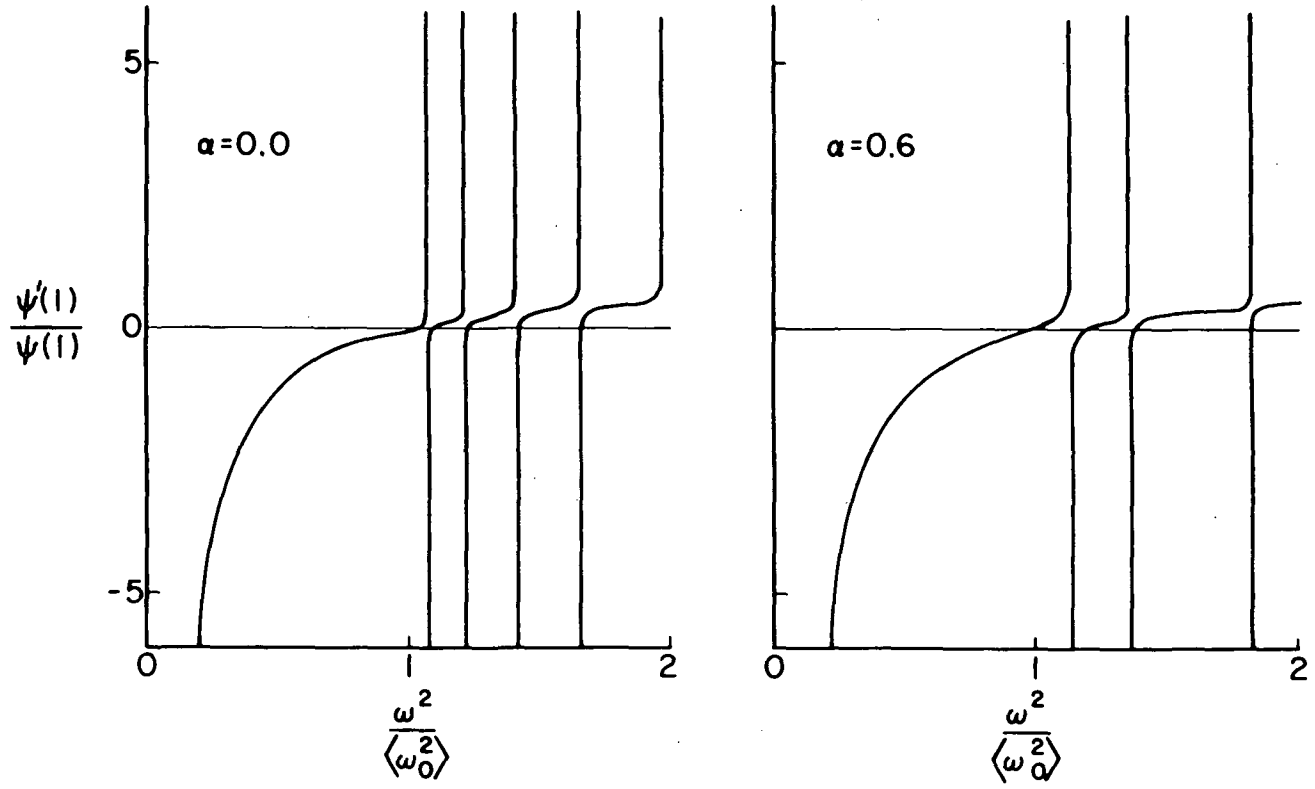

Fig. 5.2 Frequency dependence of $\psi'(1)/\psi(1)$: $a^2/\lambda_D^2 = 1000$.

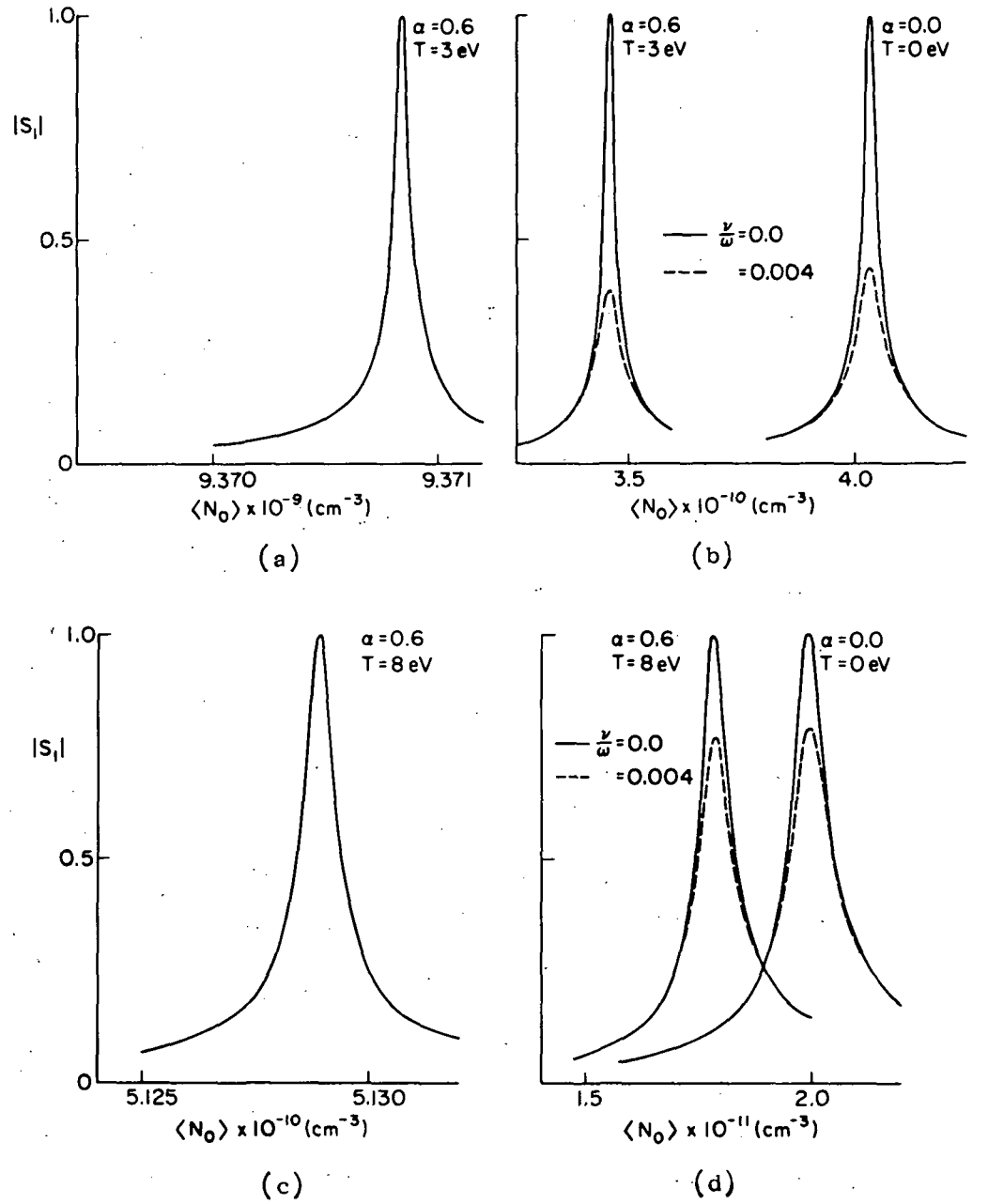

Fig. 5.3 Linear scattering amplitude as a function of electron density. (a) TD1 at 1.0 GHz; (b) MR at 1.0 GHz; (c) TD1 at 2.2 GHz; (d) MR at 2.2 GHz.

numerical integration, even using double precision, failed to converge with decreasing step size for $a/\lambda_D \gtrsim 80$, for a nonuniform plasma. For the same reason, Parker et al. could not obtain any results for $a/\lambda_D \gtrsim 70$.[44]

A singular perturbation analysis of the type developed by Miura and Barston[54] would be necessary to reach all of the values of temperature and electron density corresponding to the experiments reported in Chapter VI. Most of the nonlinear theory presented in this thesis was completed at the time of the publication of Ref. 54, which in any case only contains a one-dimensional analysis of linear scattering. Consequently, the development of the singular perturbation analysis for nonlinear scattering from a two-dimensional plasma was not attempted.

A summary of the calculations performed for linear scattering is given in Table 5.1. Only the main resonance (MR), and the first Tonks-Dattner resonance (TD1) were considered. The $\ell = 1$ and $\ell = 2$ terms in the plane wave expansion were included. The Q of the resonances is defined as

$$Q = \frac{\langle N_0 \rangle_{res}}{\langle \Delta N_0 \rangle} , \qquad (5.53)$$

where $\langle \Delta N_0 \rangle$ is taken at $|S_\ell|_{max}/2^{1/2}$. The collision factor, ν/ω , used in the computations corresponds to collision frequencies of 2.5×10^7/s, for $\omega/2\pi = 1.0$ GHz, and 1.14×10^7/s, for $\omega/2\pi = 2.2$ GHz. The collision frequency in a 1.1 m Torr mercury discharge tube is about 2.5×10^7/s.[70] It can be seen from the results given in Table 5.1 that, the larger the Q of a resonance, the more sensitive it is to collisional damping. This means that, in practice, the $\ell = 2$ resonances are excited to a much lower level than the $\ell = 1$ resonance, in tubes such as those used in our experiments. Furthermore, the resonance frequencies of the $\ell = 1$ and $\ell = 2$ resonances considered in Table 5.1 differ enough to preclude the simultaneous excitation of two resonances at one frequency, even for a cold plasma. This fact will simplify the calculations in the nonlinear scattering due to one strong incident wave. The first

TABLE 5.1

SUMMARY OF THE NUMERICAL RESULTS FOR LINEAR SCATTERING:

$a = 0.31$ cm, $b = 0.42$ cm, $\epsilon_g = 4.65$.

Type	$\omega/2\pi$ GHz.	T °K	α	ν/ω GHz.	$\lvert S_1 \rvert_{max}$	$\langle N_0 \rangle_{res}$ $10^9/cm^3$	Q_1	$\lvert S_2 \rvert_{max}$	$\langle N_0 \rangle_{res}$ $10^9/cm^3$	Q_2
MR	1.0	0.0	0.0	0.0	1.0	40.3	161	1.0	51.6	2.72×10^5
MR	1.0	0.0	0.0	0.004	0.435	40.3	88	4.0×10^{-4}	51.6	130
MR	1.0	3.0	0.6	0.0	1.0	34.6	173	1.0	41.81	2.6×10^5
MR	1.0	3.0	0.6	0.004	0.389	34.6	71	2.7×10^{-4}	41.81	10
TD1	1.0	3.0	0.6	0.0	1.0	9.3708	1.56×10^5	1.0	8.506	$> 10^8$
TD1	1.0	3.0	0.6	0.004	0.001	9.40	-	-	-	-
MR	2.2	0.0	0.0	0.0	1.0	199.8	33	1.1	251.3	1.25×10^4
MR	2.2	0.0	0.0	0.004	0.745	199.8	25	9.4×10^{-3}	251.4	105
MR	2.2	8.0	0.6	0.0	1.0	178.8	34	1.0	225.6	1.13×10^4
MR	2.2	8.0	0.6	0.004	0.77	179.0	30	0.007	225.6	75
TD1	2.2	8.0	0.6	0.0	1.00	51.29	9×10^3	1.0	4.8809	$> 10^6$
TD1	2.2	8.0	0.6	0.004	0.014	51.4	-	-	-	-

Tonks-Dattner resonance for $\ell = 2$ would have an extremely high Q and hence would be affected by collisional damping even more than the $\ell = 2$ main resonances, which can be neglected for all practical purpose. Consequently, computations for the first $\ell = 2$ Tonks-Dattner resonance were not performed.

5.2 Nonlinear Scattering from a Plasma Column

When one or two large amplitude waves are incident on a plasma column, the nonlinear terms appearing in Eqs. (5.1)-(5.3) may no longer be neglected. If the incident waves have angular frequencies ω_1 and ω_2, a nonlinearly scattered wave of angular frequency ω_3, where $\omega_3 = \omega_1 \pm \omega_2$, will appear. In this section, we shall obtain the power scattered at ω_3 in the case of weak nonlinearity, i.e. when the power scattered at ω_3 is much smaller than the power scattered at ω_1 and ω_2. In this case, it is sufficient to use the linear solutions obtained in Section 5.1 in the driving term of the nonhomogeneous differential equation for the potential derived in Section 5.2.1. As before, the quasistatic approximation will be used to obtain the solution inside the plasma column. Because of the angular variations of the linear solutions, the space dependent part of the magnetic field varying at frequency ω_3 can be written as

$$H_{z3}(\underline{r}) = H_{01}H_{02} \sum_{\ell=-\infty}^{+\infty} H_{z3\ell}(r)\exp(j\ell\theta) , \qquad 0 \le r \le a , \qquad (5.54)$$

$$H_{z3}(\underline{r}) = H_{01}H_{02} \sum_{\ell=-\infty}^{+\infty} \left[W_{3\ell}H_\ell^{(1)}(k_{g3}r) + X_{3\ell}H_\ell^{(2)}(k_{g3}r)\right]\exp(j\ell\theta) , \qquad a \le r \le b , \qquad (5.55)$$

$$H_{z3}(\underline{r}) = H_{01}H_{02} \sum_{\ell=-\infty}^{+\infty} Y_{3\ell}H_\ell^{(2)}(k_3 r)\exp(j\ell\theta) , \qquad b \le r , \qquad (5.56)$$

where H_{01} and H_{02} are the magnetic field amplitudes of the incident waves. An expression for the power scattered at ω_3 is derived in Section 5.2.2 and numerical results for a nonuniform plasma column are presented in Section 5.2.3.

5.2.1 Nonlinear Potential inside the Plasma Column

The nonlinear equations are obtained by expanding Eqs. (5.7) and (5.8) up to second order. If terms involving products of first order quantities are put on the RHS of the equations, the equation of motion becomes

$$m_e N_0 f \frac{\partial \underset{\sim}{v}}{\partial t} + m_e \nu N_0 f \underset{\sim}{v} + e N_0 f \nabla\varphi - \kappa T \frac{\nabla f}{f} n + \gamma \kappa T \nabla n$$

$$= - m_e N_0 f (\underset{\sim}{v}\cdot\nabla)\underset{\sim}{v} - m_e n \frac{\partial \underset{\sim}{v}}{\partial t} - en\nabla\varphi - m_e \nu n \underset{\sim}{v} - \frac{\gamma(\gamma-1)}{2} \frac{\kappa T}{N_0} \nabla \left(\frac{n^2}{f}\right) , \tag{5.57}$$

and the continuity equation may be written as

$$N_0 \nabla\cdot(f\underset{\sim}{v}) + \frac{\partial n}{\partial t} = - \nabla\cdot(n\underset{\sim}{v}) . \tag{5.58}$$

We can Fourier analyze Eq. (5.57) and (5.58) in time to obtain

$$j m_e N_0 \Gamma_3 f \omega_3 \underset{\sim}{v}_3 + e N_0 f \nabla\varphi_3 - \kappa T \frac{\nabla f}{f} n_3 + \gamma \kappa T \nabla n_3$$

$$= - \sum_{\alpha,\beta} \left[m_e N_0 f (\underset{\sim}{v}_\alpha\cdot\nabla)\underset{\sim}{v}_\beta + j m_e \omega_\beta \Gamma_\beta n_\alpha \underset{\sim}{v}_\beta + e n_\alpha \nabla\varphi_\beta + \frac{\gamma(\gamma-1)}{2} \frac{\kappa T}{N_0} \nabla \left(\frac{n_\alpha n_\beta}{f}\right) \right] , \tag{5.59}$$

$$N_0 \nabla\cdot(f\underset{\sim}{v}_3) + j\omega_3 n_3 = - \sum_{\alpha,\beta} \nabla\cdot(n_\alpha \underset{\sim}{v}_\beta) , \tag{5.60}$$

where

$$\Gamma_\lambda = 1 - \frac{j\nu}{\omega_\lambda} . \tag{5.61}$$

In these equations, the quantities $\underset{\sim}{v}_\alpha$, φ_α, n_α, Γ_α are associated with the wave of angular frequency ω_α, and $\sum_{\alpha,\beta} A_\alpha B_\beta = A_1B_2+A_2B_1$.

After taking the divergence of Eq. (5.59), and using Eq. (5.60) and Poisson's equation in the LHS of the resulting equation, we obtain

$$\nabla^4\varphi_3 - \frac{1}{\gamma}\nabla\cdot\left(\frac{\nabla f}{f}\nabla^2\varphi_3\right) + \frac{1}{\gamma\lambda_D^2}\left[\left(\frac{\omega_3^2\Gamma_3}{\omega_0^2} - f\right)\nabla^2\varphi_3 - \nabla f\cdot\nabla\varphi_3\right]$$

$$= \frac{e}{\gamma\kappa T\epsilon_0}\sum_{\alpha,\beta}\left\{m_e N_0\nabla\cdot\left[f(\underset{\sim}{v}_\alpha\cdot\nabla)\underset{\sim}{v}_\beta\right] - jm_e\omega_\alpha\nabla\cdot(n_\alpha\underset{\sim}{v}_\beta) + e\nabla\cdot(n_\alpha\nabla\varphi_\beta) + \frac{\gamma(\gamma-1)}{2}\frac{\kappa T}{N_0}\nabla^2\left(\frac{n_\alpha n_\beta}{f}\right)\right\}. \tag{5.62}$$

The LHS of Eq. (5.62) is identical to the LHS of Eq. (5.15) obtained for the potential in the linear scattering case. The following expansions are used in Eq. (5.62)

$$\varphi_\lambda(\underset{\sim}{r}) = H_{0\lambda}\sum_{\ell=-\infty}^{+\infty}{}' \psi_{\lambda\ell}(r)\exp(j\ell\theta), \qquad \lambda=1,2,$$

$$\varphi_3(\underset{\sim}{r}) = H_{01}H_{02}\sum_{\ell=-\infty}^{+\infty}{}' \psi_{3\ell}(r)\exp(j\ell\theta), \tag{5.63}$$

$$n_\lambda(\underset{\sim}{r}) = H_{0\lambda}\sum_{\ell=-\infty}^{+\infty} N_{\lambda\ell}(r)\exp(j\ell\theta),$$

$$\underset{\sim}{v}_\lambda(r) = H_{0\lambda}\sum_{\ell=-\infty}^{+\infty}{}' \left[V_{r\lambda\ell}(r)\underset{\sim}{i}+V_{\theta\lambda\ell}(r)\underset{\sim}{j}\right]\exp(j\ell\theta), \qquad \lambda=1,2,$$

where $H_{0\lambda}\psi_{\lambda\ell}$, $H_{0\lambda}N_{\lambda\ell}$, $H_{0\lambda}V_{r\lambda\ell}$ and $H_{0\lambda}V_{\theta\lambda\ell}$, for $\lambda=1,2$, are the linear quantities associated with an incident wave of angular frequency ω

and azimuthal wavenumber ℓ . The sign $\sum_{\ell=-\infty}^{+\infty}{}'$ means that the term with $\ell=0$ has been excluded from the sum since it would lead to an infinite magnetic field, as noted in Section 5.1.1.

Lengthy manipulations finally yield for $\psi_{3\ell}(r)$

$$D_\ell \psi_{3\ell} = \frac{e}{\gamma \kappa T \epsilon_0} \sum_{\alpha,\beta} \sum_{\ell=m+n}{}' \Bigg\{ m_e N_0 \Bigg[\left(\frac{f}{r}+f'\right) V'_{r\alpha m} V_{r\beta n} + f\left(V_{r\alpha m}' V_{r\beta n}' - \frac{1}{r}\left(V_{\theta\alpha m}' V_{\theta\beta n} + V_{\theta\alpha m} V_{\theta\beta n}'\right)\right.$$

$$\left. + V_{r\alpha m}'' V_{r\beta n} + \frac{jn}{r}\left(V_{\theta\alpha m}' V_{r\beta n} + V_{\theta\alpha m} V_{r\beta n}'\right) - \frac{\ell^2}{2r^2} V_{\theta\alpha m} V_{\theta\beta n} + \frac{j\ell}{r^2} V_{r\alpha m}\left(V_{\theta\beta m+r} V_{\theta\beta n}'\right)\right)$$

$$- \frac{f'}{r} V_{\theta\alpha m}\left(V_{\theta\beta n} - jn V_{r\beta n}\right)\Bigg] - j m_e \omega_m \left[\frac{N_{\alpha m} V_{r\beta n}}{r} + N_{\alpha m}' V_{r\beta n} + N_{\alpha m} V_{r\beta n}' + \frac{j\ell}{r} N_{\alpha m} V_{\theta\beta n}\right]$$

$$+ e\left[\frac{N_{\alpha m} \psi_{\beta n}'}{r} + N_{\alpha m}' \psi_{\beta n}' + N_{\alpha m} \psi_{\beta n}'' - \frac{\ell n}{r^2} N_{\alpha m} \psi_{\beta n}\right] + \frac{\gamma(\gamma-1)}{2} \frac{\kappa T}{f N_0}\left[\left(N_{\alpha m}'' N_{\beta n} + N_{\alpha m} N_{\beta n}''\right)\right.$$

$$\left. + \left(\frac{1}{r} - \frac{2f'}{f}\right)\left(N_{\alpha m}' N_{\beta n} + N_{\alpha m} N_{\beta n}'\right) + 2 N_{\alpha m}' N_{\beta n}' - \left(\frac{f''}{f} - \frac{2f'^2}{f^2} + \frac{f'}{rf} + \frac{\ell^2}{r^2}\right) N_{\alpha m} N_{\beta n}\right]\Bigg\} . \tag{5.64}$$

where D_ℓ is the differential operator defined in Eq. (5.17).

The solution of Eq. (5.64) can be written as

$$\psi_{3\ell}(r) = A_{3\ell} \psi_{3\ell 1}(r) + B_{3\ell} \psi_{3\ell 2}(r) + \psi_{3\ell p}(r) , \tag{5.65}$$

where $\psi_{3\ell 1}(r)$ and $\psi_{3\ell 2}(r)$ are two linearly independent solutions of the homogeneous equation $D_\ell \psi_{3\ell} = 0$ which are regular at $r = 0$, and $\psi_{3\ell p}(r)$ is a particular solution of Eq. (5.64). The solutions of $D_\ell \psi_3 = 0$ were obtained in Section 5.1.1 for a nonuniform plasma. A series solution for $\psi_{3\ell p}(r)$, obtained in Appendix E, will be used to start the numerical integration of Eq. (5.64).

Equation (5.65) contains two arbitrary constants. One of them can be determined by requiring that the radial velocity vanish up to second order at r=a. The velocity can be obtained from the equation of motion [Eq. (5.43)],

$$\underset{\sim}{v}_{3}(r) = \frac{je}{m_e \omega_3 \Gamma_3}\left\{\nabla\varphi_3 + \lambda_D^2 \frac{f'}{f^2}\nabla\varphi_3^2 - \frac{\gamma\lambda_D^2}{f}\nabla(\nabla^2\varphi_3)\right.$$

$$\left. + \sum_{\alpha,\beta}\left[\frac{m_e}{e}(\underset{\sim}{v}_\alpha\cdot\nabla)\underset{\sim}{v}_\beta + \frac{jm_e\omega_\beta\Gamma_\beta}{N_0 fe}\, n_\alpha \underset{\sim}{v}_\beta + \frac{n_\alpha\nabla\varphi_\beta}{N_0 f} + \frac{\gamma(\gamma-1)}{2}\frac{\kappa T}{n_0 f}\nabla\left(\frac{n_\alpha n_\beta}{f}\right)\right]\right\}, \tag{5.66}$$

$$\underset{\sim}{v}_{3}(r) = \sum_{\ell=-\infty}^{+\infty}{}' \underset{\sim}{v}_{3\ell}(r)\exp(j\ell\theta)\,. \tag{5.66}$$

This equation can be expanded using Eq. (5.63) to yield

$$\underset{\sim}{v}_{3\ell}(\underset{\sim}{r}) = \frac{je\lambda_D^2 H_{01}H_{02}}{m_e\omega_3\Gamma_3 f}\left\{\left[T_{3\ell}(r) + \frac{f}{\lambda_D^2}\sum_{\alpha,\beta}\sum_{\ell=m+n}{}' U_{mn}(r)\right]\hat{\underset{\sim}{i}}\right.$$

$$\left. + \left[Z_{3\ell}(r) + \frac{f}{\lambda_D^2}\sum_{\alpha,\beta}\sum_{\ell=m+n}{}' G_{mn}(r)\right]\hat{\underset{\sim}{j}}\right\}\exp(j\ell\theta)\,, \tag{5.67}$$

where

$$T_{3\ell}(r) = -\gamma\psi_{3\ell}''' + \left(\frac{f'}{f} - \frac{\gamma}{r}\right)\psi_{3\ell}'' + \left[\frac{f}{\lambda_D^2} + \frac{f'}{rf} + (\ell^2+1)\frac{\gamma}{r^2}\right]\psi_{3\ell}' - \frac{\ell^2}{r^2}\left(\frac{f'}{f} + \frac{2\gamma}{r}\right)\psi_{3\ell}\,, \tag{5.68}$$

$$U_{mn}(r) = \frac{m_e}{e}\left[V'_{r\alpha m}V_{r\beta n} - \frac{V_{\theta\alpha m}}{r}\left(V_{\theta\beta n} - jnV_{r\beta n}\right)\right] + \frac{jm_e\omega_\beta\Gamma_\beta}{N_0 ef}\, N_{\alpha m}V_{r\beta n} + \frac{N_{\alpha m}\psi'_{\beta n}}{N_0 f}$$

$$+ \frac{\gamma(\gamma-1)}{2}\frac{\kappa T}{N_0^2 ef}\left[N'_{\alpha m}N_{\beta n} + N_{\alpha m}N'_{\beta n} - \frac{f'}{f}N_{\alpha m}N_{\beta n}\right], \tag{5.69}$$

$$Z_{3\ell}(r) = \frac{j\ell}{r}\left[-\gamma\left(\psi_{3\ell}'' + \frac{\psi_{3\ell}'}{r}\right) + \left(\frac{f}{\lambda_D^2} + \frac{\gamma\lambda_D^2}{r^2}\right)\psi_{3\ell}\right] , \qquad (5.70)$$

$$G_{mn}(r) = \frac{m_e}{e}\left[\frac{j\ell}{2r} V_{\theta\alpha m}V_{\theta\beta n} + V_{r\alpha m}\left(\frac{V_{\theta\beta n}}{r} + V_{\theta\beta n}'\right)\right] + \frac{jm_e\omega\Gamma_{\beta\beta}}{N_0 ef} N_{\alpha m}V_{\theta\beta n} + \frac{jn}{N_0 fr} N_{\alpha m}\psi_{\beta n}$$

$$+ \frac{j\gamma(\gamma-1)\ell}{2r} \frac{\kappa T}{N_0^2 ef^2} N_{\alpha m}N_{\beta n} . \qquad (5.71)$$

The condition that the radial velocity vanish at r=a is

$$T_{3\ell}(a) + \frac{f(a)}{\lambda_D^2} \sum_{\alpha,\beta} \sum_{\ell=m+n}{}' U_{mn}(a) = 0 . \qquad (5.72)$$

We can use Eq. (5.65) in the first term of Eq. (5.72) to obtain

$$A_{3\ell}h_{3\ell 1}(a) + B_{3\ell}h_{3\ell 2}(a) + h_{3\ell p}(a) + \frac{f(a)}{\lambda_D^2} \sum_{\alpha,\beta} \sum_{\ell=m+n} U_{mn}(a) = 0 , \qquad (5.73)$$

where

$$h_{3\ell j}(r) = -\gamma\psi_{3\ell j}''' + \left(\frac{f'}{f} - \frac{\gamma}{r}\right)\psi_{3\ell j}'' + \left[\frac{f}{\lambda_D^2} + \frac{f'}{fr} + (\ell^2+1)\frac{\gamma}{r^2}\right]\psi_{3\ell j}'$$

$$- \frac{\ell^2}{r^2}\left(\frac{f'}{f} + \frac{2\gamma}{r}\right)\psi_{3\ell j} , \quad j = 1,2,p. \qquad (5.74)$$

5.2.2 Nonlinear Scattered Power

As in the calculation of the linear scattered power, the solution inside the column must be matched to the solution outside in order to determine the constants in Eqs. (5.55), (5.56) and (5.65). It is more convenient to use the boundary conditions on the electric field

than those on the magnetic field. The radial displacement and the tangential electric field must be continuous at $r=a$ and $r=b$. The displacement in the plasma can be obtained by writing Poisson's equation

$$\nabla \cdot \epsilon_0 \underset{\sim}{E}_{3} = n_{3} e \ , \tag{5.75}$$

and using the continuity equation to obtain

$$\nabla \cdot \epsilon_0 \underset{\sim}{E}_{3} = \frac{je}{\omega_{3}} \left[N_0 \nabla \cdot (f \underset{\sim}{v}_{3}) + \sum_{\alpha,\beta} \nabla \cdot (n_{\alpha} \underset{\sim}{v}_{\beta}) \right] \ . \tag{5.76}$$

The displacement can be written as

$$\underset{\sim}{D}_{3} = \epsilon_0 \underset{\sim}{E}_{3} - \frac{je}{\omega_{3}} \left[N_0 f \underset{\sim}{v}_{3} + \sum_{\alpha,\beta} n_{\alpha} \underset{\sim}{v}_{\beta} \right] \ . \tag{5.77}$$

Since both the first and second order radial velocities are assumed to vanish at $r=a$, the radial displacement at the boundary is

$$D_{3r} = \epsilon_0 E_{3r} = - \epsilon_0 \varphi_{3}' \ . \tag{5.78}$$

The constants are found to be

$$A_{3\ell} = \frac{C_{\ell p} I_{\ell 2} + h_{3\ell 2} I_{\ell p}}{h_{3\ell 1}(a) I_{\ell 2} - h_{3\ell 2}(a) I_{\ell 1}} \ , \quad B_{3\ell} = - \frac{h_{3\ell 1}(a) I_{\ell p} + C_{\ell p} I_{\ell 1}}{h_{3\ell 1}(a) I_{\ell 2} - h_{3\ell 2}(a) I_{\ell 1}} \ ,$$

$$W_{3\ell} = - \frac{F_{3\ell 2}}{F_{3\ell 1}} X_{3\ell} \ , \quad X_{3\ell} = - \frac{j\pi \omega_{3} \epsilon_0 \epsilon_g a}{4} \left[A_{3\ell} G_{\ell 1} + B_{3\ell} G_{\ell 2} + G_{\ell p} \right] , \quad Y_{3\ell} = - \frac{4j X_{3\ell}}{\pi k_{3} b F_{3\ell 1} \epsilon_g^{1/2}} \ , \tag{5.79}$$

$$F_{3\ell 1} = \epsilon_g^{1/2} H_{\ell}^{(1)}(k_{g3} b) H_{\ell}^{(2)\prime}(k_{3} b) - H_{\ell}^{(1)\prime}(k_{g3} b) H_{\ell}^{(2)}(k_{3} b) \ ,$$

$$F_{3\ell 2} = \epsilon_g^{1/2} H_{\ell}^{(2)}(k_{g3} b) H_{\ell}^{(2)\prime}(k_{3} b) - H_{\ell}^{(2)\prime}(k_{g3} b) H_{\ell}^{(2)}(k_{3} b) \ ,$$

$$G_{\ell j} = \frac{\ell}{a} H_\ell^{(1)}(k_{g3}a)\psi_{3\ell j}(a) - \frac{k_3 a}{\ell \epsilon_g^{1/2}} H_\ell^{(1)'}(k_{g3}a)\psi_{3\ell j}(a) \quad , \quad j=1,2,p$$

$$d_\ell = \frac{\ell^2 \epsilon_g^{1/2}}{k_3 a^2} \left[\frac{F_{3\ell 1} H_\ell^{(2)}(k_{g3}a) - F_{3\ell 2} H_\ell^{(1)}(k_{g3}a)}{F_{3\ell 1} H_\ell^{(2)}(k_{g3}a) - F_{3\ell 2} H_\ell^{(1)'}(k_{g3}a)} \right] , \tag{5.80}$$

$$I_{\ell j} = \psi'_{3\ell j}(a) - d_\ell \psi_{3\ell j}(a) \quad , C_{\ell p} = -h_{3\ell p}(a) - \frac{f(a)}{\lambda_D^2} \sum_{\alpha,\beta} \sum_{\ell=m+n} U_{mn} \, .$$

The symmetry, or antisymmetry, with respect to interchanges between ℓ and $-\ell$ must be determined for the various quantities used in this section in order to obtain the angular variation of $\psi_{3\ell}$, $H_{3z\ell}$, and of the nonlinear scattered power. It can be seen from Eq. (5.65) that $\psi_{3\ell}$ will have the same symmetry as $\psi_{3\ell p}$, which has the same symmetry as the RHS of Eq. (5.64). A typical term in the RHS of Eq. (5.64) is $N_{\alpha m}\psi''_{\beta n}$. It was seen in Section 5.1.3 that the linear magnetic field was symmetric with respect to interchanges between ℓ and $-\ell$. Since the magnetic field and the potential are antisymmetric, we obtain

$$N_{\alpha -m} = -N_{\alpha m} \, , \quad \psi''_{\beta -n} = -\psi''_{\beta n} \, , \quad N_{\alpha -m}\psi''_{\beta -m} = N_{\alpha m}\psi''_{\beta n} \, . \tag{5.81}$$

Thus, the nonlinear quantities $\psi_{3\ell}$ and $H_{3z\ell}$ must be symmetric and antisymmetric, respectively, with respect to interchanges between ℓ and $-\ell$. The nonlinear scattered magnetic field is

$$H_{zs}(\underline{r}) = 2H_{01}H_{02} \sum_{\ell=1}^{\infty} Y_{3\ell} H_\ell^{(2)}(k_3 r) \sin \ell\theta \, , \tag{5.82}$$

and, for $kr \gg 1$, the nonlinear scattered power is

$$P_s = \frac{16}{\pi} \frac{\mu_0 H_{01}^2 H_{02}^2}{k_3 r} \left[\sum_{\ell=1}^{\infty} Y_{3\ell} \sin \ell\theta \right]^2 \tag{5.83}$$

It can be seen from Eq. (5.83) that no scattered power is directed in the $\theta=0$ and $\theta=\pi$ directions for any ℓ .

5.2.3 Numerical Results

Some results of nonlinear scattering amplitude are presented, in this section, for harmonic generation produced by a large amplitude incident wave. Since the different multipole resonances occur at different electron densities, as was seen in Section 5.1.4, the nonlinear scattering produced at each linear multipole resonance can be considered separately. We shall only consider linear dipole excitation, which produces a nonlinear quadrupolar radiation pattern. The physical characteristics of the tubes used in experiments to be described in Chapter VI were used in the computations. The other parameters were chosen to illustrate the general behavior of the solutions while avoiding the numerical difficulties mentioned in Section 5.1.4.

Figure 5.4 shows the nonlinear scattering amplitude, Y_{32} , as a function of the electron temperature, for a uniform and a nonuniform plasma column. Some radial potential profiles, shown in Fig. 5.5, suggest that electron plasma waves at the second harmonic are excited in the plasma by the nonlinear driving terms in Eq. (5.64). The boundary conditions at $r = a$ provide some constraints on the potential, however. It can be seen from Eq. (5.55), (5.56), (5.65), (5.79) and (5.80) that the ratio $\psi'_{3\ell}(a)/\psi_{3\ell}(a)$ can be written as

$$\frac{\psi'_{3\ell}(a)}{\psi_{3\ell}(a)} = -\frac{\ell^2 \epsilon_g}{k_3 a^2}\left[\frac{F_{\ell 1}H_\ell^{(2)'}(k_{g3}a)-F_{\ell 2}H_\ell^{(1)'}(k_{g3}a)}{F_{\ell 1}H_\ell^{(2)}(k_{g3}a)-F_{\ell 2}H_\ell^{(1)}(k_{g3}a)}\right] . \qquad (5.84)$$

The RHS of Eq. (5.84) is a function of the geometry and of the frequency only. As the temperature increases, the wavelength of the electron plasma wave changes, and the number of periods of the wave inside the column decreases, as can be seen in Fig. 5.5. This means that $\psi'_{3\ell}(a)$ might vary between zero, if the wavelength is such that $\psi_{3\ell}(a)$ is a maximum of the potential, and the maximum slope of the potential curve, if $\psi_{3\ell}(a) = 0$. Since the ratio $\psi'_{3\ell}(a)/\psi_{3\ell}(a)$ is constant, at a given frequency, $\psi_{3\ell}(a)$ can also vary between zero and a maximum value, and so will the scattering amplitude, which is proportional to $\psi_{3\ell}(a)$.

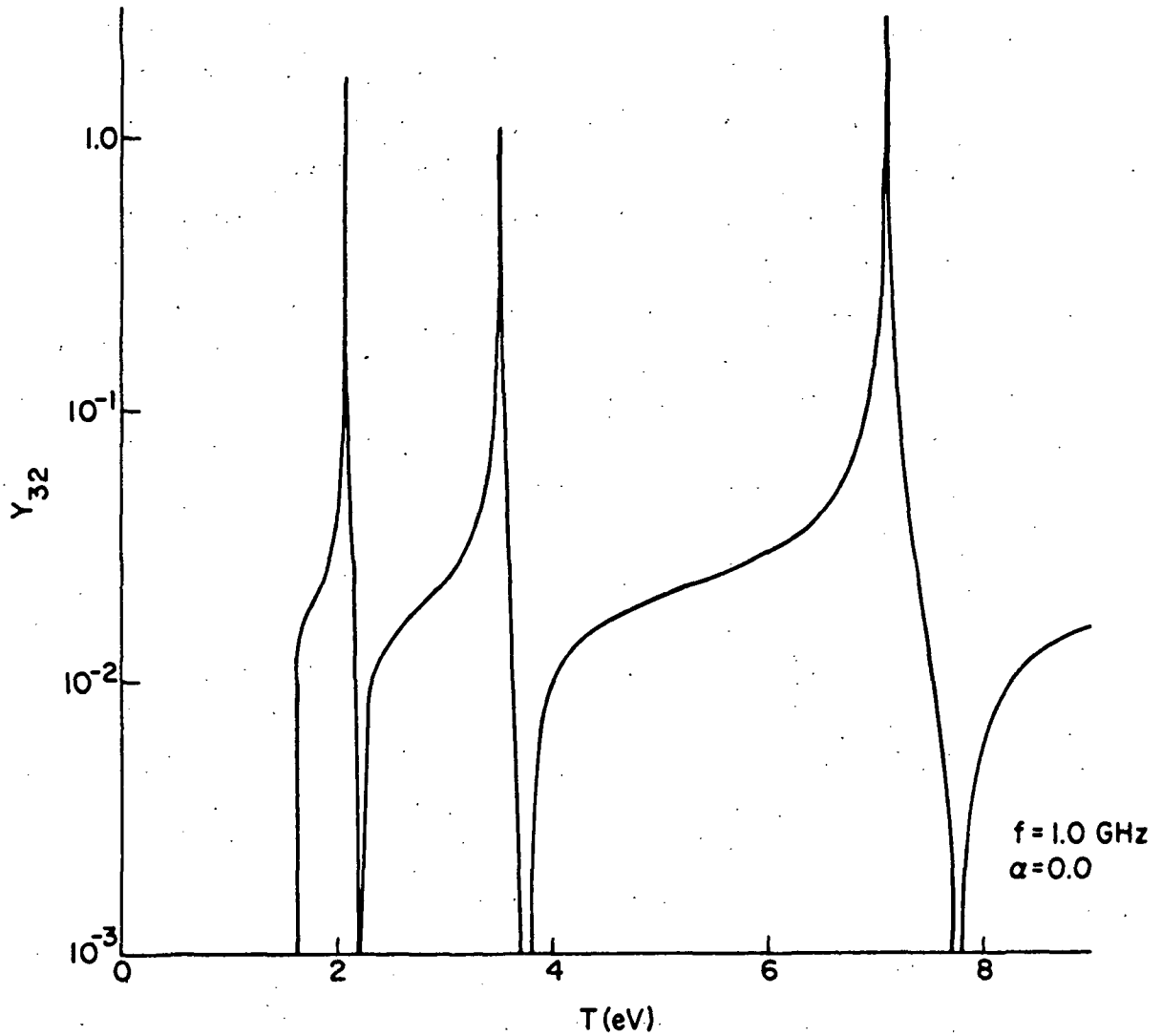

(a)

Fig. 5.4 Nonlinear scattering amplitude as a function of electron temperature: (a) uniform plasma.

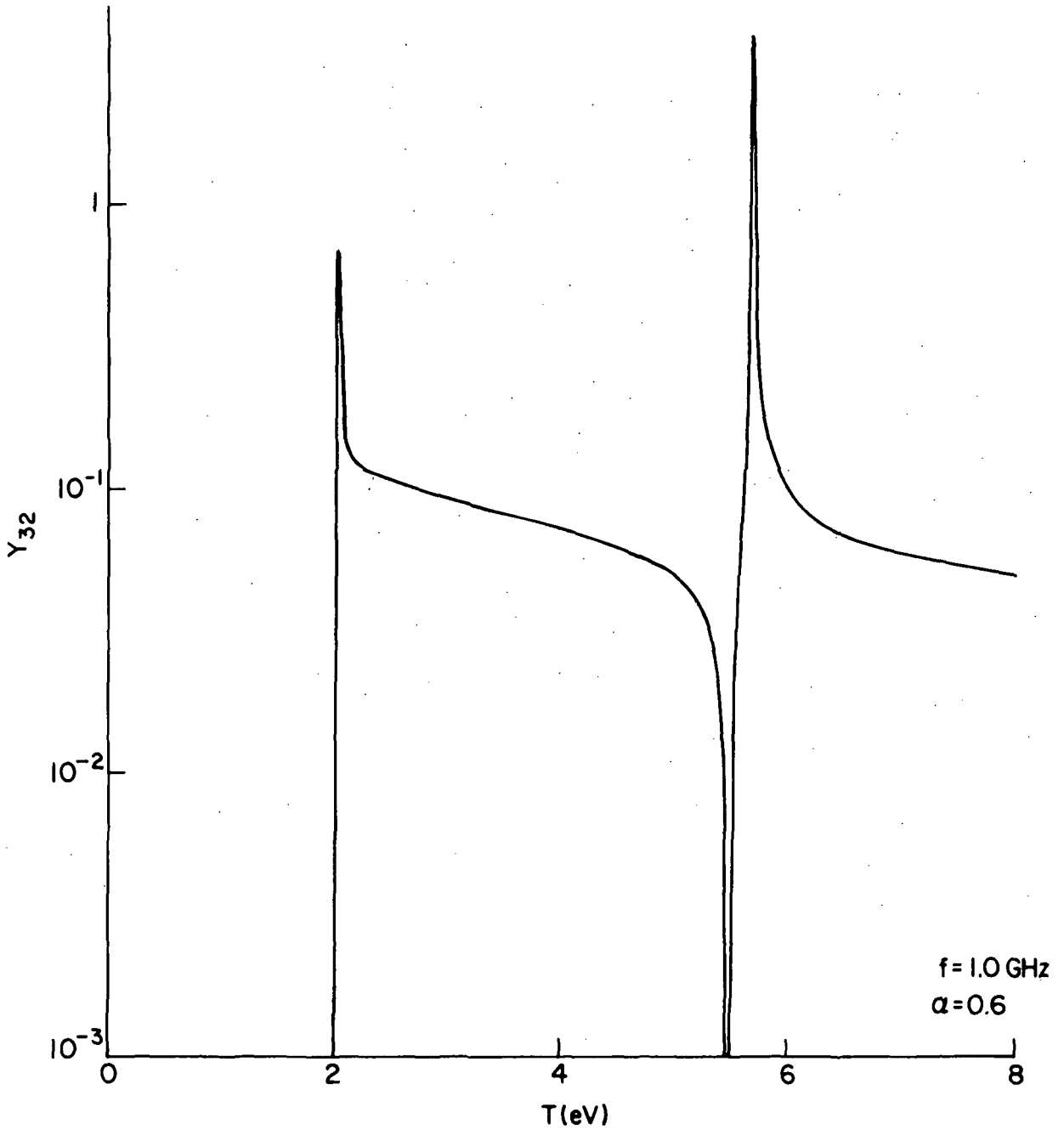

Fig. 5.4 (Cont.) (b) nonuniform plasma.

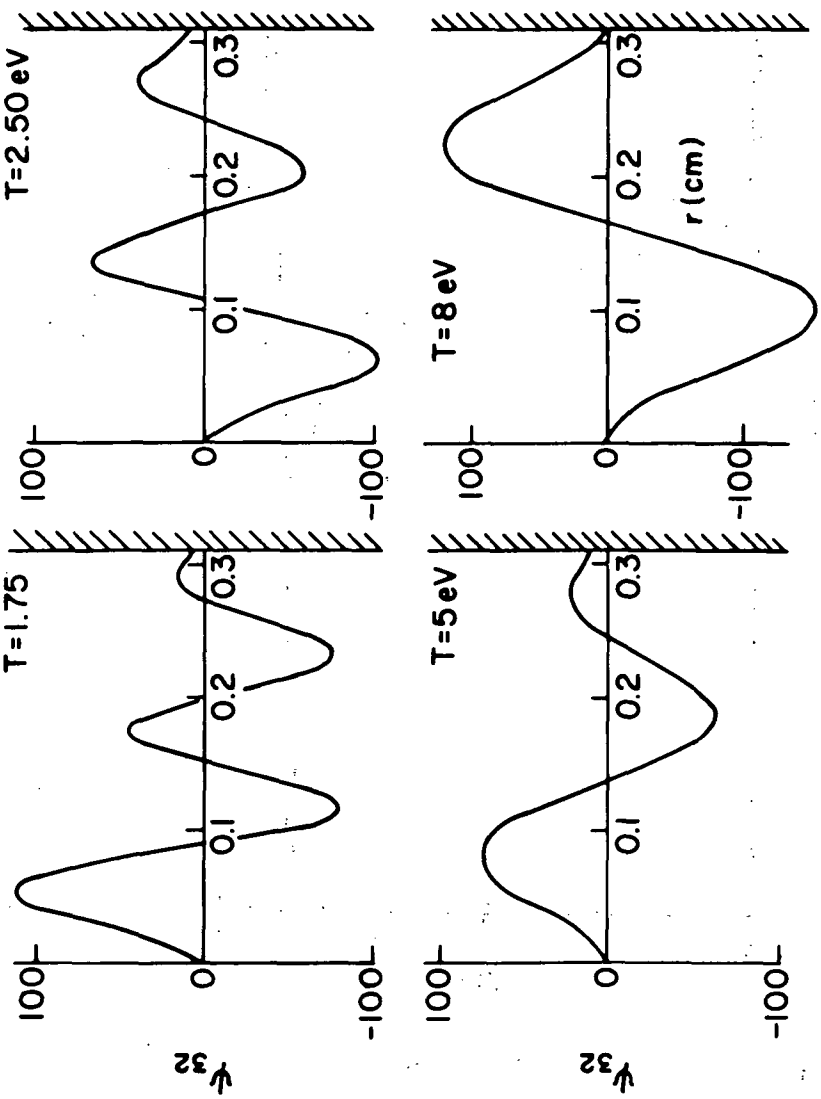

Fig. 5.5 Radial potential profile at second harmonic.
(a) uniform plasma.

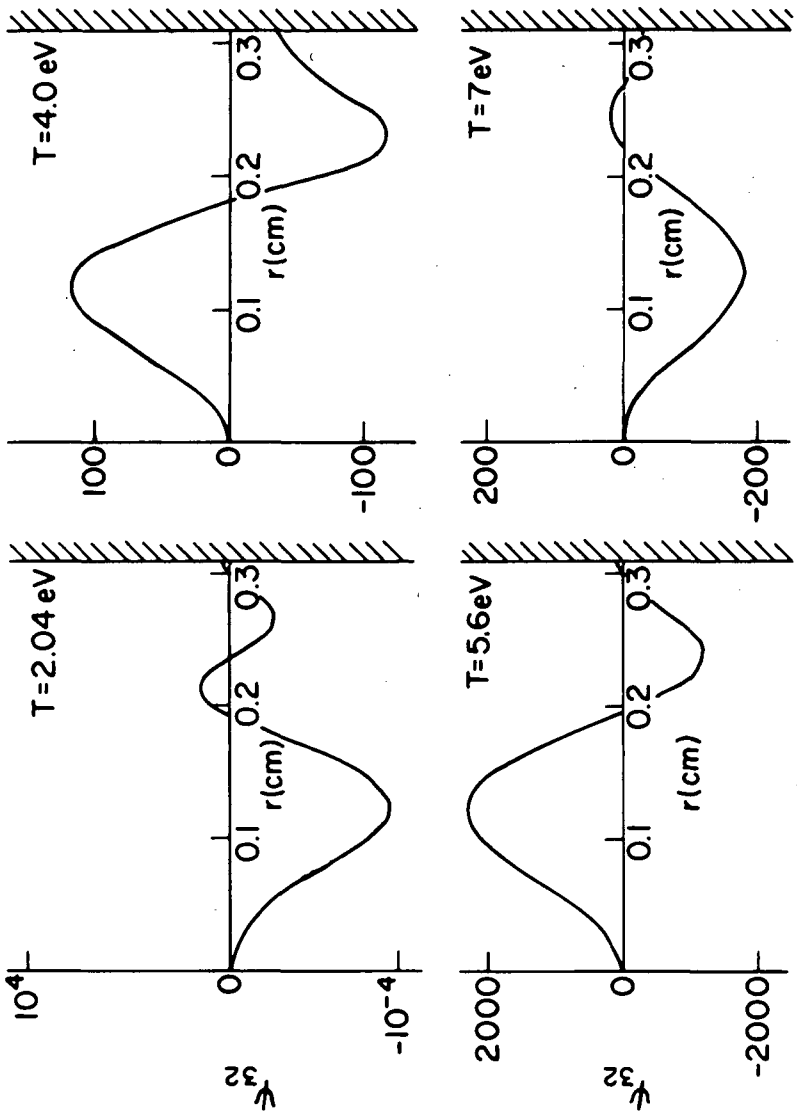

Fig. 5.5 (Cont.) (b) Nonuniform plasma.

This explains roughly the large variations in Y_{32} found in Fig. 5.4. The boundary condition on $v_{r3\ell}(a)$ and the nonuniformity of the excitation provided by the products of linear quantities also influence the potential in the column. This is well illustrated in Fig. 5.5(b). The curves for $T = 4.0$ and 5.6 eV have approximately the same wavelength, but the sign of $\psi_{32}(a)$ is different in the two cases. We would even expect to find $\psi_{32}(a)|_{T=4.0} \geq \psi_{32}(a)|_{T=5.6}$ since the wavelength at $T = 4.0$ is smaller than at $T = 5.6$. Furthermore, the curve for $T = 7.0$ eV has a very short wavelength oscillation which seems to be introduced by the excitation and the boundary conditions.

It can be seen from Fig. 5.6 that Y_{32} varies with frequency in a similar way. It is more difficult to predict what happens in this case since the RHS of Eq. (5.84) depends on frequency.

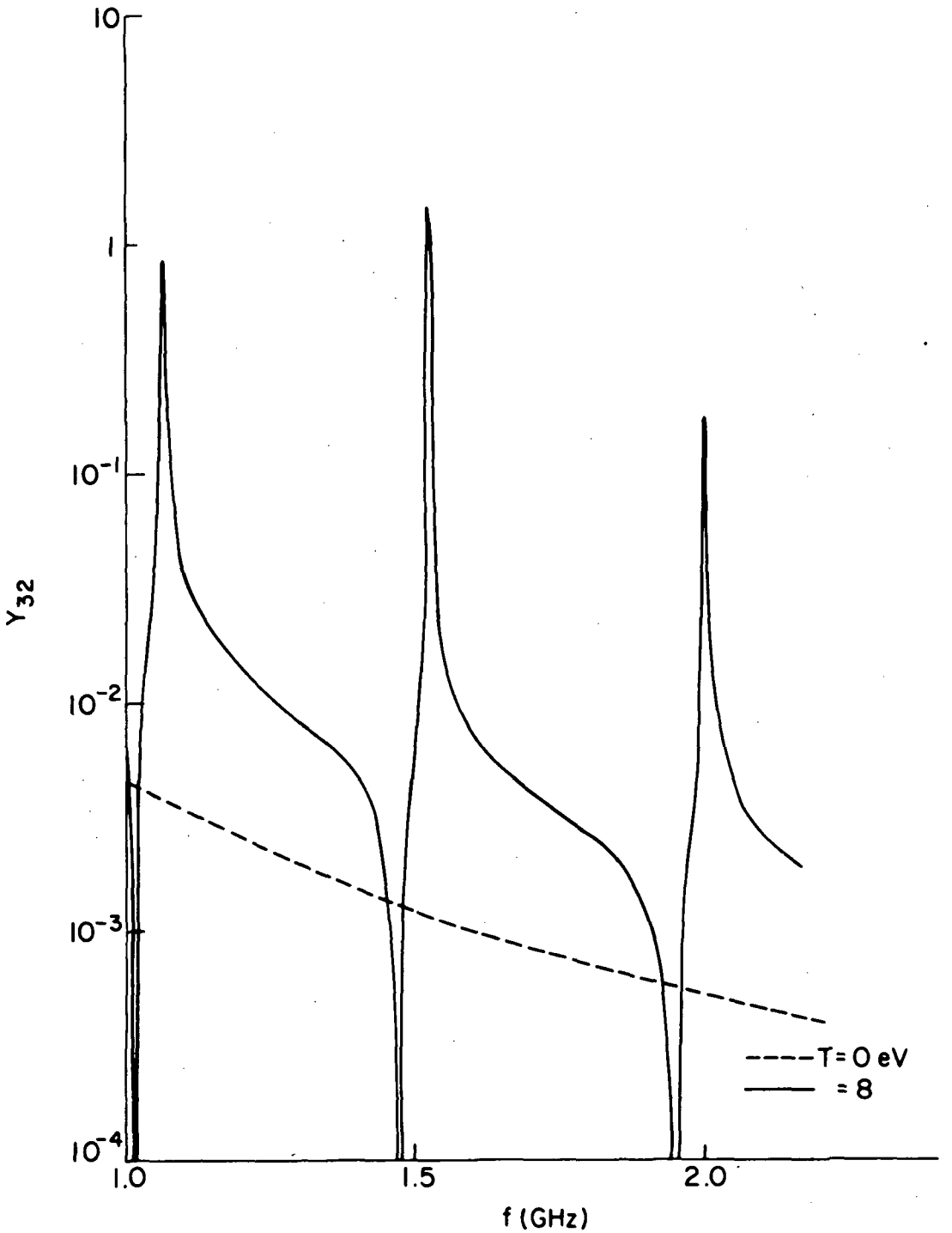

Fig. 5.6 Nonlinear scattering amplitude as a function of frequency. (a) Uniform plasma.

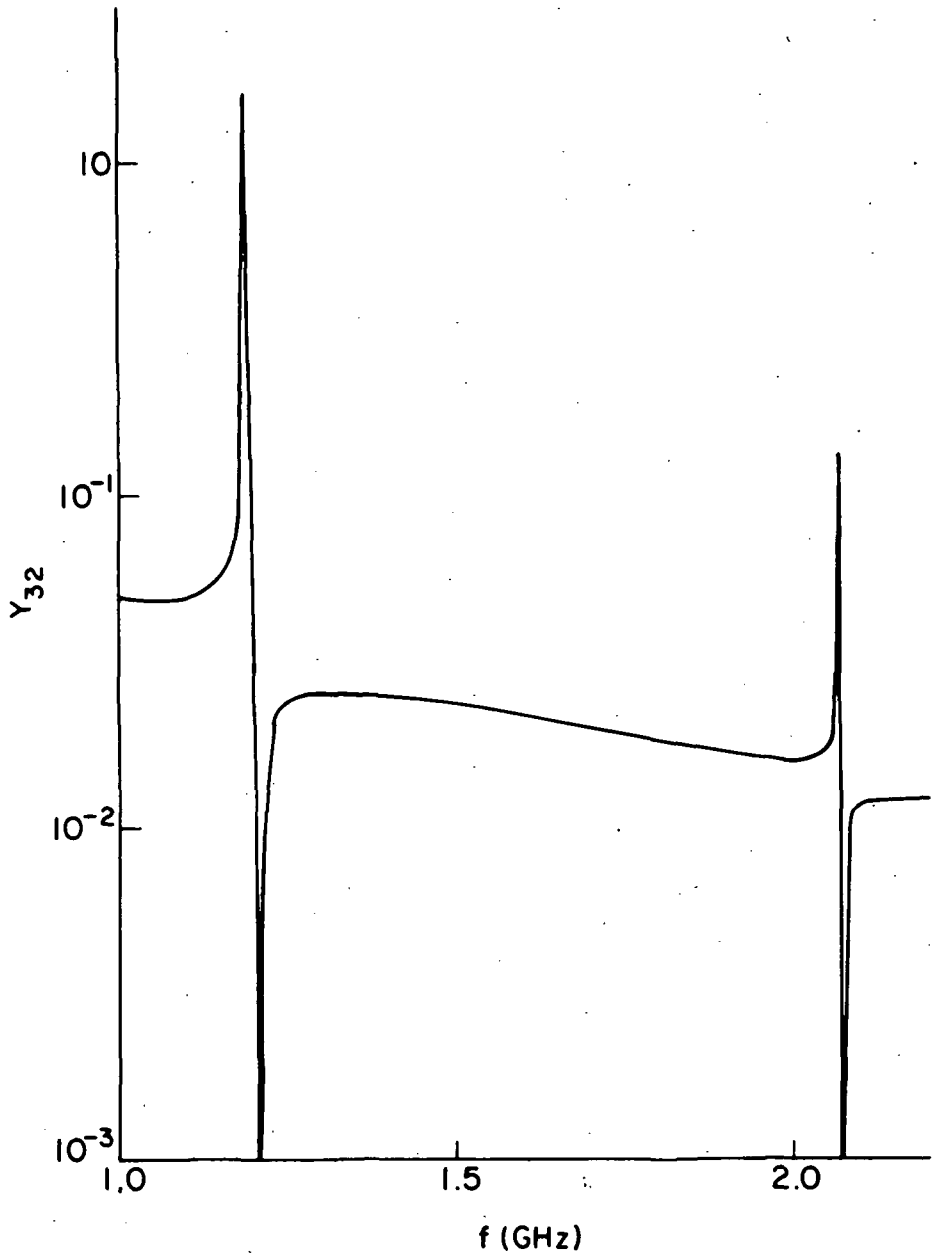

Fig. 5.6 (Cont.) (b) Nonuniform plasma.

Chapter VI

NONLINEAR SCATTERING FROM A PLASMA COLUMN: EXPERIMENTS

In this chapter, we present some experimental results of linear and nonlinear scattering at the resonances of a plasma column. Since many investigators have observed these resonances in the linear regime, we shall limit our study of linear resonances to a few selected results which are important in relation to our nonlinear scattering experiments. As was mentioned at the beginning of this thesis, experiments in the nonlinear regime are often sensitive to effects which do not disturb appreciably linear phenomena. Some experiments performed by Stern,[55] and by Messiaen and Vandenplas,[56] showed the existence of nonlinear scattering, but their results seem to be incompatible with the radiation pattern predicted by theory. Our experiments illustrate some effects which can explain their results.

6.1 Experimental Set-up

Our experiments were performed by illuminating a plasma column suspended in free space with a signal launched from a microwave horn. The scattered signal was picked up by a small dipole antenna. Figure 6.1 shows the arrangement of the plasma and antennas used in our experiments. Various conflicting requirements had to be considered in the realization of the set-up. In order to approach free space propagation in the experiments, the distance between the plasma and the antennas should be larger than the free space wavelength and the dimensions of the antennas. Since the limited space, time and resources at our disposal permitted only the construction of a small anechoic chamber, it was desirable to use signals of high enough frequencies that the fields set up by the antennas could still approximate free space propagation. On the other hand, the discharge current should be small enough to prevent overheating of the discharge tube. This is especially important for the mercury discharge tubes used in some of the experiments since the neutral gas pressure, and hence the collision frequency, depend strongly on temperature. It turned out that these requirements could not all be met simultaneously. The compromise finally made is described in the following subsections.

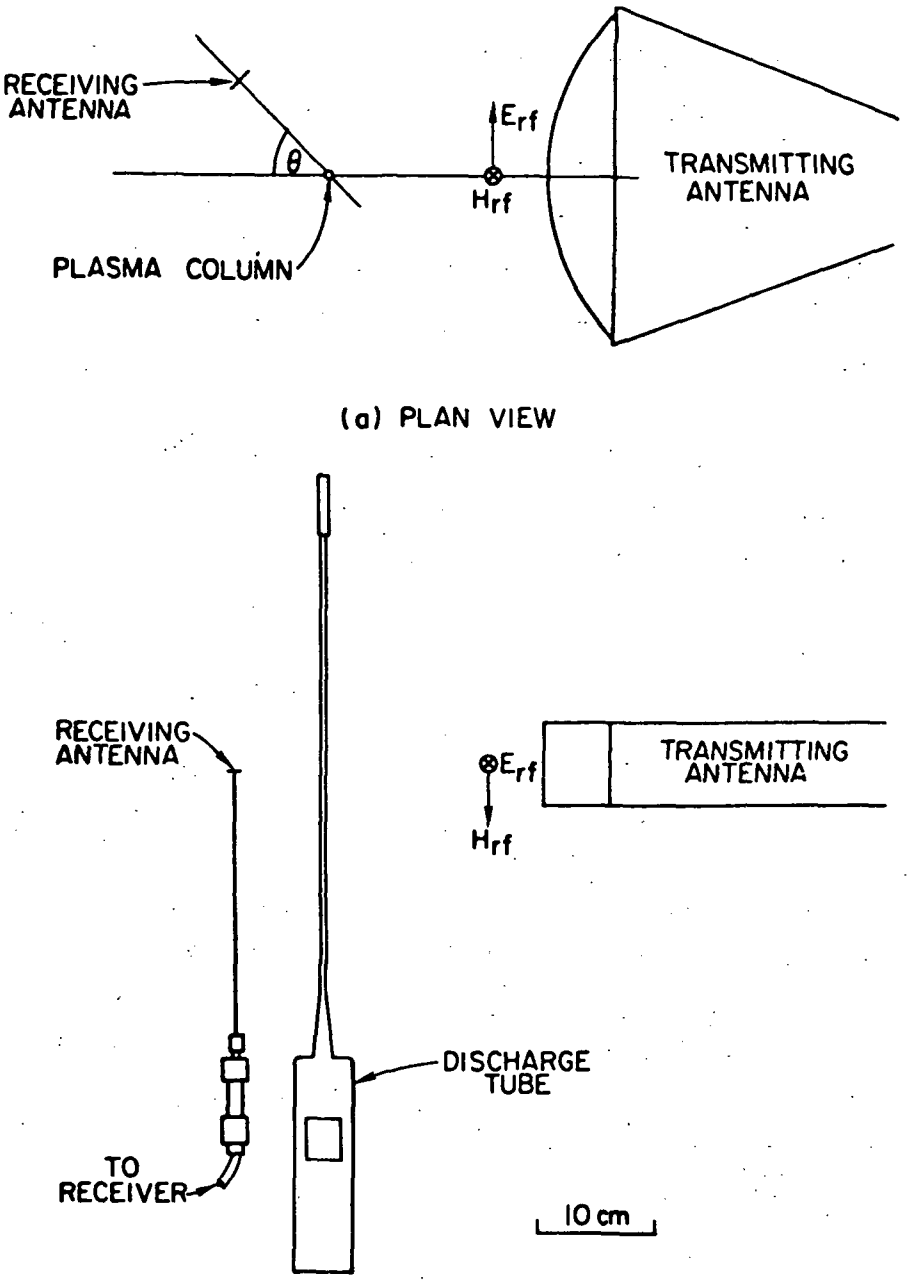

Fig. 6.1 Set-up for studying scattering from a plasma column.

6.1.1 RF System

The waves were launched from an E-plane sectional horn fitted with a dielectric lens. The horn was connected to a piece of S-band waveguide, which had a cut-off frequency of 2.08 GHz. The scattered signal was received on small dipole antennas which could be moved in a circular trajectory around the column by means of a motorized support. A sketch of one of these antennas with its balun is shown in Fig. 6.2. The balun is made of a cylindrical can concentric with the input coaxial line.

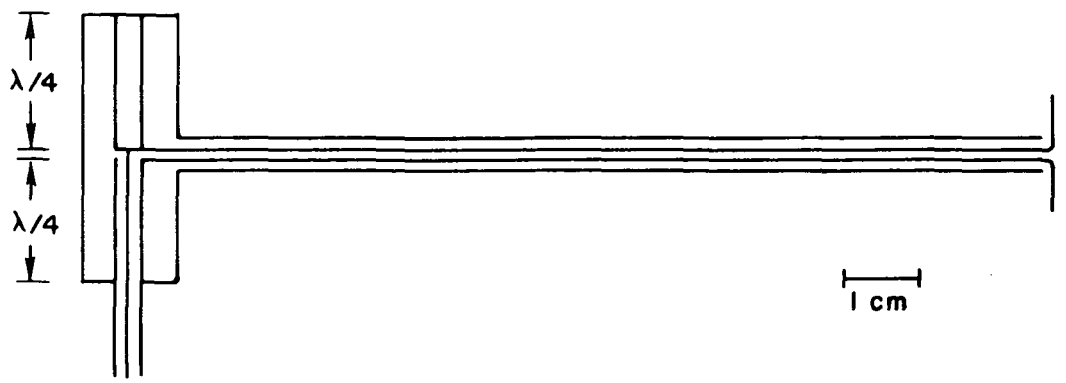

FIG. 6.2 Dipole antenna with balun.

The experimental area was enclosed in a 48 X 61 X 61 cm box lined with microwave absorbent material.

A block diagram of the RF system used in linear measurements is presented in Fig. 6.3. This set-up made possible the cancellation of the direct signal propagating from the horn to the dipole in order to observe only the scattered signal. The direct signal was cancelled out in the absence of a plasma by adjusting the phase and the amplitude of a sample of the transmitted signal fed into the receiver. This feature was used in some of the experiments. Figure 6.4 shows a schematic of the RF set-up used in nonlinear scattering studies. The transmitting system was carefully designed to prevent the radiation of second harmonic signals. The transmitted signal was amplitude modulated by a 1 kHz square wave. The receiver was preceded by a G-band directional coupler acting

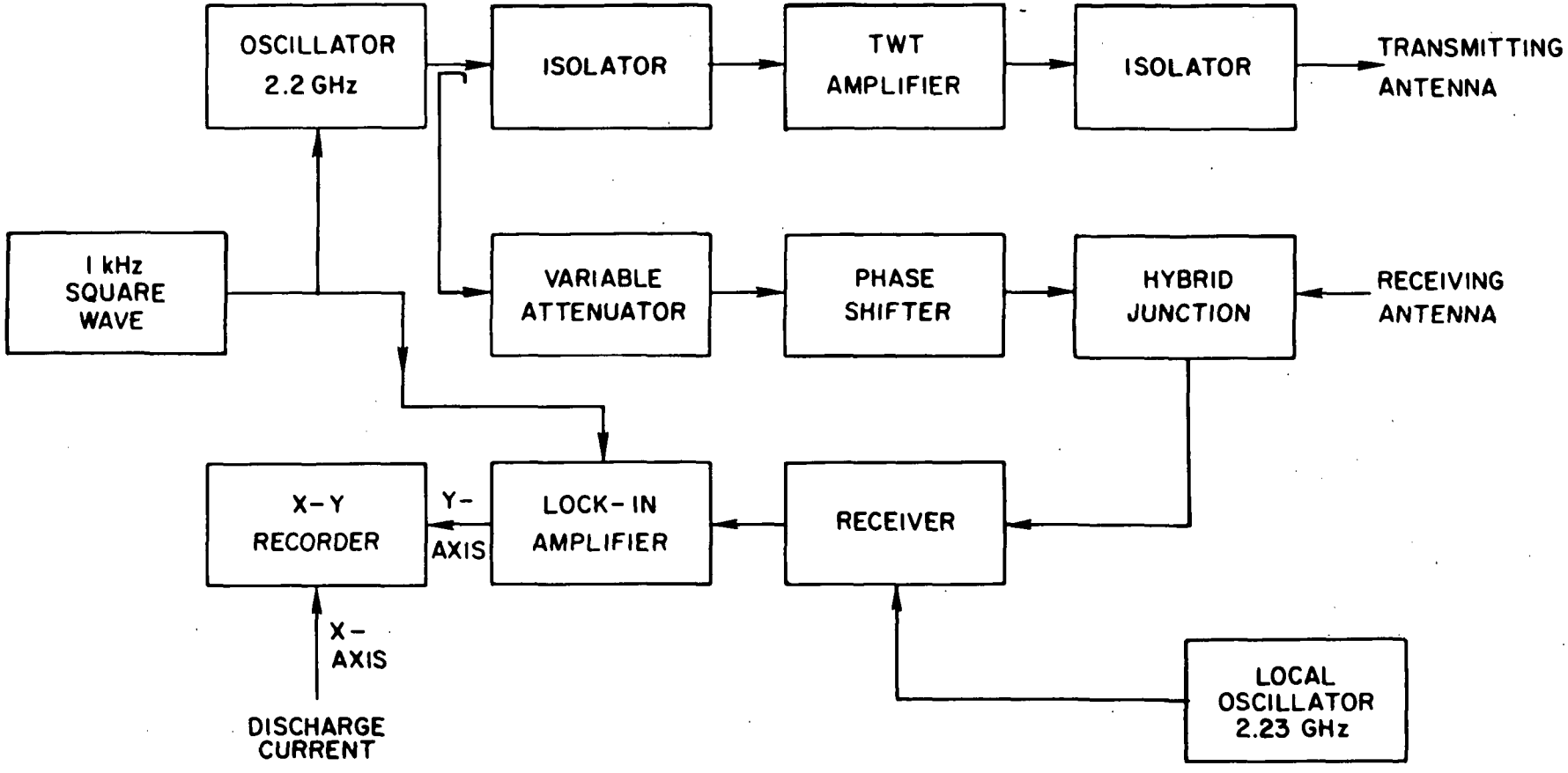

Fig. 6.3 RF system used in linear scattering experiments

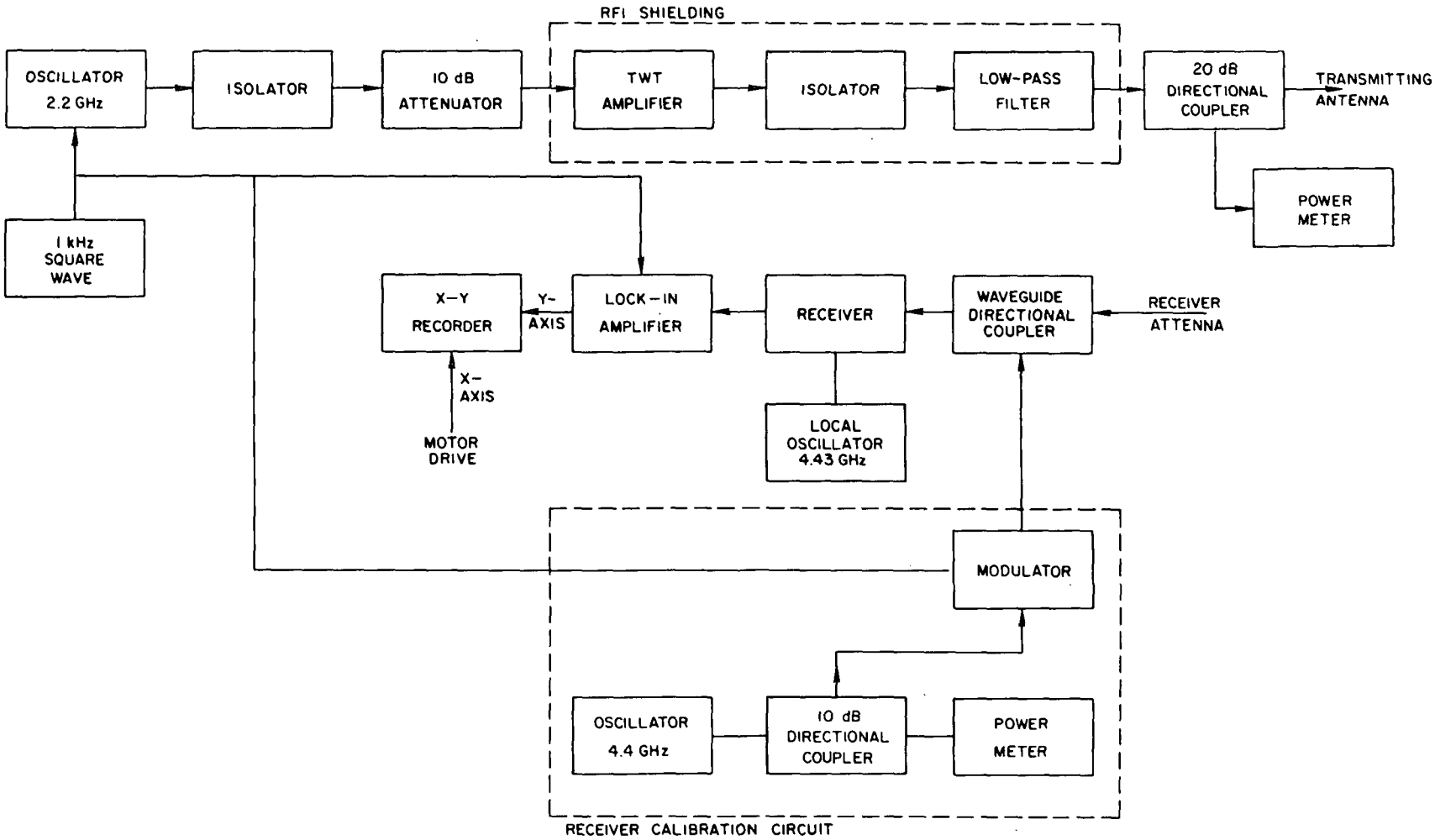

Fig. 6.4 RF system used in nonlinear scattering experiments.

as a high-pass filter as well as providing a calibration signal to the receiver. The audio signal detected in the receiver was then fed into a narrow-band lock-in amplifier. Signals down to -125 dBm could be detected with a bandwidth of 0.25 Hz (time constant of 1 sec). In most experiments, some sensitivity was sacrificed in order to obtain a faster time response.

The antennas were calibrated by comparison with known waveguide fields.

6.1.2 Plasma Columns

Mercury discharge tubes have been used in most of the previous experiments on resonant scattering from a plasma column. The convenience of using a sealed-off tube, as well as the ease of observation of a large number of resonances in a mercury plasma, have been the main reasons for this choice. The mercury vapor pressure in the tube is determined, in theory, by the temperature of the coldest point of the tube. At room temperature, the pressure is of the order of 1 m Torr. We found, however, that the actual Hg pressure in the column depended strongly on the discharge current density, which was as high as $1 A/cm^2$, in some cases. This dependence was illustrated in different ways which shall be mentioned later, as the experimental results are presented. The external temperature of the glass discharge tube was controlled by forced air cooling, which helped to a certain extent in reducing pressure variations in the tube. An argon discharge tube, attached to a vacuum system, was also used in order to study the effect of collision frequency variations on the resonances. The physical characteristics of the various tubes used in our experiments were: $a = 0.31$ cm, $b = 0.42$ cm, $\epsilon_g = 4.65$.

6.2 Linear Scattering

6.2.1 Resonance Frequencies

The resonance frequencies of a plasma column can be measured by sweeping either the incident frequency, at a fixed discharge current, or the discharge current, at a fixed incident frequency. While the first method is preferable, because it does not change the operating conditions of the discharge, we did not use it because of the difficulties associated with obtaining constant incident power levels and receiver

sensitivities at microwave frequencies. Since our only purpose in finding the resonance frequencies was to determine the discharge currents at which the column was resonating, no independent electron density measurements were performed. Examples of resonance frequency spectra obtained in transmission, with the dipole antenna at 0°, are shown in Fig. 6.5 and 6.6. The measurements of Fig. 6.5 were obtained by sweeping the discharge current over the range 50-380 mA in 10 seconds. Those of Fig. 6.6 were obtained point by point, by varying the discharge current manually, and waiting a sufficient time for the tube to attain thermal equilibrium before taking the measurement. The difference in the position of the resonances in Fig. 6.5 and 6.6 shows the effect of the pressure variations in the tube. The relatively fast increase in the discharge current in the measurements of Fig. 6.5 produced less heating of the tube than the slow current variation of the point by point measurements of Fig. 6.6. Hence, the resonances shown in Fig. 6.5 occurred at a higher discharge current, or lower Hg pressure, than those in Fig. 6.6. Any variations in either the cooling rate of the tube, or the sweep rate of the current, produced variations of the resonance current consistent with the results of Fig. 6.5 and 6.6.

6.2.2 Scattering Amplitude and Q of the Resonance

The dipole resonance of a mercury discharge was examined further after cancelling out the direct signal from the horn to the dipole antennae. Figure 6.7 shows the power scattered at $\theta = 0$ as a function of the discharge current. This curve was obtained by sweeping the discharge current over the range 260-330 mA in about 1 minute. Using a loop antenna calibrated against known waveguide fields, the scattering amplitude at the maximum of the resonance, $|S_1|_{max}$, was found to be 0.715. Since this result involved the measurement of H_0 and H_{zs}, given by Eq. (5.43), it is a relative measurement because the two quantities are proportional to each other. The only cause of error comes from reading the instruments and positioning the probe properly. A conservative estimate of the error, in this case, would be ± 25%, which corresponds to an error of ± 2 db in the relative power. It is then obvious that collisional damping has to be considered if an accurate comparison between theory and experiment is to be obtained. The Q of the resonance, as obtained from Fig. 6.7, was 45.

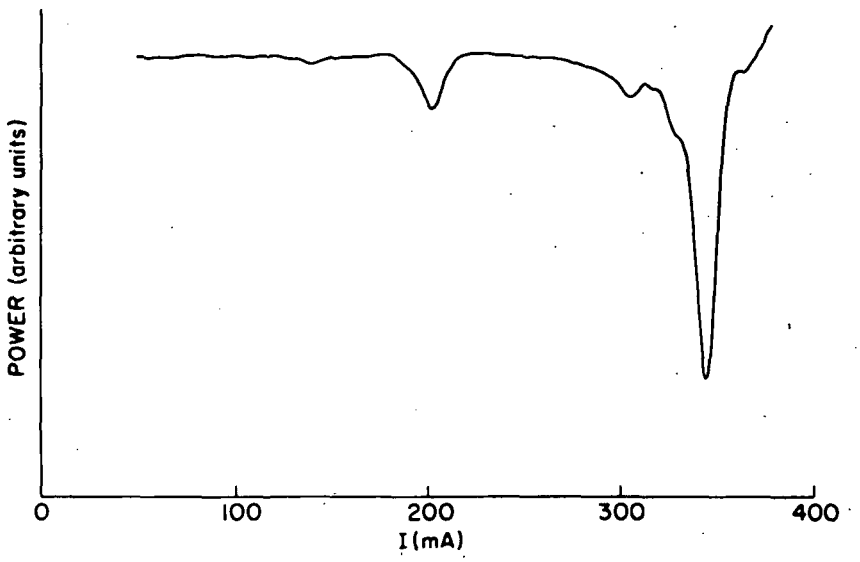

Fig. 6.5 Linear scattering obtained by the current sweep method.

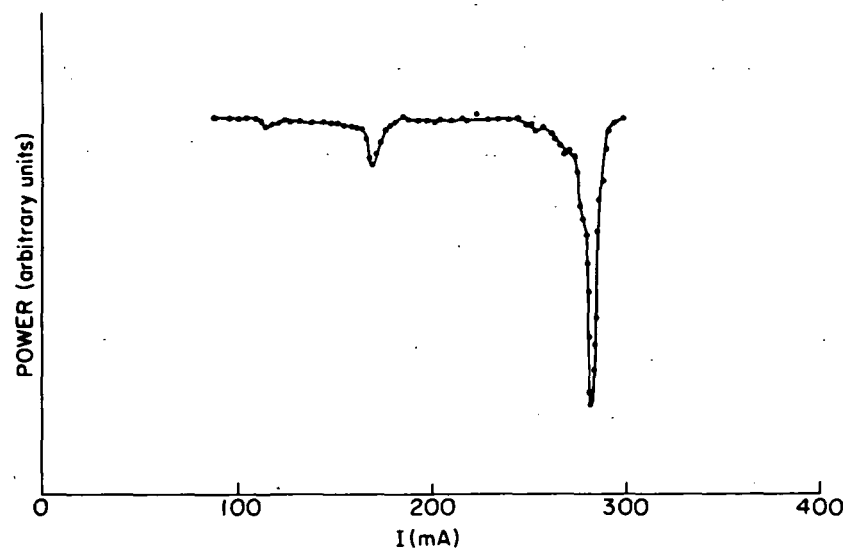

Fig. 6.6 Linear scattering obtained by the point-by-point method.

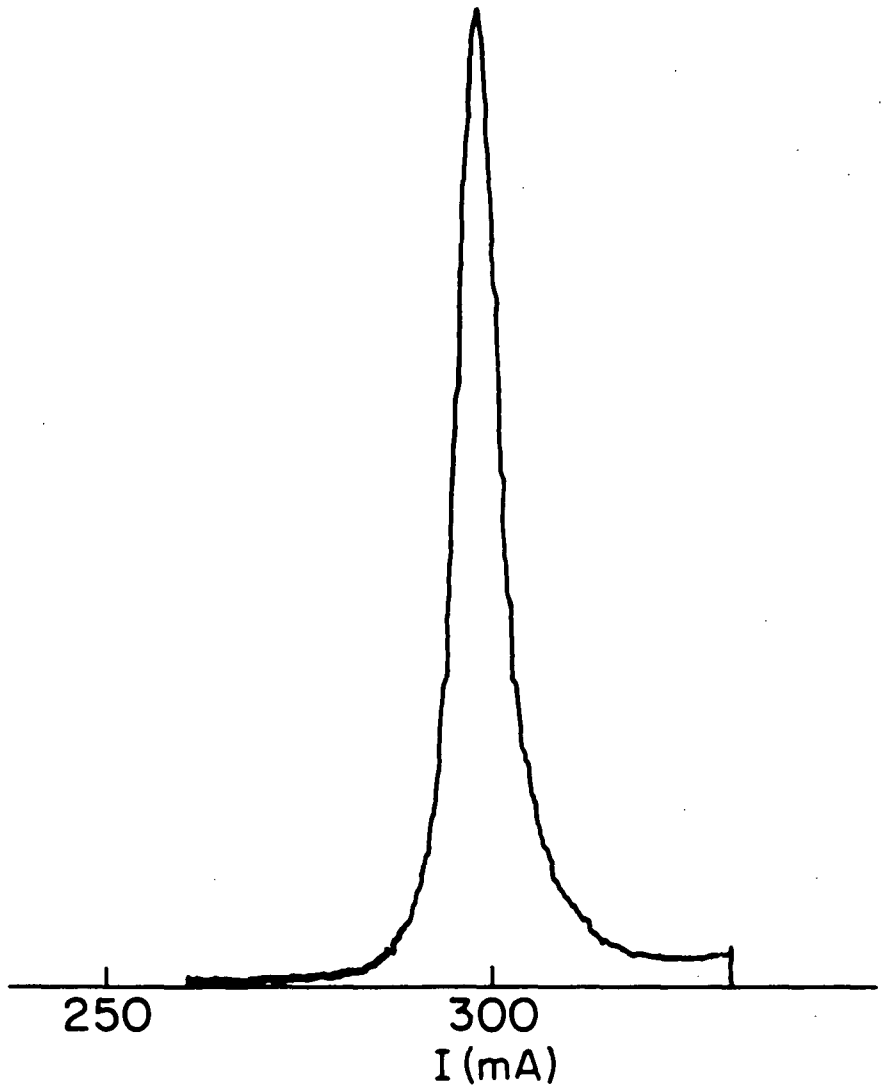

Fig. 6.7 Linear scattered power at 2.2 GHz with θ=0.

6.2.3 Radiation Pattern

The radiation pattern at 2.2 GHz was measured with the mercury discharge, and is shown in Fig. 6.8. Each point on the curve was obtained after cancelling the direct signal from the horn to the dipole antenna. The curve for $\cos^2\theta$ vs θ is plotted with the experimental points. The finite beam width of the antenna caused the experimental points to lie above the theoretical curve except in the regions around $\pm 180^\circ$, where the shadow cast by the dipole antenna, between the horn and the column, produced less scattered power than predicted.

6.3 Nonlinear Scattering

The experiments described in this section involved harmonic generation in a plasma column illuminated by a 2.2 GHz large amplitude wave. While it was relatively easy to observe harmonic generation, it was difficult to measure unequivocally some of the properties of the phenomenon predicted by theory. For instance, if a linear dipolar resonance is excited, the second harmonic radiation pattern should be quadrupolar, with maxima at $\pm \pi/4$ and $\pm 3\pi/4$. As mentioned in Chapter I, this behavior was observed only after cancelling out the transverse component of the Earth's magnetic field. The situation is not as simple as indicated by the preliminary results obtained by Bruce[62] over a limited range of angles. Our experiments uncovered some additional difficulties.

6.3.1 Radiation Pattern of Nonlinear Scattering

The influence of the Earth's magnetic field on the radiation pattern of nonlinear scattering is illustrated in Fig. 6.9, which display the power received as a function of the angle for different values of the transverse DC magnetic field. A pair of Helmholtz coils was used to cancel out the transverse component of the Earth's magnetic field, $B_\perp$, which was perpendicular to the direction of the incident wave. With no cancellation, the radiation pattern, shown in Fig. 6.9(a), is dipolar, and the maximum radiated power is in the direction of $B_\perp$. It is interesting to note that Bruce's measurements,[62] performed with the magnetic field parallel to the incident wave, also show maximum power radiated parallel to $B_\perp$. It can be seen from Fig. 6.9

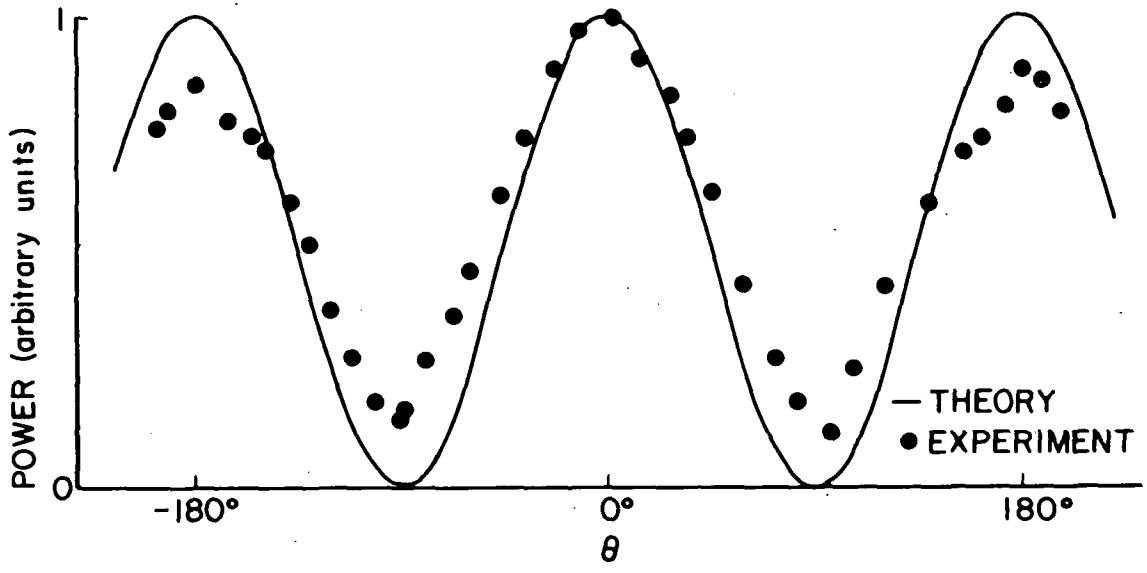

Fig. 6.8 Radiation pattern of linear scattered power at 2.2 GHz.

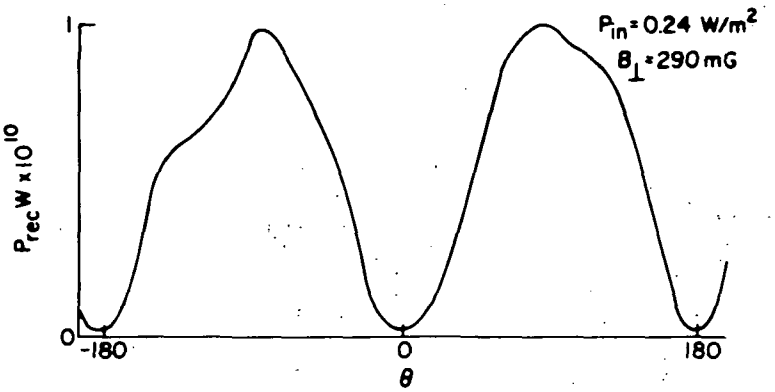

(a)

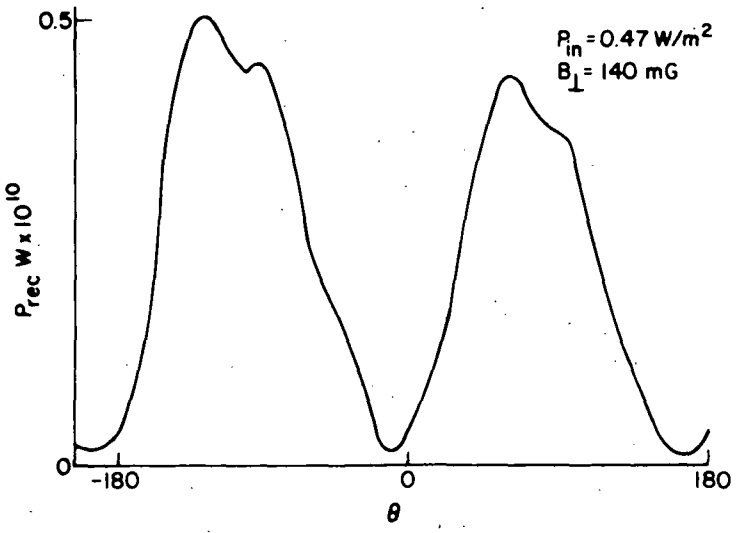

(b)

Fig. 6.9 Radiation pattern of nonlinear scattered power as a function of the transverse DC magnetic field.

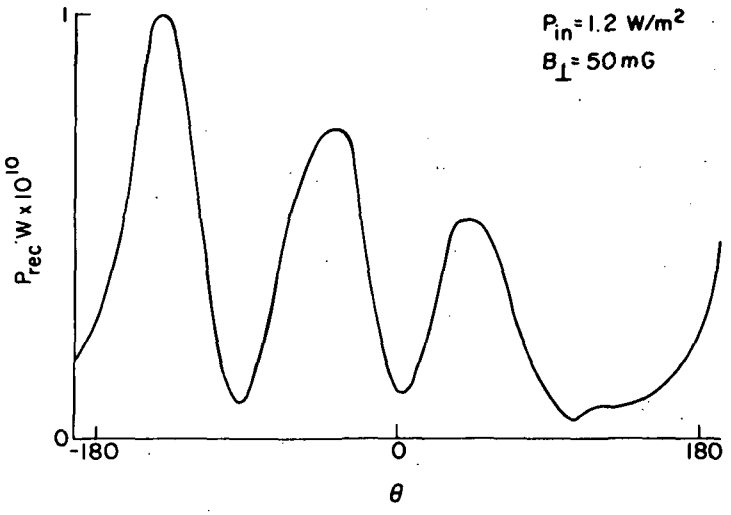

(c)

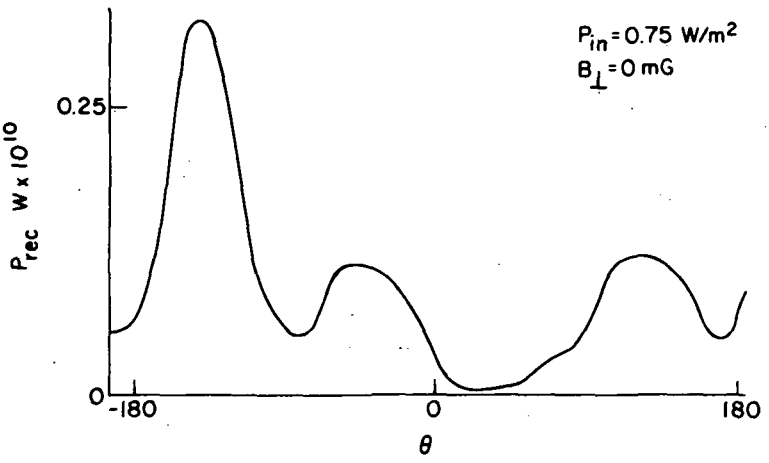

(d)

Fig. 6.9 (Cont.)

that the radiation pattern goes from dipolar to more or less quadrupolar, when the cancellation is complete. The radiated power also goes down significantly as $B_\perp$ is decreased. In our measurements, the incident power was increased while the received power was kept within a narrow range. This illustrates the importance of cancelling the Earth's magnetic field for scattering amplitude measurements as well as radiation pattern measurements. A possible mechanism for the observed behavior is a slight deformation of the DC electron density profile due to the Hall potential produced by electrons drifting in a transverse magnetic field.

The departure of the observed pattern from a pure quadrupole, and more surprisingly, its lack of symmetry, were first thought to come from imperfect cancellation of the Earth's field. Various experiments, using different discharge tubes, produced inconsistent results. We finally found that a rotation of the discharge tube produced a considerable variation in the second harmonic power scattered at a given angle. The radiation pattern in Fig. 6.10 was obtained after rotating the

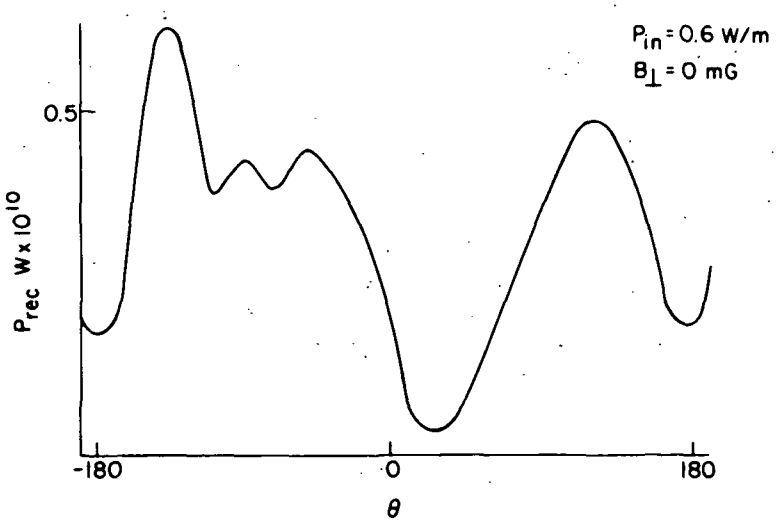

Fig. 6.10. Radiation pattern of nonlinear scattered power after 90° rotation of discharge tube.

discharge tube 90° from its position in the measurements shown in Fig. 6.9. We verified that lateral variations in the position of the discharge tube produced only minor disturbances in the radiation pattern, compared to those coming from a rotation of the tube. This indicated that the rotational asymmetry of the discharge tube was responsible for the asymmetric radiation patterns measured.

Various possible causes for the asymmetry of the tube were investigated. The use of a discharge tube made of pyrex tubing shrunk over a precision ground mandrel improved the radiation pattern only slightly: the curves in Figs. 6.9 and 6.10 were obtained with such a discharge tube. The effect of variations in the wall thickness of the tube were negligible. This was verified by inserting glass tubes of various diameters and wall thicknesses around the discharge tube and observing that the radiation pattern was unchanged, even when the axis of the outside tube was at an angle with the axis of the discharge tube. The condition of the inside surface of the discharge tube was found to influence the radiation pattern in an argon discharge. This was indicated by the changes with time in the observed radiation pattern after cleaning the glass tube with an HF acid solution. None of the results were more symmetric than the others, however: they were only different. The negligible effect on the radiation pattern of cleaning the discharge tube with organic solvents suggested that the condition of the glass surface itself, and possible some metallic deposits of evaporated cathode material, were responsible for the asymmetry of the discharge. It should be remembered that the power received at the second harmonic was about 90-100 dB below the input power to the waveguide. As indicated previously by the influence of the Earth's magnetic field on the radiation pattern, very small deformations of the static electron density profile in the column have a very important influence on the nonlinear scattering. Further studies of surface effects on a plasma column would be of great interest, in the present case, but it was not considered worthwhile to pursue them for the purpose of this thesis.

6.3.2 Scattering Amplitude

Because of the difficulties encountered in measuring the radiation pattern of nonlinear scattering, it is clear that only order of magnitude results can be obtained for the scattering amplitude. For example, the scattering amplitude, Y_{32}, obtained at the maximum in the radiated power, is 1.36×10^{-2} in Fig. 6.9(d), and 2.42×10^{-2} in Fig. 6.10. This compares with 4.17×10^{-3} predicted by the cold plasma theory without collisional damping. As indicated in Section 5.1.4, we could not obtain numerical results for the case of a warm plasma column with electron temperature of approximately 3 eV, and an incident frequency of 2.2 GHz. The nonlinear scattering amplitude predicted at 2.2 GHz, for an electron temperature of 8 eV, is 0.123, without collisions. In view of the large variations of Y_{32} as a function of electron temperature, as seen in Fig. 5.4(b), it is impossible to compare the theory and the experiment, in this case.

Some additional measurements were obtained with the argon discharge. The first Tonks-Dattner resonance was excited. We can see in Fig. 6.11 that the power received at the second harmonic is proportional to the square of the input power to the horn. Actually, the slope of the straight line is 2.12. The influence of collisions on the nonlinear scattering was also studied by varying the argon pressure in the discharge tube and adjusting the discharge current to follow the linear resonance. The collision frequency was obtained by assuming an electron temperature of 8 eV, and using data obtained by Frost and Phelps[71] for the momentum transfer collision cross-section of electrons in argon. The results are shown in Fig. 6.12, along with a theoretical curve obtained for the same conditions. The experimental results show a variation similar to the theoretical curve, and the scattering amplitudes agree within an order of magnitude.

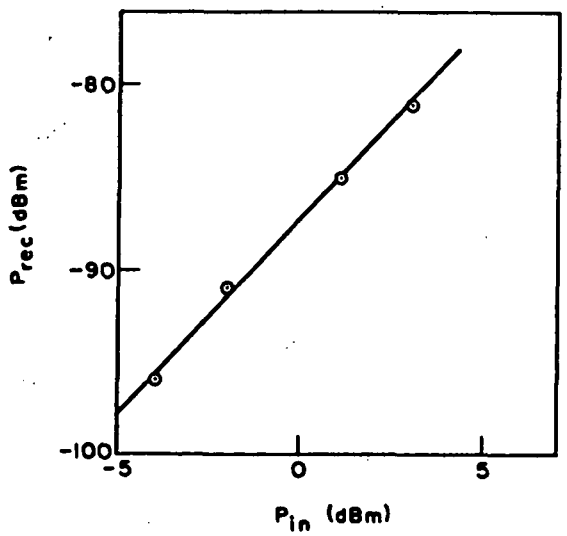

Fig. 6.11 Power received at 4.4 GHz vs power emitted at 2.2 GHz.

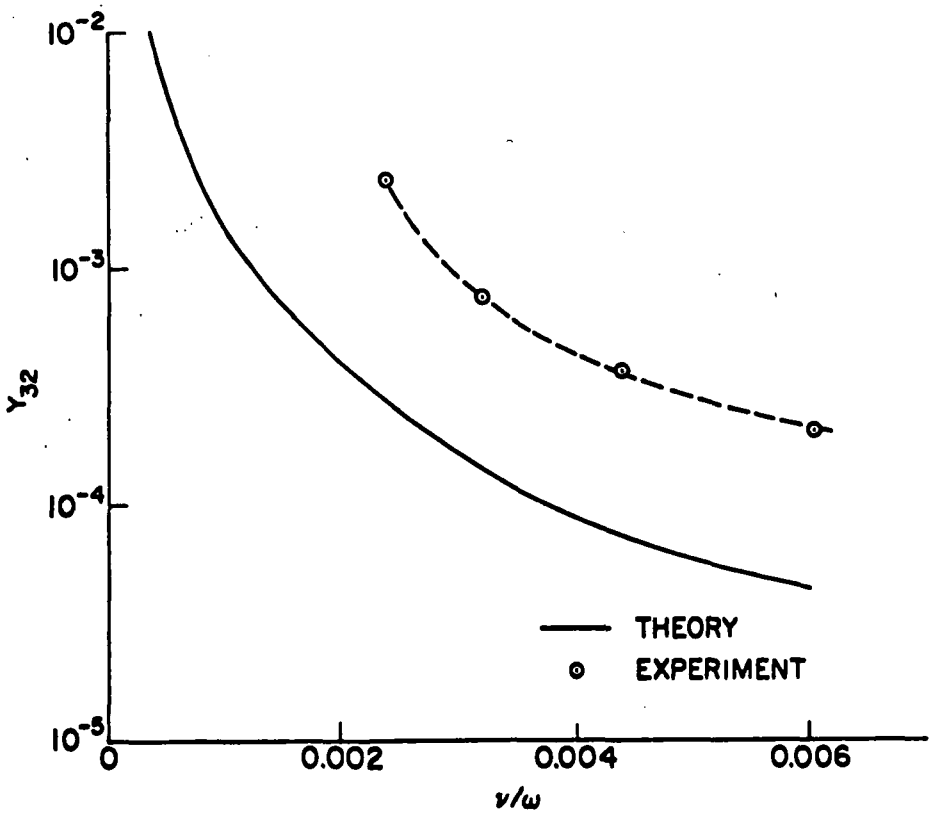

Fig. 6.12 Nonlinear scattering amplitude as a function of the collision frequency.

Chapter VII

CONCLUSIONS

The purpose of this work has been to study two special cases of nonlinear wave interactions on a plasma column. The first part of the thesis was devoted to the nonlinear coupling of slow waves on a plasma column. Slow waves in the presence of an infinite magnetic field were considered theoretically in Chapter II. The coupled mode equations and the coupling coefficient for three wave coupling were derived using an expansion of the Lagrangian density for a cold plasma. The coupled mode equations were then solved for the special cases of parametric amplification and mode conversion. The effects of linear wave damping and of a departure from synchronism due to the dispersion of the interacting modes were also considered in order to determine the bandwidth of the interaction. The linear wave damping was introduced in the coupled mode equations by means of a phenomenological loss factor.

Some experimental results of mode conversion on a plasma column in a strong magnetic field were presented in Chapter III. While qualitative agreement with theory was obtained, it was not possible to compare directly theory and experiment. It was found that the most important factor in determining the properties of the coupling is Δk, the departure from synchronism. Any difference between the theoretical and the experimental dispersion characteristics which causes the theoretical and experimental values of Δk to be significantly different makes an exact comparison between theory and experiment impossible. This is what prevented a quantitative comparison between the theory of Chapter II and the experiments of Chapter III. The inclusion of the radial nonuniformity of the column, and of finite electron temperature, might have provided the required correspondence between theory and experiment. For this reason, the theory presented in this work is only a first step in solving the problem completely.

Slow waves on a column in the absence of a magnetic field were also considered briefly in Chapter IV to illustrate the power of the Lagrangian formalism. Previous attempts to solve this problem[28,29] led to theories valid only in the small-ka limit and did not present any numerical

values of the gain obtained. In addition to developing a theory valid for any ka, in a lossless cold plasma, we also presented numerical results of the gain for parametric interaction, taking into account the dispersion of the interacting modes.

A study of nonlinear scattering from a plasma column made up the second part of this thesis. In this case, the equations of the problem were expanded up to second order to derive a nonlinear equation for the potential inside the column. The first and second order solutions in the plasma were then matched to solutions of the wave equation outside to obtain the linear and nonlinear scattering amplitudes. Numerical results obtained by computer solution of the equations showed that the linear resonances of different multipole order occur at different electron densities for a given incident wave frequency. Furthermore, collisional damping was found to reduce the scattering amplitude of the quadrupole resonances, in small diameter plasma columns, to such an extent that only dipole resonances would be excited strongly by an incident plane wave. This justified the consideration of individual linear dipole resonances and the resultant nonlinear quadrupolar scattering. The nonlinear scattering amplitudes from a uniform and nonuniform column were computed for selected ranges of frequencies and electron temperature. The range of the parameters was restricted by the nature of the linear and nonlinear solutions, which could not be computed for $a/\lambda_D \gtrsim 80$.

In Chapter VI, some experiments of linear and nonlinear scattering from a plasma column were described. The quadrupolar nature of the nonlinear scattering could only be verified approximately due to the asymmetry of the plasma column. For the same reason, the measurements of nonlinear scattering amplitude reported can be expected to be valid only within an order of magnitude. No direct comparison with theory could be achieved because the experimental parameters were outside the range where the equations could be solved numerically. This limitation could be overcome in future experiments by using a lower incident frequency. This would require either a large anechoic chamber, or a combination of dipolar and quadrupolar couplers which would permit the excitation of a dipole resonance, and the reception of the quadrupolar

nonlinear scattering. Another approach might be the use of a rectangular waveguide of suitable frequency range, and equipped with couplers sensitive to the mode excited by the quadrupolar nonlinear scattering. While this method would not yield the radiation pattern of nonlinear scattering, it would be useful in measuring the frequency dependence of the scattering because of the relative ease of calibration of a waveguide system, compared to antennas.

It should be remembered, as this work is brought to a close, that the interacting modes considered in this work are not, by any means, the only ones that could interact in a plasma column. Combinations of electromagnetic waves and plasma waves on a column have also been considered,[33] as well as combination of two resonances and one slow wave.[72] Ion-acoustic waves have been produced by exciting a column resonance at power levels much higher than those used in this work.[73] Another possibility would be incoherent scattering by fluctuations in the plasma.[74]

Appendix A

POWER FLOW IN SLOW WAVES ON A PLASMA COLUMN IN AN INFINITE MAGNETIC FIELD SURROUNDED BY AN INFINITE DIELECTRIC

The modes obtained by an exact solution for slow waves in the presence of an infinite magnetic field are transverse magnetic.[10] This means that a slow wave is not purely electrostatic; it has a Poynting vector. The magnetic field, $\underset{\sim}{H}$, can be obtained from the scalar potential, φ, by means of the Maxwell equation

$$\nabla \times \underset{\sim}{H} = \frac{\partial \underset{\sim}{D}}{\partial t} . \tag{A.1}$$

Using the permittivity tensor for a cold plasma in an infinite magnetic field

$$\underset{\sim}{\overset{\leftrightarrow}{\epsilon}}_p = \begin{pmatrix} \epsilon_\perp & 0 & 0 \\ 0 & \epsilon_\perp & 0 \\ 0 & 0 & \epsilon_\parallel \end{pmatrix} , \quad \epsilon_\perp = \epsilon_0 , \quad \epsilon_\parallel = \epsilon_0 \left(1 - \frac{\omega_0^2}{\omega^2}\right) , \tag{A.2}$$

Eq. (A.1) can be written, in component form,

$$- \frac{\partial H_\theta}{\partial z} = jkH_\theta = j\epsilon_0 \omega E_r , \tag{A.3}$$

$$\frac{\partial H_r}{\partial z} = - jkH_r = j\omega\epsilon_0 E_\theta , \tag{A.4}$$

$$\frac{1}{r} \frac{\partial}{\partial r} (rH_\theta) - \frac{1}{r} \frac{\partial H_r}{\partial \theta} = j\omega\epsilon_0 \left(1 - \frac{\omega_0^2}{\omega^2}\right) E_z . \tag{A.5}$$

Using Eqs. (2.7)-(2.9), the magnetic field components inside the plasma column become

$$H_r = \frac{\epsilon_0}{r} \frac{\omega}{k} \frac{\partial \varphi}{\partial \theta} = - jn \frac{\epsilon_0}{kr} \psi J_n(\beta r) \exp j(\omega t - n\theta - kz) , \tag{A.6}$$

$$H_\theta = - \epsilon_0 \frac{\omega}{k} \frac{\partial \varphi}{\partial r} = - \epsilon_0 \beta \frac{\omega}{k} \psi \, J_n'(\beta r) \exp j(\omega t - n\theta - kz) \quad . \qquad (A.7)$$

Outside the plasma, H_r and H_z are given by

$$H_r = - jn \frac{\epsilon_0}{r} \frac{\omega}{k} \psi \frac{J_n(\beta a)}{K_n(\beta a)} K_n(kr) \exp j(\omega t - n\theta - kz) \quad ,$$

$$H_\theta = - \epsilon_0 \omega \psi \frac{J_n(\beta a)}{K_n(\beta a)} K_n'(kr) \exp j(\omega t - n\theta - kz) \quad . \qquad (A.9)$$

The average axial power flow associated with the wave is given by

$$P = \frac{1}{2} \mathrm{Re}\left\{ \int_S (\underset{\sim}{E} \times \underset{\sim}{H}^*)_z d^2r \right\} = - \frac{1}{2} \mathrm{Re}\left\{ \int_S \left[\frac{\partial \varphi}{\partial r} H_\theta^* - \frac{\partial \varphi}{\partial \theta} H_r^* \right] d^2r \right\} , \quad (A.10)$$

where S is a plane perpendicular to the axis of the plasma column. Using the expressions for φ, given by Eq. (2.9) and (2.12), and $\underset{\sim}{H}$, given by Eq. (A.6)-(A.9), we obtain

$$P = \frac{\epsilon_0}{2} \frac{\omega}{k} |\psi|^2 \mathrm{Re}\left\{ \int_{S_p} \left[\beta^2 J_n'^2(\beta r) + \frac{n^2}{r^2} J_n^2(\beta r) \right] d^2r \right.$$

$$\left. + \frac{J_n^2(\beta a)}{K_n^2(ka)} \int_{S_g} \left[k^2 K_n'^2(kr) + \frac{n^2}{r^2} K_n^2(kr) \right] d^2r \right\} , \qquad (A.11)$$

where S_p and S_g are the parts of S inside and outside the plasma column, respectively. The integrals in Eq. (A.11) can be evaluated analytically to yield the power flow as

$$P = \frac{\pi\epsilon_0}{2}\frac{\omega}{k}|\psi|^2\left\{\left[k^2a^2\frac{K_n'^2(ka)}{K_n^2(ka)} + \beta^2a^2 - n^2\right]J_n^2(\beta a)\right.$$

$$\left. - \left[\beta^2a^2\frac{J_n'^2(\beta a)}{J_n^2(\beta a)} + k^2a^2 - n^2\right]K_n^2(ka)\right\} \quad . \qquad (A.12)$$

This result can be reduced further, by using the dispersion relation given by Eq. (2.13),

$$P = \frac{\pi\epsilon_0}{2}\frac{\omega_0^2}{\omega}\frac{ka^2}{\omega}|\psi|^2 J_n^2(\beta a) \quad . \qquad (A.13)$$

The same result could be obtained by taking the product of the group velocity and of the time-averaged energy density. Equation (A.13) can also be written as in Eq. (3.2).

Appendix B

COUPLING ENERGY DENSITY

In this Appendix, we shall make use of vector identities and of properties of the solutions $\underset{\sim}{\varphi}_\lambda$ given by Eq. (4.4) to transform Eq. (4.21). The following vector identity is used in the first and the second term of Eq. (4.21),

$$(\underset{\sim}{A}\cdot\nabla)\underset{\sim}{C} = \nabla(\underset{\sim}{A}\cdot\underset{\sim}{C}) - (\underset{\sim}{C}\cdot\nabla)\underset{\sim}{A} - \underset{\sim}{A}\times(\nabla\times\underset{\sim}{\ }) - \underset{\sim}{C}\times(\nabla\times\underset{\sim}{A}). \tag{B.1}$$

Since $\underset{\sim}{A}$ and $\underset{\sim}{C}$ are gradients of the potential, in Eq. (4.21), the last two terms on the RHS of Eq. (B.1) are identically zero, and Eq. (4.21) becomes

$$e_c = \frac{j\omega_0^2 e\epsilon_0}{8m_e}\iint_P \left\{ \frac{\nabla\underset{\sim}{\varphi}_\beta}{\omega_\alpha^2\omega_\beta^2}\cdot\nabla(\nabla\underset{\sim}{\varphi}_\alpha^*\cdot\nabla\underset{\sim}{\varphi}_\gamma) + \frac{\nabla\underset{\sim}{\varphi}_\gamma}{\omega_\alpha^2\omega_\gamma^2}\cdot(\nabla\underset{\sim}{\varphi}_\alpha^*\cdot\nabla\underset{\sim}{\varphi}_\beta) \right.$$
$$\left. + \left(\frac{1}{\omega_\beta^2\omega_\gamma^2} - \frac{1}{\omega_\alpha^2\omega_\beta^2} - \frac{1}{\omega_\alpha^2\omega_\gamma^2}\right)\nabla\underset{\sim}{\varphi}_\beta\cdot[(\nabla\underset{\sim}{\varphi}_\gamma\cdot\nabla)\nabla\underset{\sim}{\varphi}_\alpha^*\right\} d^2r + (c.c.) . \tag{B.2}$$

The factor in the third term on the RHS of Eq. (B.2) can be transformed using the synchronism condition for the frequencies. The energy density then becomes

$$e_c = \frac{j\omega_0^2 e\epsilon_0}{8m_e\omega_\alpha^2}\iint_P \left\{ \frac{\nabla\underset{\sim}{\varphi}_\beta}{\omega_\beta^2}\cdot\nabla(\nabla\underset{\sim}{\varphi}_\alpha^*\cdot\nabla\underset{\sim}{\varphi}_\gamma) + \frac{\nabla\underset{\sim}{\varphi}_\gamma}{\omega_\gamma^2}\cdot\nabla(\nabla\underset{\sim}{\varphi}_\alpha^*\cdot\nabla\underset{\sim}{\varphi}_\beta) + \frac{2\nabla\underset{\sim}{\varphi}_\beta}{\omega_\beta\omega_\gamma}\cdot\left[(\nabla\underset{\sim}{\varphi}_\gamma\cdot\nabla)\nabla\underset{\sim}{\varphi}_\alpha^*\right]\right\} d^2r \tag{B.3}$$
$$+ (c.c.) .$$

This expression can be reduced further by using the properties of the solutions $\underset{\sim}{\varphi}_\lambda$. Consider the following integral

$$\iint_P \nabla\underline{\varphi}_\beta \cdot \nabla\psi \, d^2r = \int_0^{2\pi} \int_0^a \left\{ \frac{\partial \underline{\varphi}_\beta}{\partial r} \frac{\partial \psi}{\partial r} + \frac{1}{r^2} \frac{\partial \underline{\varphi}_\beta}{\partial \theta} \frac{\partial \psi}{\partial \theta} + \frac{\partial \underline{\varphi}_\beta}{\partial z} \frac{\partial \psi}{\partial z} \right\} r \, dr \, d\theta$$

$$= \int_0^{2\pi} \frac{\partial \underline{\varphi}_\beta}{\partial r} \psi \, r \, d\theta \Big|_0^a - \int_0^a \int_0^{2\pi} \frac{1}{r} \frac{\partial}{\partial r} \left(r \frac{\partial \underline{\varphi}_\beta}{\partial r} \right) \psi \, r \, dr \, d\theta$$

$$+ \int_0^{2\pi} \int_0^a \left\{ \frac{1}{r^2} \frac{\partial \underline{\varphi}_\beta}{\partial \theta} \frac{\partial \psi}{\partial \theta} + \frac{\partial \underline{\varphi}_\beta}{\partial z} \frac{\partial \psi}{\partial z} \right\} r \, dr \, d\theta \, , \qquad \text{(B.4)}$$

where

$$\psi = \nabla\underline{\varphi}^*_\alpha \cdot \nabla\underline{\varphi}_\gamma \qquad \text{(B.5)}$$

Laplace's equation, which is satisfied by $\underline{\varphi}_\lambda$, can be used to simplify the second and third terms on the RHS of Eq. (B.4), and the result is

$$\iint_P \nabla\underline{\varphi}_\beta \cdot \nabla\psi \, d^2r = \int_0^{2\pi} \frac{\partial \underline{\varphi}_\beta}{\partial r} \psi r d\theta \Big|_0^a + \int_0^{2\pi} \int_0^a \left\{ \frac{1}{r^2} \left[\frac{\partial^2 \underline{\varphi}_\beta}{\partial \theta^2} \psi + \frac{\partial \underline{\varphi}_\beta}{\partial \theta} \frac{\partial \psi}{\partial \theta} \right] \right.$$

$$\left. + \left[\frac{\partial^2 \underline{\varphi}_\beta}{\partial z^2} \psi + \frac{\partial \underline{\varphi}_\beta}{\partial z} \frac{\partial \psi}{\partial z} \right] \right\} r \, dr \, d\theta \, . \qquad \text{(B.6)}$$

We can use Eqs. (4.4) and (4.6) in Eq. (B.5) to obtain

$$\psi = \left[\frac{\partial \hat{\varphi}^*_\alpha}{\partial r} \frac{\partial \hat{\varphi}_\gamma}{\partial r} + \left(\frac{n_\alpha n_\gamma}{r^2} + k_\alpha k_\gamma \right) \hat{\varphi}^*_\alpha \hat{\varphi}_\gamma \right] \exp j\left[(\omega_\gamma - \omega_\alpha)t - (k_\gamma - k_\alpha)z - (n_\gamma - n_\alpha)\theta \right] \, . \qquad \text{(B.7)}$$

This result is then substituted in the first term of the second integral on the RHS of Eq. (B.6), and we obtain

$$\frac{\partial^2 \underline{\varphi}_\beta}{\partial \theta^2} \psi + \frac{\partial \underline{\varphi}_\beta}{\partial \theta} \frac{\partial \psi}{\partial \theta} = - n_\beta (n_\beta + n_\gamma - n_\alpha) \underline{\varphi}_\beta \psi = 0 \, , \qquad \text{(B.8)}$$

because the n_λ satisfy a synchronism condition. In a similar way,

$$\frac{\partial^2 \varphi_\beta}{\partial z^2}\,\psi + \frac{\partial \varphi_\beta}{\partial z}\,\frac{\partial \psi}{\partial z} = -\,k_\beta(k_\beta + k_\gamma - k_\alpha)\,\varphi_\beta\psi = k_\beta \Delta k \varphi_\beta \psi \ , \qquad (B.9)$$

where $\Delta k = k_\alpha - k_\beta - k_\gamma$. After substituting Eqs. (B.8) and (B.9) in Eq. (B.6) and performing the integration over θ in the RHS of the resulting equation, we obtain

$$\iint_P \nabla\varphi_\beta \cdot \nabla\psi \; d^2r = 2\pi a \; \psi(a) \left.\frac{\partial \varphi_\beta}{\partial r}\right|_{r=a} + 2\pi k_\beta \Delta k \int_0^a \varphi_\beta \psi \; r \; dr \ . \qquad (B.10)$$

Equations (B.3), (B.7) and (B.10) are combined, and the final result can be found in Eq. (4.22).

Appendix C

SOLUTION OF EQUATION (5.17) FOR A PARABOLIC DENSITY PROFILE

In this Appendix, we shall obtain series solutions of Eq. (5.17) by the method of Frobenius. It is convenient to introduce

$$\xi = \frac{r}{a} \quad , \qquad \zeta_D = \frac{a}{\lambda_D} \, , \qquad f(\xi) = 1 - \alpha \xi^2 \, . \tag{C.1}$$

We can write Eq. (5.17) in the form:

$$\xi^4 \psi_\ell'''' + P_1(\xi)\xi^3\psi_\ell''' + P_2(\xi)\xi^2\psi_\ell'' + P_3(\xi)\xi\psi_\ell' + P_4(\xi)\psi_\ell = 0 \, , \tag{C.2}$$

where

$$P_1(\xi) = 2\left[\frac{\gamma+(1-\gamma)\alpha\xi^2}{\gamma(1-\alpha\xi^2)}\right], \tag{C.3}$$

$$P_2(\xi) = -(2\ell^2+1) + k_p^2 a^2 \xi^2 + \frac{\alpha\zeta_D^2\xi^4}{\gamma} + \frac{2\alpha\xi^2(3-\alpha\xi^2)}{\gamma(1-\alpha\xi^2)^2} \, , \tag{C.4}$$

$$P_3(\xi) = 2\ell^2+1 + k_p^2 a^2 \xi^2 + \frac{3\alpha\zeta_D^2\xi^4}{\gamma} + \frac{2\alpha\xi^2[1-\ell^2+(1+\ell^2)\alpha\xi^2]}{\gamma(1-\alpha\xi^2)^2} \, , \tag{C.5}$$

$$P_4(\xi) = -\ell^2\left[4-\ell^2+k_p^2 a^2 \xi^2 + \frac{\alpha\zeta_D^2\xi^4}{\gamma} + \frac{4\alpha^2\xi^4}{\gamma(1-\alpha\xi^2)^2}\right] , \tag{C.6}$$

and

$$k_p^2 = \frac{1}{\gamma\lambda_D^2}\left(\frac{\Gamma\omega^2}{\omega_0^2} - 1\right) . \tag{C.7}$$

Equation (C.2) has a regular singularity at the origin. We assume that we can find solutions of Eq. (C.2) of the form

$$\psi_\ell(\xi) = \sum_{i=0}^{\infty} c_{\ell i}\, \xi^{s+i} \qquad (C.8)$$

where ξ^s is the leading term in the expansion. We can substitute Eq. (C.8) in Eq. (C.2) to obtain

$$\sum_{i=0}^{\infty} \{(s+i)(s+i-1)(s+i-2)(s+i-3) + P_1(\xi)(s+i)(s+i-1)(s+i-2)$$

$$+ P_2(\xi)(s+i)(s+i-1) + P_3(\xi)(s+i) + P_4(\xi)\}\, c_{\ell_i}\, \xi^{s+i} = 0 \ . \qquad (C.9)$$

The functions $P_j(\xi)$ must be expanded in power series around the origin in order to obtain a power series in ξ^{s+i}. The results of the expansions are

$$P_1(\xi) = 2\left[1 + \frac{1}{\gamma} \sum_{i=1}^{\infty} (\alpha\, \xi^2)^i\right] , \qquad (C.10)$$

$$P_2(\xi) = -(2\ell^2+1) + \left(k_p^2 a^2 + \frac{6\alpha}{\gamma}\right)\xi^2 + \left(\frac{\zeta_D^2 \alpha}{\gamma} + \frac{10\alpha^2}{\gamma}\right)\xi^4 + \frac{2}{\gamma}\sum_{i=3}^{\infty}(2i+1)(\alpha\, \xi^2)^i \ , \qquad (C.11)$$

$$P_3(\xi) = 2\ell^2+1 + \left[k_p^2 a^2 + \frac{2\alpha}{\gamma}(1-\ell^2)\right]\xi^2 + \left[\frac{3\zeta_D^2\alpha}{\gamma} + \frac{2\alpha^2}{\gamma}(3-\ell^2)\right]\xi^4$$

$$+ \frac{2}{\gamma}\sum_{i=3}^{\infty}(2i-1-\ell^2)(\alpha\, \xi^2)^i \ , \qquad (C.12)$$

$$P_4(\xi) = -\ell^2\left[4-\ell^2+k_p^2a^2\xi^2+\left(\frac{\zeta_D^2\alpha}{\gamma}+\frac{4\alpha^2}{\gamma}\right)\xi^4+\frac{4}{\gamma}\sum_{i=3}^{\infty}(i-1)(\alpha\xi^2)^i\right]. \quad (C.13)$$

Equations (C.10)-(C.13) can be substituted in Eq. (C.9) to obtain an equation of the following form

$$\sum_{i=0}^{\infty} Q_i \xi^{s+i} = 0 . \quad (C.14)$$

Since the equation must be satisfied for all ξ within the radius of convergence of the solution (C.8), we must have

$$Q_i = 0 \quad (C.15)$$

for all i .

We will now consider the first few Q_i in order to determine the coefficients $c_{\ell i}$. First, we have

$$Q_0 = (s+\ell)(s-\ell)(s+\ell-2)(s-\ell-2)c_{\ell 0} = 0 . \quad (C.16)$$

Equation (C.16) is the indicial equation associated with Eq. (C.2). Since $c_{\ell 0}$ is assumed to be nonzero, four values of s satisfy Eq. (C.16),

$$s = \ell, -\ell, \ell+2, -\ell+2 . \quad (C.17)$$

These values of s may not all yield linearly independent solutions of the form given by Eq. (C.3) because they differ by integers. This question will be examined further after deriving the recursion relation for the $c_{\ell i}$.

The coefficient of ξ in Eq. (C.14) is

$$Q_1 = (s+\ell+1)(s-\ell+1)(s+\ell-1)(s-\ell-1)c_{\ell 1} = 0 . \quad (C.18)$$

Since none of the roots of Eq. (C.16) makes Q_1 vanish, $c_{\ell 1}$ must be

zero. This is to be expected since the series expansions for the $P_j(\xi)$ only involve even powers of ξ. We obtain for the next two nonzero coefficients

$$Q_2 = (s+\ell+2)(s-\ell+2)(s+\ell)(s-\ell)c_{\ell 2} + (s+\ell)(s-\ell)\left[\frac{2\alpha s}{\gamma} + k_p^2 a^2\right]c_{\ell 0} = 0 \ , \tag{C.19}$$

$$Q_4 = (s+\ell+4)(s-\ell+4)(s+\ell+2)(s-\ell+2)c_{\ell 4} + (s+\ell+2)(s-\ell+2)\left[\frac{2\alpha}{\gamma}(s+2)+k_p^2 a^2\right]c_{\ell 2}$$

$$+ \left[\frac{2\alpha^2}{\gamma}(s+\ell)(s-\ell)(s+2) + \frac{\zeta_D^2\alpha}{\gamma}(s^2+2s-\ell^2)\right] c\ell 0 = 0 \tag{C.20}$$

Finally, for $m \geq 6$ and even, we have the following four-term recursion relation

$$Q_m = (s+\ell+m)(s-\ell+m)(s+\ell+m-2)(s-\ell+m-2)c_{\ell m}$$

$$+ (s+\ell+m-2)(s-\ell+m-2)\left[\frac{2\alpha}{\gamma}(s+m-2) + k_p^2 a^2\right]c_{\ell m-2}$$

$$+ \left\{\frac{2\alpha^2}{\gamma}(s+\ell+m-4)(s-\ell+m-4)(s+m-2)+ \frac{\zeta_D^2\alpha}{\gamma}[(s+m-4)^2+2(s+m-4)-\ell^2]\right\} c_{\ell m-4}$$

$$+ \frac{2\alpha\frac{m}{2}}{\gamma}(s+\ell+m-6)(s-\ell+m-6)(s+m-2)c_{\ell m-6} = 0 \ . \tag{C.21}$$

The coefficients $c_{\ell m}$ can all be determined by an expression of the form

$$c_{\ell m} = \frac{A_{m-2}\, c_{\ell m-2} + A_{m-4}c_{\ell m-4} + A_{m-6}c_{\ell m-6}}{F(s,\ell,m)} \ , \tag{C.22}$$

where

$$F(s,\ell,m) = (s+\ell+m)(s-\ell+m)(s+\ell+m-2)(s-\ell+m-2) \ . \tag{C.23}$$

Consider $\ell \geq 0$. Equation (C.22) is valid provided $F(s,\ell,m)$ does not vanish for all even $m \geq 2$. For the root $s_1 = \ell+2$, which is the largest,

$$F(s_1,\ell,m) = m(m+2)(m+2+2\ell)(m+\ell) \ . \qquad (C.24)$$

There is always a solution of the form of Eq. (C.8) with $s = \ell+2$. For the root $s_2 = \ell$, we obtain

$$F(s_2,\ell,m) = m^2(2\ell+m)(m-2) \ . \qquad (C.25)$$

The factor (m-2) in Eq. (C.25) comes from $(s-\ell+m-2)$ in Eq. (C.23). It is impossible to determine $c_{\ell 2}$ unless the numerator of Eq. (C.22) also contains $(s-\ell)$. As seen from Eq. (C.19), it does, and there exists another linearly independent solution of the form of Eq. (C.8) with $s = \ell$. The root $s_3 = -\ell+2$ does not yield a new solution since $F(s_3,\ell,m) = 0$ for $m = \ell, 2\ell$, and ℓ -+ for $\ell > 5$, and since nothing can be factored out of Eq. (C.20). We obtain for the root $s_4 = -\ell$

$$F(s_4,\ell,m) = m(m-2\ell)(m-2)(m-2-2\ell) \ . \qquad (C.26)$$

Even if the zero of $F(s_4,\ell,m)$ at $m = 2$ is cancelled by a corresponding zero in the numerator of Eq. (C.22), the ones at $m = 2\ell$ and $m = 2\ell+2$ are not, and $s = -\ell$ does not yield a linearly independent solution. A similar result could be obtained for the case $\ell < 0$ since all the equations in this Appendix are symmetrical with respect to an interchange between ℓ and $-\ell$.

The method has yielded two linearly independent solutions of the form of Eq. (C.8) with

$$s = |\ell| \ , \ s = |\ell| + 2 \ .$$

Two other linearly independent solutions containing logarithms could also be found.[69] They have to be rejected as nonphysical, however, because they are infinite at the origin. The potential can then be written formally as in Eq. (5.19).

Appendix D

NONLINEAR SCATTERING FROM A COLD UNIFORM PLASMA COLUMN

The purpose of this Appendix is to present an adaptation of the theory of Ref. 62, for the nonlinear scattering from a cold uniform plasma column in free space, to the case where a glass tube surrounds the plasma. This case has also been studied by Messiaen and Vandenplas,[56] who developed their theory in a different way. The geometry considered here is shown in Fig. 5.1. The equations of the problem are the equation of motion for a cold plasma, given by Eq. (2.1), and Maxwell's equations, given by Eq. (2.3).

D.1 Linear Regime

The expressions for the $\underline{H}$ field in the three regions formed by the plasma, glass, and free space are given by Eqs. (5.4)-(5.6). In the present case, the wave equation in the plasma yields

$$H_{z\ell}(r) = J_\ell(k_p r) \ , \tag{D.1}$$

where

$$k_p = \epsilon_p^{1/2} \ , \qquad \epsilon_p = \left(1 - \frac{\omega_0^2}{\Gamma\omega^2}\right) . \tag{D.2}$$

The constants in Eqs. (5.4)-(5.6) are determined by requiring the continuity of H_z and E_θ at r=a and r=b . The results are

$$M_\ell = \frac{-8\epsilon_p^{1/2} j^{-\ell}}{\pi^2 k^2 ab\, R_\ell} \ , \tag{D.3}$$

$$F_{\ell j} = \epsilon_g^{1/2} H_\ell^{(j)}(k_g a) J_\ell'(k_p a) - \epsilon_p^{1/2} H_\ell^{(j)'}(k_g a) J_\ell(k_p a) \ , \ j = 1,2 \ . \tag{D.4}$$

The constants B_ℓ, C_ℓ, S_ℓ, R_ℓ, V_ℓ, and V_ℓ' are given in Eqs. (5.40)-(5.42).

Although the RF space-charge density is zero in the column, there is a discontinuity in E_r at $r=a$, indicating a surface charge density given by

$$\rho_s = -\frac{(\epsilon_g-\epsilon_p)}{\omega a \epsilon_g \epsilon_p} H_0 \sum_{\ell=-\infty}^{+\infty} \ell\, M_\ell J_\ell(k_p a)\exp j\ell\theta \ . \qquad (D.5)$$

D.2 Nonlinear Regime

The $\underset{\sim}{H}$ *fields in the plasma, glass, and free space, are given by* Eqs. (5.54)-(5.56). Since the Maxwell curl equations can be combined to yield a wave equation for H_z containing no nonlinear driving term, we obtain

$$H_{z3\ell}(r) = A_{3\ell} J_\ell(k_{p3} r) \ , \qquad r \le a \ . \qquad (D.6)$$

The nonlinear electric field can be obtained by means of the equation

$$\underset{\sim}{E}_3 = \frac{1}{j\omega_3 \epsilon_0 \epsilon_{p3}} \left[\nabla \times \underset{\sim}{H}_3 + \frac{j N_0 e^3}{m_e^2 \omega_1 \omega_2 \omega_3} \nabla(\underset{\sim}{E}_1 \cdot \underset{\sim}{E}_2) \right] . \qquad (D.7)$$

The nonlinear surface current is given by

$$J_{s3} = \sum_{\alpha,\beta} \rho_{s\alpha}(a) v_{\theta\beta}(a) = \sum_{\ell=-\infty}^{+\infty} J_{s3\ell} \exp j\ell\theta \ , \qquad (D.8)$$

where

$$J_{s3\ell} = \frac{e H_{01} H_{02}}{\epsilon_0 m_e \epsilon_g \omega_{p1} \epsilon_{p2} \omega_1 \omega_2 a} \sum_{\alpha,\beta} \sum_{\ell=m+n} m M_{\alpha m} M_{\beta n} \frac{k_{p\beta}}{\omega_\beta} (\epsilon_{p\alpha}-\epsilon_g) J_m(k_{p\alpha} a) J_n'(k_{p\beta} a) \ . \qquad (D.9)$$

The continuity of H_{z3} at $r=a$ and $r=b$ yields

$$A_{3\ell}J_\ell(k_{p3}a) - \left[W_{3\ell}H_\ell^{(1)}(k_{g3}a) + X_{3\ell}H_\ell^{(2)}(k_{g3}a)\right] = J_{s3\ell} \ , \quad (D.10)$$

$$W_{3\ell}H_\ell^{(1)}(k_{g3}b) + X_{3\ell}H_\ell^{(2)}(k_{g3}b) = Y_{3\ell}H_\ell^{(2)}(k_3 b) \ . \quad (D.11)$$

The continuity of $E_{\theta 3}$ gives

$$k_3\epsilon_{p3}\left[W_{3\ell}H_\ell^{(1)'}(k_{g3}a) + X_{3\ell}H_\ell^{(2)'}(k_{g3}a)\right] - A_{3\ell}k_{p3}\epsilon_g^{1/2}J_\ell'(k_{p3}a) = f_\ell \ , \quad (D.12)$$

where

$$f_\ell = \frac{\ell\,\epsilon_g^{1/2}\epsilon\omega_0^2}{\epsilon_0 m e\,\omega_1^2\omega_2^2\omega_3\epsilon_{p1}\epsilon_{p2}} \sum_{\ell=m+n} M_{1m}M_{2n}\Big[mnJ_m(k_{p1}a)J_n(k_{p2}a) - k_{p1}k_{p2}a^2J_m'(k_{p1}a)J_n'(k_{p2}a)\Big] \ , \quad (D.13)$$

$$W_{3\ell}H_\ell^{(1)'}(k_{g3}b) + X_{3\ell}H_\ell^{(2)'}(k_{g3}b) = \epsilon_g^{1/2}Y_{3\ell}H_\ell^{(2)}(k_3 b) \ . \quad (D.14)$$

The constants are found to be

$$A_{3\ell} = \frac{J_{s3\ell} + Q_\ell f_\ell}{J_\ell(k_{p3}a) - Q_\ell\epsilon_g^{1/2}k_{p3}J_\ell'(k_{p3}a)} \ , \qquad W_{3\ell} = -\frac{F_{\ell 2}}{F_{\ell 1}}X_{3\ell} \ ,$$
$$X_{3\ell} = \frac{F_{\ell 1}\left[A_{3\ell}J_\ell(k_{p3}a) - J_{s3\ell}\right]}{F_{\ell 1}H_\ell^{(2)}(k_{g3}a) - F_{\ell 2}H_\ell^{(1)}(k_{g3}a)} \ , \qquad Y_{3\ell} = -\frac{4_j X_{3\ell}}{\pi k_{g3}bF_{\ell 1}} \ , \quad (D.15)$$

where

$$F_{\ell j} = \epsilon_g^{1/2}H_\ell^{(j)}(k_{g3}b)H_\ell^{(2)'}(k_3 b) - H_\ell^{(j)'}(k_{g3}b)H_\ell^{(2)}(k_3 b) \ . \quad (D.16)$$

The results of this Appendix are used in Section 5.1.4, for linear scattering, and 5.2.3, for nonlinear scattering, in comparison with the warm plasma model.

Appendix E

PARTICULAR SOLUTION OF EQ. (5.64)

The solution of Eq. (5.64) is similar to that of Eq. (5.17), obtained in Appendix C. We can write Eq. (5.64) in the form

$$\xi^4\psi_\ell'''' + P_1(\xi)\xi^3\psi_\ell''' + P_2(\xi)\xi^2\psi_\ell'' + P_3(\xi)\xi\psi_\ell' + P_4(\xi)\psi_\ell = \xi^4 G_\ell(\xi), \quad (E.1)$$

where the $P_i(\xi)$ are given by Eqs. (C.3)-(C.6), and $G_\ell(\xi)$ is the RHS of Eq. (5.64) expressed as a function of ξ. In order to find a particular solution of Eq. (5.64), the RHS is expanded for small ξ. Because of the complexity of $G_\ell(\xi)$, this expansion is performed on the computer. It turns out the the leading term of $G_\ell(\xi)$ is $g_{\ell 0}\,\xi^\ell$ and that $G_\ell(\xi)$ can be written as

$$G_\ell(\xi) = \sum_{i=0}^{\infty} g_{\ell i}\xi^{i+\ell}, \quad (E.2)$$

with $g_{\ell i} = 0$ for i odd. We can then assume a solution of the form

$$\psi_{\ell p}(\xi) = \sum_{i=0}^{\infty} c_{\ell i}\,\xi^{i+\ell+4}, \quad (E.3)$$

with $c_{\ell i} = 0$ when i is odd. The coefficients $c_{\ell i}$ for i even can be obtained by replacing Eqs. (C.16), and (C.18)-(C.21) by

$$Q_{\ell i} = g_{\ell i},$$

with the $Q_{\ell i}$ defined as before and s replaced by $\ell+4$. The complete solution of Eq. (5.64) is given formally in Eq. (5.65).

REFERENCES

1. R. Z. Sagdeev and A. A. Galeev, Nonlinear Plasma Theory, (W. A. Benjamin, Inc., New York, N. Y., 1969).

2. W. H. Louisell, Coupled Mode and Parametric Electronics, (John Wiley, New York, N. Y., 1960).

3. J. A. Armstrong, N. Bloembergen, J. Ducuing and P. S. Pershan, Phys. Rev. 127, 1918 (1962).

4. B. B. O'Brien, R. W. Gould and J. V. Parker, Phys. Rev. Lett. 14, 630 (1965).

5. S. Ramo, Phys. Rev. 56, 276 (1939).

6. W. C. Hahn, Gen. El. Rev. 42, 258 (1939).

7. L. D. Smullin and P. Chorney, Proc. IRE 46, 360 (1958); W. O. Schumann, Z. Angew. Phys. 8, 482 (1956); J. Dawson and C. Oberman, Phys. Fluids 2, 103 (1959).

8. A. W. Trivelpiece and R. W. Gould, J. Appl. Phys. 30, 1784 (1959); A. W. Trivelpiece, Slow Wave Propagation in Plasma Waveguides, (San Francisco Press Inc., San Francisco, Ca., 1967).

9. V. Bevc and T. E. Everhart, J. Electron. Contr. 13, 185 (1962); M. Camus and J. LeMezec, Proc. of the Symposium at Copenhagen, on Electromagnetic Theory and Antennas (The Macmillan Company, New York, N. Y., 1963), Part I, p. 323.

10. V. L. Granatstein, S. P. Schlesinger and A. Vigants, Trans. IEEE APll, 489 (1963).

11. V. L. Granatstein and S. P. Schlesinger, J. Appl. Phys. 36, 3503 (1965).

12. R. N. Carlisle, J. Appl. Phys. 35, 1384 (1964).

13. H. L. Stover and G. S. Kino, Proc. Fifth International Conference on Microwave Tubes, Paris, France, September 1964 (Academic Press, New York, N. Y., 1965), p. 374.

14. R. J. Briggs and S. F. Paik, Int. J. Electron. 23, 163 (1968).

15. E. M. Barston, Stanford University Microwave Laboratory Rept. No. 1064 (July 1963).

16. C. B. Wharton and J. H. Malmberg, Proc. VIIth International Conference on Phenomena in Ionized Gases, Belgrade, Yugoslavia, August 1965, (Gradevinska Knjiga Publishing House, Belgrade, 1966).

17. H. L. Stover, Stanford University Microwave Laboratory Rept. No. 1140 (October 1964).

18. J. H. Malmberg, C. B. Wharton and W. E. Drummond, Proc. Second Conference on Plasma Physics and Controlled Nuclear Fusion Research, Culham (IAEA, Vienna, 1966), Vol. 1, p. 485.

19. P. Diament, V. L. Granatstein and S. P. Schlesinger, J. Appl. Phys. 37, 1771 (1966).

20. F. W. Crawford and J. A. Tataronis, Int. J. Electron. 19, 557 (1965).

21. B. B. O'Brien, Plasma Phys. 9, 369 (1967).

22. R. L. Gunshor, J. Appl. Phys. 37, 3630 (1966); H. H. Kuehl and G. E. Stewart, J. Appl. Phys. 37, 1724 (1966); K. F. Lee, J. Appl. Phys. 37, 4367 (1966).

23. P. A. Sturrock, Proc. Roy. Soc. A242, 277 (1957); Ann. Phys. 9, 422 (1960).

24. F. E. Low, Proc. Roy. Soc. A248, 282 (1958).

25. J. J. Galloway and F. W. Crawford, Proc. Fourth European Conference on Controlled Fusion and Plasma Physics, Rome, Italy, September 1970 (CNEN, Rome, 1970), p. 161.

26. K. J. Harker, Stanford University Institute for Plasma Research Rept. No. 395 (November 1970).

27. J. J. Galloway and H. Kim, J. Plasma Phys. 6, 53 (1971).

28. G. S. Kino, J. Appl. Phys. 31, 1449 (1960).

29. S. F. Paik, J. Appl. Phys. 33, 1017 (1962).

30. G. S. Kino and B. F. Ludovici, Proc. Fourth International Conference on Ionization Phenomena in Gases, Uppsala, Sweden, 1959 (North Holland Publishing Co., Amsterdam, 1960), Vol. 2, p. 762.

31. M. Pérulli, Thèse de Doctorat, Faculté des Sciences de Paris, (1968); G. Laval, R. Pellat and M. Pérulli, Plasma Phys. 11, 579 (1969).

32. E. N. Spithas and W. M. Manheimer, Phys. Fluids 13, 1110 (1970).

33. D. Phelps, N. Rynn and G. Van Hoven, Phys. Rev. Lett. 26, 688 (1971).

34. L. Tonks, Phys. Rev. 37, 1458 (1931); Phys. Rev. 38, 1219 (1931).

35. N. Herlofson, Arkiv Fysik 3, 247 (1959).

36. A. Dattner, Ericsson Technics 2, 309 (1957); 8, 1 (1963); Phys. Rev. Lett. 10, 205 (1963).

37. P. E. Vandenplas, Electron Waves and Resonances in Bounded Plasmas (Interscience Publishers, New York, N. Y., 1968).

38. T. R. Kaiser and R. L. Closs, Phil. Mag. 43, 1 (1952).

39. G. Keitel, Proc. IRE 43, 1481 (1955).

40. R. W. Gould, Proc. Conference on Plasma Oscillation, Linde Company, Indianapolis, 1959, p. 167.

41. R. W. Gould, California Institute of Technology, Electron Tube and Microwave Laboratory Report No. 7, Contract DA-039-SC-85317 (1 July - 30 September 1961).

42. P. Weissglas, Phys. Rev. Lett. 10, 206 (1963).

43. F. W. Crawford, Phys. Lett. 5, 244 (1963).

44. J. V. Parker, J. C. Nickel and R. W. Gould, Phys. Fluids 7, 1489 (1964).

45. J. V. Parker, Phys. Fluids 6, 1657 (1963).

46. G. Bryant and R. N. Franklin, Proc. Phys. Soc. 81, 531 (1963); 81, 790 (1963); R. N. Franklin, J. Electr. Control 17, 513 (1964).

47. W. D. Hershberger, Phys. Fluids 4, 740 (1961).

48. K. J. Parbhakar and B. C. Gregory, Can. J. Phys. 49, 2578 (1971).

49. W. M. Leavens, Radio Science, J. Res. NBS 69D, 1310 (1965).

50. K. J. Harker, G. S. Kino and D. Eitelbach, Phys. Fluids 11, 425 (1968).

51. D. E. Baldwin, Phys. Fluids 12, 279 (1969).

52. D. W. Ignat, Phys. Fluids 13, 1771 (1970).

53. G. Dorman, J. Plasma Phys. 2, 557 (1968); 3, 387 (1969); 4, 127 (1970).

54. R. M. Miura and E. M. Barston, J. Plasma Phys. 6, 271 (1971).

55. R. A. Stern, Phys. Rev. Lett. 14, 538 (1965).

56. A. M. Messiaen and P. E. Vandenplas, Plasma Phys. 10, 851 (1968).

57. J. A. Green, J. Geophys. Res. 70, 3244 (1965).

58. Semiannual Report No. 9, NASA Grant NGR 05-020-077, Stanford University Institute for Plasma Research Rept. No. 356 (February 1970).

59. J. L. Yen and N. C. McDermott, Appl. Phys. Lett. 7, 253 (1965).

60. Semiannual Report No. 8, NASA Grant NGL 05-020-176, Stanford University Institute for Plasma Research Rept. No. 412 (February 1971).

61. R. L. Bruce, F. W. Crawford and K. J. Harker, Proc. Tenth International Conference on Phenomena in Ionized Gases, Oxford, England, September 1971 (Donald Parsons and Co., Oxford, England, 1971), p. 326.

62. R. L. Bruce, F. W. Crawford and K. J. Harker, Proc. Third International Conference on Quiescent Plasmas, Elsinore, Denmark, September 1971: Published as Danish Atomic Energy Commission, Risø Report No. 250 (October 1971).

63. R. J. Briggs, Electron-Stream Interaction with Plasmas (M.I.T. Press, Cambridge, Mass., 1964).

64. E. S. Cassedy and A. A. Oliner, Proc. IEEE 51, 1342 (1963); E. S. Cassedy, Proc. IEEE 55, 1154 (1967).

65. F. F. Chen, Plasma Phys. 7, 47 (1965).

66. J. E. Allen, R. F. Boyd and P. Reynolds, Proc. Phys. Soc. LXX, 297 (1957).

67. J. G. Laframboise, University of Toronto Institute for Aerospace Studies Rept. No. 100 (1966).

68. F. F. Chen, C. Etiévant and D. Mosher, Phys. Fluids 11, 811 (1968).

69. E. L. Ince, Ordinary Differential Equations, (Dover Publications, Inc., New York, N. Y., 1965), pp. 395-403.

70. F. W. Crawford and G. S. Kino, Proc. IRE 49, 1767 (1961).

71. L. S. Frost and A. V. Phelps, Phys. Rev. 136A, 1538 (1964).

72. P. Leprince and M. Moisan, Plasma Phys. 13, 659 (1971).

73. R. A. Stern and N. Tzoar, Phys. Rev. Lett. 17, 903 (1966).

74. J. V. Evans, Proc. IEEE, 57, 496 (1969).

JOINT SERVICES ELECTRONICS PROGRAM
REPORTS DISTRIBUTION LIST

Department of Defense

No. of Copies	
1	Director for Materials Sciences Advanced Research Projects Agency 1400 Wilson Boulevard Arlington, Virginia 22209
1	Chief, R&D Division (340) Defense Communications Agency Washington, D.C. 20301
12	Defense Documentation Center Attn: DDC-TCA Cameron Station Alexandria, Virginia 22314
1	Colonel Norman D. Jorstad Weapons Systems Evaluation Group 400 Army-Navy Drive Arlington, Virginia 22202
1	Dr. A. D. Schnitzler Institute for Defense Analyses Science and Technology Division 400 Army-Navy Drive Arlington, Virginia 22202
1	Dr. George H. Heilmeier Office of Director of Defense Research and Engineering The Pentagon Washington, D.D. 20315

Department of the Air Force

No. of Copies	
1	Headquarters/USAF (AF/RDPE) Washington, D.C. 20330
1	Headquarters USAF/RDPS Washington, D.C. 20330
1	Colonel E. P. Gaines, Jr. ESD (XR) L.G. Hanscom Field Bedford, Massachusetts 01730
5	Lt. Col. Jack W. Gregory Electronic & Solid State Sciences Air Force Office of Scientific Research 1400 Wilson Boulevard Arlington, Virginia 22209
1	Rome Air Development Center Attn: Documents Library (TDLD) Griffiss AFB, New York 13440
1	Mr. H. E. Webb, Jr. (ISCP) Rome Air Development Center Griffiss AFB, New York 13440
1	AFSC (CCJ/Mr. Irving R. Mirman) Andrews AFB Washington, D.C. 20331
1	Directorate of Electronics Headquarters AFSC/DLC Andrews AFB Washington, D.C. 20331
1	Directorate of Science Headquarters AFSC/DLS Andrews AFB Washington, D.C. 20331
1	Mr. Carl Sletten AFCRL/LZ L.G. Hanscom Field Bedford, MA 01730
1	Dr. Richard Picard AFCRL/OP L.G. Hanscom Field Bedford, MA 01730
1	Mr. Robert Barrett AFCRL/LQ L.G. Hanscom Field Bedford, MA 01730

No. of Copies	
1	Mr. L. B. Holman ASD/ENV Directorate Wright-Patterson AFB, Ohio 45433
1	Dr. John N. Howard AFCRL (CA) L.G. Hanscom Field Bedford, Massachusetts 01730
1	Headquarters ESD (TRI) L.G. Hanscom Field Bedford, MA 01730
1	Professor R. E. Fontana Head Dept. of Electrical Eng. AFIT/ENE Wright-Patterson AFB, Ohio 45433
1	Dr. H. V. Noble, AFAL/TE Chief, Electronics Technology Div. Air Force Avionics Laboratory Wright-Patterson AFB, Ohio 45433
1	AF Avionics Lab/CA Attn Dr. Bernard H. List Chief Scientist AF Avionics Laboratory Wright-Patterson AFB, Ohio 45433
1	AFAL/TEA (Mr. R. D. Larson) Wright-Patterson AFB, Ohio 45433
1	Faculty Secretariat (DFSS) US Air Force Academy Colorado 80840
1	Mr. Jules I. Wittebort Chief, Electronics Branch AF Materials Lab. AFAL/LTE Wright-Patterson AFB, Ohio 45433
1	Director of Aerospace-Mechanics Sciences Frank J. Seiler Research Lab. (OAR) USAF Academy, Colorado 80840

No. of Copies	
1	Major Richard J. Gowen Tenure Professor Dept. of Electrical Eng. USAF Academy, Colorado 80840
1	Director, USAF Project RAND Via: Air Force Liaison Office The RAND Corporation Attn: Library D 1700 Main Street Santa Monica, CA 90406
1	AUL/LSE-9663 Maxwell AFB, Alabama 36112
1	AFETR Technical Library (MU-135) Patrick AFB, Florida 32925
1	ADTC (SSLT) Eglin AFB, Florida 32542
1	Headquarters AMD (RDR/Col. Godden) Brooks AFB, Texas 78235
1	USAFSAM (RAT) Brooks AFB, Texas 78235
2	Commanding General Attn: STEWS-AD-L, Technical Library White Sands Missile Range New Mexico 88002
1	USAF European Office of Aerospace Research Technical Information Office Box 14, FPO New York 09510
1	VELA Seismological Center 312 Montgomery Street Alexandria, Virginia 22314
1	Dr. Carl E. Baum AFWL (ES) Kirtland AFB New Mexico 87117

Department of the Army

No. of Copies

1 Headquarters, DA (DARD-ARP-P)
Washington, D.C. 20310

1 Commanding General
US Army Security Agency
Attn: IARD-T
Arlington Hall Station
Arlington, Virginia 22212

1 Commanding General
US Army Materiel Command
Attn: AMCRD-TP (Dr. Zarwyn)
Washington, D.C. 20315

1 Director
US Army Advanced Materiel Concepts Agency
2461 Eisenhower Avenue
Alexandria, Virginia 22314

1 Mr. H. T. Darracott (AMXAM-TF)
US Army Advanced Materiel Concepts Agency
2461 Eisenhower Avenue
Alexandria, Virginia 22314

1 Commanding Officer (AMXRD-BAD)
US Army Ballistics Research Lab.
Aberdeen Proving Ground
Aberdeen, Maryland 21005

1 US Army Munitions Command
Attn: Science & Technology Info. Branch, Bldg. 59
Picatinny Arsenal, SMUPA-RT-S
Dover, New Jersey 07801

1 Dr. Herman Robl
Deputy Chief Scientist
US Army Research Office (Durham)
Box CM, Duke Station
Durham, North Carolina 27706

1 Richard O. Ulsh (CRDARD-IP)
US Army Research Office (Durham)
Box CM, Duke Station
Durham, North Carolina 27706

No. of Copies

1 Commandant
U.S. Army Command & Gen. Staff College
Attn: Acquisitions, Lib. Div
Fort Leavenworth, Kansas 66027

1 Technical Director (SMUFA-A1000TD-107-1)
Frankford Arsenal
Philadelphia, Penn. 19137

1 Redstone Scientific Info. Ctr.
Attn: Chief, Document Section
US Army Missile Command
Redstone Arsenal, Alabama 35809

1 Commanding General
US Army Missile Command
Attn: AMSMI-RR
Redstone Arsenal, Alabama 35809

1 Commanding General
US Army Strategic Communications Command
Attn: SCC-ATS (Mr. Peter B. Pichetto)
Fort Huachuca, Arizona 85613

1 Dr. Homer F. Priest
Chief, Materials Sciences Division, Bldg. 292
Army Materials and Mechanics Research Center
Watertown, Mass. 02172

1 John E. Rosenberg
Harry Diamond Laboratories
Connecticut Ave. & Van Ness Street N. W.
Washington, D.C. 20438

1 Commanding General
USACDC Concepts and Force Design Group
Attn: Technical Library, Room 636
2461 Eisenhower Avenue
Alexandria, Virginia 22314

1 Commandant
US Army Air Defense School
Attn: Missile Science Div., C&S Dept.
P. O. Box 9390
Fort Bliss, Texas 79916

No. of Copies	
1	Dr. Hans K. Zielger (AMSEL-TL-DC) Army Member, TAC/JSEP US Army Electronics Command Fort Monmouth, New Jersey 07703
10	Mr. I. A. Balton, (AMSEL-TL-DC) Executive Secretary, TAC/JSEP US Army Electronics Command Fort Monmouth, New Jersey 07703
2	US Army Medical Research & Dev. Command Forrestal Building Washington, D.C. 20314
4	Director Walter Reed Army Institute of Research Walter Reed Army Medical Center Washington, D.C. 20012
1	Director Walter Reed Army Institute of Research Walter Reed Army Medical Center Attn: MEDEC-ZIF, Building 502 Washington, D.C. 20012
1	Commanding Officer Letterman Army Institute of Res. San Francisco, California 94129
1	US Army Medical Research Lab. Fort Knox, Kentucky 40121
1	Mr. A. D. Bedrosian, Room 26-131 US Army Scientific Liaison Office Mass. Institute of Technology 77 Massachusetts Avenue Cambridge, Massachusetts 02139
1	Project Manager NAVCON Attn: AMCPM-NC-TM (Mr. H. H. Bahr) Bldg. 2539 Fort Monmouth, New Jersey 07703
1	Director (NV-D) Night Vision Laboratory, USAECOM Fort Belvoir, Virginia 22060

No. of Copies	
1	Commanding Officer Atmospheric Sciences Lab. US Army Electronics Command White Sands Missile Range New Mexico 88002
1	Atmospheric Sciences Lab. US Army Electronics Command Attn: AMSEL-BL-DD (Mr. Marvin Diamond) White Sands Missile Range New Mexico 88002
1	Chief, Missile EW Tech Area Electronic Warfare Lab.; ECOM Attn: AMSEL-WL-MY White Sands Missile Range New Mexico 88002
1	US Army Weapons Command Rock Island Arsenal Rock Island, Illinois 61201
1	Mrs. E. E. Hitchingham, Science Librarian School of Engineering Oakland University Rochester, Michigan 48063
1	Harry C. Holloway, M.D. Col, MC Director, Div. of Neuropsych. Walter Reed Army Institute of Research Washington, D.C. 20012
	Commanding General US Army Electronics Command Fort Monmouth, New Jersey 07703
1	Attn: AMSEL-RD-O (Dr. W. S. McAfee)
1	AMSEL-TL-N (Dr. S. Kronenberg)
1	AMSEL-CT-L (Dr. G. Buser)
1	AMSEL-BL-FM-A
1	AMSEL-CT-D

No. of Copies	
	Commanding General US Army Electronics Command Fort Monmouth, New Jersey 07703
1	Attn: AMSEL-CT-R
1	AMSEL-CT-I
1	AMSEL-CT-A
1	AMSEL-NL-D (Dr. H. S. Bennett)
1	AMSEL-NL-A
1	AMSEL-NL-C
1	AMSEL-NL-P-2
1	AMSEL-NL-R
1	AMSEL-NL-S
1	AMSEL-TL-I
1	AMSEL-TL-S
1	AMSEL-TL-Q
1	AMSEL-TL-B
1	AMSEL-VL-D
1	AMSEL-WL-D
1	AMSEL-TL-M (Mr. Lipetz)
1	AMSEL-CT-L (Dr. Papayoanou)

Department of the Navy

3	Director, Electronic Programs Attn: Code 427 Office of Naval Research 800 North Quincy Street Arlington, Virginia 22217
1	Mr. Gordon D. Goldstein, Code 437 Information Systems Program Office of Naval Research Arlington, Virginia 22217
1	Commander Naval Security Group Command Naval Security Group Headquarters Attn: Technical Library 3801 Nebraska Avenue N.W. Washington, D.C. 20390
1	Director Naval Research Laboratory Attn: Mr. A. Brodzinsky, Supt. Electronics Division Washington, D.C. 20390
1	Director, Naval Research Laboratory Attn: Code 5200 Washington, D.C. 20390
1	Dr. Herbert Rabin, (Code 7000) Assoc. Dir. of Res. for Space Science & Technology Naval Research Laboratory Washington, D.C. 20390
2	Director Naval Research Laboratory Attn: Library, Code 2629 (ONRL) Washington, D.C. 20390
1	Dr. G. M. R. Winkler Director, Time Service Division US Naval Observatory Washington, D.C. 20390
1	Naval Air Systems Command AIR-310B Washington, D.C. 20360
1	Dr. A. L. Slafkosky Scientific Advisor Commandant of the Marine Corps (Code AX) Washington, D.C. 20380
1	US Naval Weapons Laboratory Dahlgren, Virginia 22448
1	Commander US Naval Ordnance Laboratory Attn: Librarian White Oak, Maryland 20910
1	Director Office of Naval Research Boston Branch 495 Summer Street Boston, Massachusetts 02210
1	Commander Naval Air Development Center Warminster, PA 18974 Attn: ADT

No. of Copies

1 Commanding Officer
Naval Missile Center
Attn: 5632.2, Technical Library
Point Mugu, California 93042

1 W. A. Eberspacher
Systems Effectiveness Branch (5721)
Naval Missile Center
Point Mugu, California 93041

1 Commander
Naval Electronics Laboratory Ctr.
Attn: Library
San Diego, California 92152

1 Deputy Director and Chief Scientist
Office of Naval Research Branch Office
1030 East Green Street
Pasadena, California 91106

1 Superintendent
Naval Post Graduate School
Monterey, California 93940
Attn: Library (Code 2124)

1 Officer in Charge, New London Lab.
Naval Underwater Systems Center
(Technical Library)
New London, Connecticut 06320

1 Commanding Officer
Naval Avionics Facility
Attn: D/035 Technical Library
Indianapolis, Indiana 46241

1 US Naval Oceanographic Office
Attn: M. Rogofsky, Librarian
(Code 1640)
Washington, D. C. 20390

1 Office of Naval Research
Branch Office
536 South Clark
Chicago, Illinois 60605

1 Commanding Officer
Naval Training Device Center
Attn: Technical Library
Orlando, Florida 32813

Other Government Agencies

No. of Copies

1 Dr. H. Harrison
AEC/NASA Space Nuclear Systems Office
AEC Headquarters, Mail F-309
Washington, D.C. 20545

1 Los Alamos Scientific Lab.
Attn: Reports Library
P. O. Box 1663
Los Alamos, New Mexico 87544

1 M. Zane Thornton
Deputy Director
Center for Computer Sciences and Technology
National Bureau of Standards
US Departmnet of Commerce
Washington, D.C. 20234

1 US Postal Service
Library-Room 6012
12th and Pennsylvania Ave. N.W.
Washington, D.C. 20260

1 NASA Lewis Research Center
Attn: Library
21000 Brookpak Road
Cleveland, Ohio 44135

Non-Government Agencies

1 Director
Research Laboratory of Electronics
Massachusetts Institute of Technology
Cambridge, Massachusetts 02139

1 Director
Microwave Research Institute
Polytechnic Institute of Brooklyn
Long Island Graduate Center, Route 110
Farmingdale, New York 11735

No. of Copies	
1	Mr. Jerome Fox, Research Coordinator Polytechnic Institute of Brooklyn 333 Jay Street Brooklyn, New York 11201
1	Director Columbia Radiation Laboratory Dept. of Physics Columbia University 538 West 120th Street New York, New York 10027
1	Director Coordinated Science Laboratory University of Illinois Urbana, Illinois 61801
1	Director Stanford Electronics Laboratory Stanford University Stanford, California 94305
1	Director Microwave Laboratory Stanford University Stanford, California 94305
1	Director Electronics Research Laboratory University of California Berkeley, California 94720
1	Director Electronics Sciences Laboratory University of Southern California Los Angeles, California 90007
1	Director Electronics Research Center The University of Texas at Austin Engineering-Science Bldg. 112 Austin, Texas 78712

No. of Copies	
1	Director of Laboratories Division of Engineering & Applied Physics Harvard University Pierce Hall Cambridge, Massachusetts 02138
1	Dr. G. J. Murphy The Technological Institute Northwestern University Evanston, Illinois 60201
1	Dr. John C. Hancock, Head School of Electrical Eng. Purdue University Lafayette, Indiana 47907
1	Dept. of Electrical Eng. P. O. Box 4200 Texas Technological University Lubbock, Texas 79409
1	Aerospace Corporation P. O. Box 92957 Attn: Library Acquisitions Group Los Angeles, California 90045
1	AIL, A Division of Cutler Hamer Library Walt Whitman Road Melville, New York 11746
1	The University of Arizona Dept. of Electrical Eng. Tucson, Arizona 85721
1	Engineering & Mathematical Sciences Library University of California at Los Angeles 405 Hilgred Avenue Los Angeles, California 90024
1	Sciences-Engineering Library University of California Santa Barbara, California 93106

No. of Copies	
1	Professor Nicholas George California Institute of Technology Pasadena, California 91109
1	Hunt Library Carnegie-Melon University Schenley Park Pittsburgh, Penn. 15213
1	Dr. A. G. Jordan Head of Dept. of Electrical Eng. Carnegia-Melon University Schenley Park Pittsburgh, Penn. 15213
1	Dept. of Electrical Eng. Case Western Reserve University 10900 Euclid Avenue Cleveland, Ohio 44106
1	Hollander Associates Attn: Librarian P. O. Box 2276 Fullerton, California 92633
1	Walter H. Veazie, Head Electronic Properties Information Center Mail Station E-148 Hughes Aircraft Company Culver City, California 90230
1	Illinois Institute of Technology Dept. of Electrical Engineering Chicago, Illinois 60616
1	Government Documents Dept. University of Iowa Libraries Iowa City, Iowa 52240
1	The Johns Hopkins University Applied Physics Laboratory Attn: Document Librarian 8621 Georgia Avenue Silver Spring, Maryland 20910
1	Lehigh University Dept. of Electrical Engineering Bethlehem, Pennsylvania 18015

No. of Copies	
1	Mr. E. K. Peterson Lenkurt Electric Co., Inc. 1105 County Road San Carlos, California 94070
1	MIT Lincoln Laboratory Attn: Library A-082 P. O. Box 73 Lexington, Massachusetts 02173
1	Miss Barbara H. Kohl Project MAC, Room 413 545 Main Street Cambridge, Massachusetts 02139
1	Professor R. H. Rediker Professor Electrical Eng. Mass. Institute of Technology Building 13-3050 Cambridge, Massachusetts 02139
1	Professor Joseph E. Rowe Chairman, Dept. of Electrical Computer Engineering The University of Michigan Ann Arbor, Michigan 48104
1	New York University Engineering Library Bronx, New York 10453
1	State University of New York College of Ceramics at Alfred University Alfred, New York 14802
1	Professor James A. Cadzow Dept. of Electrical Eng. State University of New York at Buffalo Buffalo, New York 14214
1	Dr. Richard H. McFarland Dept. of Electrical Eng. Ohio University Athens, Ohio 45701

No. of Copies

1 Raytheon Company
Research Division Library
28 Seyon Street
Waltham, Massachusetts 02154

1 Rice University
Dept. of Electrical Eng.
Houston, Texas 77001

1 Dr. Leo Young, Program Manager
Stanford Research Institute
Menlo Park, California 94025

1 GTE Waltham Research Lab. Library
40 Sylvan Road
Attn: Esther McLaughlin,
Documents Librarian
Waltham, Massachusetts 02154

1 Dr. W. R. LePage, Chairman
Dept. of Electrical Eng.
Syracuse University
Syracuse, New York 13210

1 Dr. F. R. Charvat
Union Carbide Corporation,
Materials Systems Division
Crystal Products Department
8888 Balboa Avenue
P. O. Box 23017
San Diego, California 92123

1 Utah State University
Dept. of Electrical Eng.
Logan, Utah 84321

1 Research Labs for the Engineering Sciences
School of Engineering and Applied Science
University of Virginia
Charlottesville, Virginia 22903

1 Yale University
Engineering & Applied Science Library
15 Prospect Street
New Haven, Connecticut 06520

No. of Copies

1 Rensselaer Polytechnic Institute
Systems Engineering
School of Engineering
Attn: Dr. Dean Arden
Troy, New York 12181

DOCUMENT CONTROL DATA - R & D

(Security classification of title, body of abstract and indexing annotation must be entered when the overall report is classified)

1. ORIGINATING ACTIVITY (Corporate author)
Institute for Plasma Research
Stanford University
Stanford, California 94305

2a. REPORT SECURITY CLASSIFICATION
UNCLASSIFIED

2b. GROUP

3. REPORT TITLE

NONLINEAR WAVE INTERACTION IN A PLASMA COLUMN

4. DESCRIPTIVE NOTES (Type of report and inclusive dates)

SCIENTIFIC INTERIM

5. AUTHOR(S) (First name, middle initial, last name)

Jean-Marc Larsen

6. REPORT DATE	7a. TOTAL NO. OF PAGES	7b. NO. OF REFS
October 1972	164	74

8a. CONTRACT OR GRANT NO	9a. ORIGINATOR'S REPORT NUMBER(S)
N00014-67-A-0112-0044 NASA NGL-05-020-176	I.P.R. No. 493
b. PROJECT NO	
c.	9b. OTHER REPORT NO(S) (Any other numbers that may be assigned this report)
d.	

10. DISTRIBUTION STATEMENT

This document has been approved for public release and sale; its distribution is unlimited. Reproduction in whole or in part is permitted for any purpose of the United States Government.

11. SUPPLEMENTARY NOTES	12. SPONSORING MILITARY ACTIVITY
	U.S. Navy, Office of Naval Research National Aeronautics and Space Administration

13. ABSTRACT

This work is a theoretical and experimental study of two particular cases of nonlinear wave interaction in a plasma column. The frequencies of the waves are of the order of magnitude of the electron plasma frequency. Ion motions are neglected.

In the first part of the thesis, the nonlinear coupling of slow waves on a plasma column is studied by means of cold plasma theory. The quasistatic approximation is used to simplify the analysis. The case of a plasma column surrounded by an infinite dielectric in the absence of a magnetic field is also examined. The linear properties of slow waves are reviewed, and solutions are obtained for use in the nonlinear theory.

The second part of the thesis is devoted to nonlinear scattering from a plasma column in an electromagnetic field having its magnetic field parallel to the axis of the column. In the linear regime, the plasma column exhibits series of multipole resonances. A warm plasma analysis using a scalar electron pressure and a nonuniform electron density profile is presented.

Some observations of nonlinear scattering are presented, and the effect of the Earth's magnetic field and of discharge symmetry on the radiation pattern are discussed. The influence of collisional loss on the nonlinear scattering amplitude is also considered.

DD FORM 1 NOV 68 1473

14 KEY WORDS	LINK A		LINK B		LINK C	
	ROLE	WT	ROLE	WT	ROLE	WT
WAVE-WAVE INTERACTION IN PLASMAS						
SURFACE WAVE INTERACTION ON A PLASMA COLUMN						
PARAMETRIC AMPLIFICATION IN A PLASMA COLUMN						
MODE CONVERSION IN A PLASMA COLUMN						
NONLINEAR SCATTERING FROM A PLASMA COLUMN						